

**Characterization of molecular properties of propylene impact
copolymers**

M.S. Pretorius



**Thesis presented in partial fulfillment of the requirements for the
degree of Master of Science at the University of Stellenbosch.**

Study Leader: Dr A.J. van Reenen

March 2007

I, the undersigned, hereby declare that the work contained in this thesis is my own original work and that I have not previously in its entirety or in part submitted it at any university for a degree.

Date:07/03/2007.....

Opsomming

Hierdie navorsing behels die fraksionering en karakterisering van vyf propileen impak kopolimere, sowel as die gebruik van preparatiewe temperatuutstyging eluering fraksionering (prep-TREF) om bondel ooreenstemming te bestudeer. Die fraksionering tegniek wat gebruik is in die navorsing is prep-TREF. Die prep-TREF fraksies was geanaliseer deur kristallisasië analise fraksionering (CRYSTAF), differensiële skandee kalorimetrie (DSC), ^{13}C kern magnetiese resonans spektroskopie (^{13}C NMR) en hoë-temperatuur jel-permeasie kromatografie (HT-GPC). Die molekulêre heterogeniteit van die kopolimere was ook geïllustreer, terwyl die fraksionering tegniek geoptimaliseer was. Ook, die propileen impak kopolimere wat eenders voorkom, sowel as totaal en al verskillend is in molekulêre samestelling, is vergelyk om bondel ooreenstemming te illustreer.

Die resultate vir die oorspronklike polimere het gewys dat die etileen inhoud, soos bepaal deur ^{13}C NMR, verskil van dit wat die vervaardigers aanspraak op maak. CRYSTAF analise het verskille opgelewer tussen twee oënskynlik eenderse polimere van verskillende bondels. Die prep-TREF tegniek is geoptimaliseer vir hierdie materiale, veral met respek tot die elueringstemperatuur sowel as die temperatuur intervale van die materiale. 15 duidelike onderskeibare fraksies, waarvan 7 ongeveer 90 % van die totale gewig van die polimeer wat gefraksioneer is opmaak, is verkry. Drie vername komponente is geïsoleer. Dit is 'n etileen-propileen-rubber, EPR, (50 – 60 mol %), propileen homopolimeer en etileen-ryke kopolimere. Die EPR is nie-kristallyn en grootendeels teenwoordig in die 25 en 50 °C fraksies. Meeste van die etileen is in die kopolimere teenwoordig as EPR. 'n Toename in die etileen inhoud ly gevolglik tot 'n toename in die rubberige, oplosbare deel van die polimeer. Prep-TREF is bewys as 'n nuttige tegniek om baie kompleks materiale soos hierdie propileen impak kopolimere te vergelyk.

Abstract

This study involves the fractionation and characterization of five propylene impact copolymers as well as the use of preparative temperature rising elution fractionation (prep-TREF) to study batch consistency. The fractionation technique used in the study was prep-TREF. The prep-TREF fractions were subsequently analysed off-line by crystallization analysis fractionation (CRYSTAF), differential scanning calorimetry (DSC), ^{13}C nuclear magnetic resonance (^{13}C NMR) and high-temperature gel-permeation chromatography (HT-GPC). The molecular heterogeneity of these copolymers was illustrated, while optimizing the fractionation technique. Also propylene impact copolymers that seem similar, as well as obviously different in molecular make-up, were compared to illustrate batch consistency.

The results for the original polymers show that the ethylene content, as determined by ^{13}C NMR, was significantly different from that claimed by the manufacturers. CRYSTAF analyses indicated differences between two seemingly similar polymers from different batches. The prep-TREF technique was optimized for these materials, particularly with respect to the elution temperatures and temperature intervals of these materials. Up to 15 clearly identifiable fractions, of which 7 comprised about 90 % of the total weight of the polymer fractionated, were obtained. Three major components were isolated from each of the polymers. These were ethylene-propylene-rubber, EPR, (50 – 60 mole %), propylene homopolymer and ethylene-rich copolymers. The EPR was non-crystalline and largely present in the fractions isolated at elution temperatures of 25 and 50 °C. Most of the ethylene in the copolymers is present as EPR. An increase in the ethylene content does correspondingly increase the rubbery, soluble part of the polymer. Prep-TREF was shown to be a useful technique to compare very complex materials such as the propylene impact copolymers.

Acknowledgements

I wish to thank the following people and institutions for their contributions:

Dr A.J. van Reenen, my supervisor, for his help, guidance and financial support in the completion of this study.

SASOL Polymers, for the provision of the materials needed to complete this thesis.

The people at the **Department of Chemistry and Polymer Science** at Stellenbosch University, especially the Olefins group, for their support.

Elsa Malherbe and **Jean McKenzie** for the NMR work.

Dr Valerie Grümel for the HT – GPC work.

Derrick McCauley for the CRYSTAF work.

A heart felt thank you to my **family and friends** for their constant support.

My mother, **Daneel Botha**, for her unwavering belief, support and love throughout my studies. Without you none of this would have been possible.

Finally, to my fiancée, **Liesel de Waal**, with you next to me, anything is possible.

Abbreviations

CRYSTAF	Crystallization analysis fractionation
^{13}C NMR	^{13}C nuclear magnetic resonance
DEAC	Diethyl aluminium chloride
DSC	Differential scanning calorimetry
EPC	Ethylene-propylene copolymer
EPDM	Ethylene-propylene-diene copolymer
EPR	Ethylene-propylene-rubber
FTIR	Fourier transform infrared
HDPE	High density polyethylene
HP-LDPE	High-pressure low-density polyethylene
HT-GPC	High-temperature gel permeation chromatography
i-PP	Isotactic polypropylene
LLDPE	Linear low density polyethylene
LDPE	Low density polyethylene
M_n	Number average molecular weight
M_w	Weight average molecular weight
MWD	Molecular weight distribution
PE	Polyethylene
PD	Polydispersity
PP	Polypropylene
prep-TREF	Preparative temperature rising elution fractionation
SEC	Size-exclusion chromatography
SEM	Scanning electron microscopy
SHAC	Super high activity catalyst
T_c	Crystallization temperature
T_e	Elution temperature of TREF
T_m	Melting temperature
TREF	Temperature rising elution fractionation
WAXD	Wide-angle X-ray diffraction

W_i

Weight of i number of fractions in grams

$\Sigma W_i\%$

Cumulative weight percentage of i number of fractions

Table of contents

List of contents	I
List of figures	V
List of tables	IX

List of contents

Chapter 1	Introduction and objectives	
1.1	Introduction	1
1.2	Objectives	2
1.3	References	2
Chapter 2	Historical and theoretical background	
2.1	Early developments in the field of polyolefins	3
2.1.1	Commercial production of polyolefins	4
2.2	Development of the Ziegler-Natta Catalysts	4
2.2.1	Overview of the Theory of Ziegler-Natta Polymerization	6
2.2.2.1	Early mechanisms	6
2.2.2.2	Bimetallic mechanisms	6
2.2.2.3	Monometallic mechanisms	7
2.2.2.4	The Trigger mechanism	8
2.2.2.5	Mechanism of stereoregulation in α -olefin polymerization	9
2.3	Polypropylenes	10
2.3.1	Polypropylene production processes	11
2.3.1.1	Early processes	11
2.3.1.2	Current processes	12

2.4	Impact polypropylenes	12
2.4.1	Introduction	12
2.4.2	Sequential copolymerization	13
2.4.3	Polypropylene blends	14
2.4.4	Structure/property relationships of impact polypropylene copolymers	14
2.5	Fractionation and characterization of polyolefins	16
2.5.1	Separation mechanisms of fractionation	18
2.5.2	Theory of fractionation	18
2.5.3	Application of the TREF technique	20
2.6	References	22
Chapter 3	Experimental	
3.1	Materials	28
3.1.1	Impact polypropylene copolymers	28
3.1.2	Sand	28
3.1.3	Glass wool	28
3.1.4	Solvents	28
3.1.4.1	Xylene	28
3.1.4.2	Deuterated solvents	28
3.2	Equipment	28
3.2.1	Temperature Rising Elution Fractionation (TREF)	28
3.2.1.1	Crystallization step	29
3.2.1.2	Elution step	30

3.3	Polymer characterization	31
3.3.1	Differential scanning calorimetry (DSC)	31
3.3.2	Crystallization analysis fractionation (CRYSTAF)	31
3.3.3	High temperature gel permeation chromatography (HT – GPC)	32
3.3.4	^{13}C Nuclear magnetic resonance (^{13}C NMR) spectroscopy	32
3.4	References	33
Chapter 4	Results and discussion	
4.1	Impact polypropylene copolymers	34
4.1.1	Introduction	34
4.1.2	^{13}C NMR analysis	35
4.1.2.1	Microstructure determination of unfractionated polymers	36
4.1.3	CRYSTAF analysis	41
4.1.4	DSC analysis	42
4.1.5	HT-GPC analysis	44
4.1.6	Characterization of the impact polypropylene copolymers: A summary	44
4.2	Fractionation of impact polypropylene copolymers	46
4.2.1	Introduction	46
4.2.2	Optimization of prep-TREF	46
4.2.3	Prep-TREF results of the five copolymers	51
4.3	Results and discussion of fractionated polymer C	54
4.3.1	Introduction	54
4.3.2	CRYSTAF results	55

4.3.3	DSC results	57
4.3.4	HT-GPC results	61
4.3.5	^{13}C NMR results	64
4.3.6	Summary of characterization results for the fractions from polymer C	66
4.4	Comparing batch consistency and copolymers with differing ethylene content	67
4.4.1	Introduction	67
4.4.2	Differences between polymer batches	67
4.4.2.1	Polymers A and B	67
4.4.2.2	Polymers C and D	73
4.4.3	Comparing copolymers with different ethylene content	76
4.5	References	82
Chapter 5	Conclusions and recommendations	
5.1	Introduction	83
5.2	Conclusions	83
5.3	Recommendations	84
Appendices		
Appendix A:	TREF curves and fractionation data for polymers A – E	85
Appendix B:	^{13}C NMR-; CRYSTAF-; DSC-; HT – GPC data	99

List of Figures

Chapter 2

- Figure 2.1 The Cossee mechanism for Ziegler-Natta olefin polymerization. 8
- Figure 2.2 Stereoregulation mechanisms in α -olefin polymerization. 9
- Figure 2.3 The schematic illustrations of isotactic (a), syndiotactic (b) and atactic (c) PP. 10

Chapter 3

- Figure 3.1 Crystallization step setup showing stirrer (1), oil bath (2), reflux condenser (3), the glass reactor with dissolved polymer and sand (4), thermosensor (5), temperature controller (6) and processor (7). 29
- Figure 3.2 The elution column with glass wool (1), ceramic beads (2), polymer on support (3) and the Xylene flow direction (4). 30
- Figure 3.3 Elution step setup, indicating nitrogen flow (1), the Xylene reservoir (2), copper tubing (3), the GC oven (4), control valve (5), elution column (6) and the collection beaker. 31

Chapter 4

- Figure 4.1 The backbone structure of polymer containing ethylene and propylene. 37
- Figure 4.2 ^{13}C NMR spectra of the unfractionated polymers (A-E). 38
- Figure 4.3 ^{13}C NMR spectrum of unfractionated polymer C. 39
- Figure 4.4. Possible repeat units present in unfractionated polymer C. 39
- Figure 4.5 CRYSTAF traces for the unfractionated polymers (A-E). 42
- Figure 4.6 DSC crystallization exotherms of the unfractionated polymers (A-E). 43
- Figure 4.7 DSC melting endotherms of the unfractionated polymers (A-E). 43

- Figure 4.8 HT-GPC curves of the response vs. retention time (s) of the unfractionated polymers (A-E). 44
- Figure 4.9 The curves of TREF for polymer C (9 fractions). The weight of the fractions as a function of the elution temperature ($^{\circ}\text{C}$), (a) the differential weight fraction to temperature, $W_i\%/\Delta T_i$, (b) accumulative weight fraction, $\Sigma W_i\%$. 47
- Figure 4.10 The curves of TREF for polymer D (12 fractions). The weight of the fractions as a function of the elution temperature ($^{\circ}\text{C}$), (a) the differential weight fraction to temperature, $W_i\%/\Delta T_i$, (b) accumulative weight fraction, $\Sigma W_i\%$. 48
- Figure 4.11 The curves of TREF for polymer D (16 fractions). The weight of the fractions as a function of the elution temperature ($^{\circ}\text{C}$), (a) the differential weight fraction to temperature, $W_i\%/\Delta T_i$, (b) accumulative weight fraction, $\Sigma W_i\%$. 50
- Figure 4.12 The curves of TREF for all five polymers. The weight per fraction, W_i (g), as a function of the elution temperature, ($^{\circ}\text{C}$). 51
- Figure 4.13 The curves of TREF for polymer C. The weight of the fractions as a function of the elution temperature ($^{\circ}\text{C}$), (a) $W_i\%/\Delta T_i$, (b) $\Sigma W_i\%$. 55
- Figure 4.14 The concentration in solution, determined by CRYSTAF, for the unfractionated, and fractions, of polymer C as a function of temperature. 56
- Figure 4.15 The 'undercooling' effect as demonstrated by comparing (a) the CRYSTAF crystallization temperature distribution curve and (b) the prep-TREF curve of the differential weight fraction to temperature, $W_i\%/\Delta T_i$, as a function of temperature. 57
- Figure 4.16 The DSC melting and crystallization peak maxima as a function of the TREF elution temperature for the fractions from polymer C, (a) DSC melting peak maxima, T_m , (b) DSC crystallization peak

	maxima, T_c , (c) represents the situation where T_m or $T_c = \text{TREF}$ elution temperature.	58
Figure 4.17	DSC melting curves (2 nd heating cycle) of the fractions obtained from polymer C.	60
Figure 4.18	DSC crystallization curves of the fractions from polymer C.	61
Figure 4.19	HT-GPC results for the fractions from polymer C.	62
Figure 4.20	The weight average molecular weight, of the fractions from polymer C as a function of elution temperature.	63
Figure 4.21	The number average molecular weight of the fractions from polymer C as a function of elution temperature.	63
Figure 4.22	The ^{13}C NMR spectra of the fractions from polymer C.	65
Figure 4.23.	The ^{13}C NMR spectrum of the 105 °C fraction from polymer C, showing the methine area.	65
Figure 4.24.	The ethylene content of the fractions of polymers A and B as a percentage of the total sample ethylene content vs. the elution temperature.	70
Figure 4.25	The data from TREF for polymers A and B (run 2). The weight per fraction, W_i (g), as a function of the elution temperature.	71
Figure 4.26	The DSC exotherms, (T_c), and endotherms, (T_m), for the 115 °C fractions of both polymers, A and B (run 2).	72
Figure 4.27	The weight average molecular weights for the fractions of both polymers A and B as a function of TREF elution temperature (°C) (run 2).	73
Figure 4.28	The data from TREF for polymers C and D (run 2). The weight per fraction, W_i (g), as a function of the elution temperature.	74

- Figure 4.29. The weight average molecular weights for the fractions of both polymers C and D as a function of TREF elution temperature ($^{\circ}\text{C}$) (run 2). 76
- Figure 4.30 The curves of TREF for all five polymers. The weight per fraction, W_i (g), as a function of the elution temperature. 77
- Figure 4.31 The ethylene content of the fractions of polymers A and C as a percentage of the total sample ethylene content vs. the elution temperature. 80
- Figure 4.32 The weight average molecular weights for the fractions of both polymers A and C as a function of TREF elution temperature ($^{\circ}\text{C}$) (run 2). 81

List of Tables

Chapter 4

Table 4.1	The parameters for calculating the chemical shifts of alkanes using the empirical additivity relationships..	35
Table 4.2	The correction term S_i for calculating the chemical shifts of branched alkanes using the chemical shift relationship.	36
Table 4.3	Mole% ethylene in the copolymers as supplied and as calculated from ^{13}C NMR.	41
Table 4.4	Summary of properties for the unfractionated polymers (A-E).	45
Table 4.5	Fractionation data of polymer C (9 fractions).	48
Table 4.6	Fractionation data of polymer D (12 fractions).	49
Table 4.7	Fractionation data for the five copolymers.	52
Table 4.8	Summary of properties for the fractions from polymer C.	66
Table 4.9	Components of the fractions from polymer C.	67
Table 4.10	Summary of properties for the fractions of both polymers A and B (run 2).	68
Table 4.11	Ethylene content comparisons for the fractions of both polymers A and B (run 2).	69
Table 4.12	Summary of properties for the fractions of both polymers C and D.	75
Table 4.13	Summary of properties for the fractions of both polymers A and C (run 2).	78
Table 4.14	Ethylene content comparisons for the fractions of both polymers A and C (run 2).	79

Chapter 1

Introduction and objectives

1.1 Introduction

“Fatto il polipropilene” (Made polypropylene). From this note by Giulio Natta on succeeding in polymerizing propylene in the early 1950s to having the highest production volume of all the olefin polymers in the current world market, polypropylene changed from a useless, low molecular weight, non-crystalline material into an exciting blend of new science with practical applications.^[1] The path of polypropylene, in a relatively short period of time, has truly been remarkable.

Polypropylene is a very versatile polymer with many exceptional properties. A major drawback is that it does have a low impact resistance at low temperatures. Polypropylene (PP) random copolymers have better impact resistance compared to the homopolymer. A random copolymer has lower crystallinity than the homopolymer, which results in lower melting- and softening temperature, tensile strength, dimensional stability and hardness. In many applications, such as automotive bumpers, light weight materials with good impact strength and stiffness over a wide temperature range are desirable. Food containers, on the other hand, are typically exposed to temperature extremes. In both these cases, the articles should be able to withstand low temperature impact as well as being dimensionally stable at elevated temperatures. PP random copolymers cannot meet all of these criteria.

Impact polypropylene copolymers do meet these requirements. These polymers are typically produced in a two-step cascade process where propylene is homopolymerized in the one reactor, transferred to a second reactor and copolymerized with ethylene to form the so-called impact copolymers. These copolymers are reactor blends of, (a), a polypropylene homopolymer matrix that provides stiffness, (b), a dispersed ethylene/propylene rubber (EPR) phase functioning as stress concentrators for dissipating

stresses in the matrix and, (c), a number of chains containing long sequences of both propylene and EPR to provide adhesion between the homopolymer and rubber phase.

Temperature rising elution fractionation (TREF) is a technique that fractionates heterogeneous polymers by crystallizability. Preparative temperature rising elution fractionation (prep-TREF) can be employed to separate complex polymers into discrete fractions, which can then be analyzed individually. Analytical techniques used in characterizing the fractions off-line include crystallization analysis fractionation (CRYSTAF), ^{13}C nuclear magnetic resonance spectroscopy (^{13}C NMR), differential scanning calorimetry (DSC) and high temperature gel permeation chromatography (HT-GPC). Using prep-TREF can lead to a better understanding of the molecular heterogeneity of semi-crystalline polymers.

1.2 Objectives

The two main objectives of this study were:

1. Use prep-TREF to fully fractionate and characterize impact polypropylene copolymers. This would involve the fractionation of different polypropylene impact copolymers and off-line characterization of these fractions. The first step would be to illustrate the molecular heterogeneity of these copolymers, while optimizing the fractionation technique.
2. Show that prep-TREF can be used to compare seemingly similar as well as obviously different impact copolymers with respect to molecular make-up. This could illustrate batch consistency.

1.3 References

1. Moore, E.P., *Introduction*, in *Polypropylene Handbook*, E.P. Moore, Editor. 1996, Hanser Verlag: Munich.

Chapter 2

Historical and theoretical background

2.1 Early developments in the field of polyolefins

The word *polymeric* was used first by J. Berzelius in 1832.^[1] He discussed the polymerization of organic compounds in 1863.^[2-4] The word olefin is based on the term 'olefiant' (oil forming gas), used by Dutch chemists to describe the evolved gas (ethylene) resulting from the addition of chlorine to oil (ethylene dichloride). The words alkene, ethene, propene, butene, and so on are preferred in IUPAC nomenclature, but polymer scientists have chosen to use the equivalent trivial names (i.e., olefin, ethylene, propylene, butylenes, etc).

In 1858 Goryainov and Butlerov produced polypentene by the addition of a trace of boron trifluoride to pentene. By 1869 they published a paper on the steps followed in their attempts to polymerize ethylene, propylene, pentene and pinene.^[5] While they were able to polymerize propylene and isobutylene, in the presence of traces of boron trifluoride,^[6] they failed in their attempts to polymerize ethylene.^[7] 'Polypropylene', as a word, was first used by Butlerov in 1876. Fontana repeated the methods used by Goryainov and Butlerov for the polymerization of propylene in 1952.^[8] The amorphous product obtained, while useful as an additive in lubricating oil, was useless as a structural material.

A gum-like polymer was produced by Butlerov and Goryainov in 1873 by the cationic polymerization of isobutylene in the presence of boron trifluoride.^[9] Thomas and Sparks produced butyl rubber, a copolymer of isobutylene (95 %) and isoprene (5 %) by 1944.^[10] In 1953 Natta produced an elastomer, ethylene-propylene monomer (EPM), by the copolymerization of ethylene and propylene.^[11]

2.1.1 Commercial production of polyolefins

The very first commercially produced polyolefin was highly branched low density polyethylene (LDPE), made by Imperial Chemical Industries (ICI) in 1933. Two chemists, Fawcett and Gibson, discovered polyethylene (PE) as a trace amount, scraped from the inner wall of the autoclave used in an attempt to condense ethylene and benzaldehyde at 200 °C.^[12] This resulted in the patent for the high-pressure production of LDPE in 1937.^[13] Despite initial technical problems delaying commercialization, by the time of World War II large quantities of LDPE were being produced for the coaxial cable used in radar applications.

The use of transition metal catalysts for the production of linear PE was heralded when Ziegler patented his TiCl_4 – triethyl aluminum catalyst system capable of producing PE with densities between 0.945 and 0.960 g/cm^3 at atmospheric pressure.^[14] A chromium catalyst, capable of producing PE with a density of between 0.960 and 0.970 g/cm^3 , was discovered by Hogan and Banks.^[15] Ziegler's catalyst was licensed to Petrochemicals, Montecatini, Hoechst and Hercules and the chromium catalyst to Phillips. Production started in the US by Phillips and in Europe by Hoechst in the period 1956 to 1957.^[16]

Natta was a consultant to Montecatini and, being involved in studying the kinetics of the ethylene polymerization reaction, undertook the investigation of Ziegler's new catalyst.^[17] Natta polymerized propylene with the Ziegler catalyst and discovered that it produced a mixture of amorphous and crystalline polypropylene (PP).^[18] Later, Natta's group successfully synthesized regular linear, head-to-tail polymers of α -olefins.^[19] The first company to commercially produce crystalline PP was Montecatini in Italy who went into production in 1957. Hercules followed suit and commenced production of PP in the U.S.^[20]

2.2 Development of the Ziegler-Natta Catalysts

Since Natta, using Ziegler's $\text{TiCl}_4/\text{AlR}_3$ catalyst system, succeeded in producing PP with low isotacticity in 1954, and improving on the PP isotacticity by using crystalline TiCl_3 modifications instead of the soluble TiCl_4 , isotactic PP has become one of the most

important polyolefin plastics. There has since been a relentless pursuit in the academic and industrial world to develop ever more efficient catalytic systems.

The first generation of Ziegler-Natta catalysts, $\text{TiCl}_3/\text{AlEt}_2\text{Cl}$, exhibited low polymerization activity and polymers with an isotacticity index (II) of around 90 %. Consequently, the removal of both catalyst residue and atactic material was required through expensive washing procedures.^[21] These factors made the production process both complicated and expensive. Only the Ti atoms on the surface of the TiCl_3 , which represent only a small fraction of the total Ti, is accessible to the cocatalyst. Active polymerization sites were thus limited and efforts started to improve the catalyst efficiency.

Second generation Ziegler-Natta catalysts, developed mainly by Solvay in the early 1970's, had a higher surface area ($40 \text{ m}^2/\text{g}$ as opposed to $30 \text{ m}^2/\text{g}$ of the first generation catalysts), much improved catalyst activity and an II of about 95 %.^[22] This 'Solvay' Ti_3Cl catalyst, with diethyl aluminium chloride (DEAC) as cocatalyst, is still employed today in the production of PP.

Attempts were made to develop supported catalysts by using mainly hydroxyl containing supports able to anchor the transition metal compound.^[23] Although these third generation Ziegler-Natta catalysts were to highly active for ethylene polymerization, they were not very successful for producing PP (as a result of low activity). During the late 1960's, catalysts based on 'activated' MgCl_2 were discovered by Montedison.^[24] These catalysts, which were highly active in producing both PE and PP, produced PP with low isotacticity (II < 50 %) ^[25] and were initially confined to PE production until the addition of Lewis bases ^[26] lead to a combination of high activity and good stereospecificity. A typical third generation Ziegler-Natta catalyst make-up consisted of co-milling MgCl_2 , TiCl_4 , a Lewis base (known as an internal donor), combined with an AlR_3 as cocatalyst and a second Lewis base (known as an external donor).^[23] These third generation catalysts still necessitated the removal of atactic material and research continued to find more efficient combinations of electron donors.

This search for more effective electron donors lead to the discovery of highly active and stereospecific catalysts referred to as super high activity catalysts (SHAC). Following

this, a new combination of electron donors, alkylphthalates as internal donors and alkoxy silanes as external donors, were discovered. These catalyst systems were initially called 'super-active third generation' by Galli *et al.* [27] but are labelled 'fourth generation catalysts' by Albizzati *et al.* [23] These fourth generation catalysts are currently used in most of the modern industrial processes for the production of PP.

2.2.1 Overview of the Theory of Ziegler-Natta Polymerization

2.2.2.1 Early mechanisms

Shortly after his discovery of the ethylene polymerization, Ziegler suggested his "aufbau" mechanism involving tri-ethyl aluminum, in which a polarized ethylene molecule is inserted in a stepwise manner at an anionic aluminum-carbon bond. [28] Natta extended Ziegler's "aufbau" reaction to apply to propylene, but omitted the configuration of the inserting propylene molecule. [29]

Neitzescu *et al.* [30] proposed a radical mechanism in which a chlorine atom is displaced from the TiCl_4 by an alkyl group from the aluminum alkyl. Friedlander and Oita [31] took the effects of the catalyst surface in the insertion reaction into consideration and proposed a mechanism whereby an electron is released from the transition metal surface to a chemisorbed olefin molecule which in turn transferred another electron to an adjacent molecule. It was suggested that polymer growth take place via bound radicals.

In 1959 Gilchrist [32] proposed an anionic mechanism whereby transfer of an alkyl group from the adsorbed metal alkyl to an adsorbed olefin resulted in an anionic olefin-alkyl molecule.

2.2.2.2 Bimetallic mechanisms

The bimetallic mechanism proposed by Uelzmann [33] involved a reaction between TiCl_3 and an aluminum alkyl to form the $(\text{TiCl}_2)^+(\text{AlR}_3\text{Cl})^-$ ion pair. The titanium attracts an olefin molecule which aligns itself along the Ti-Al axis and inserts into a metal-carbon bond.

In Natta and Mazzanti's [34] bimetallic mechanism the titanium, halogen, aluminum and methylene from one of the alkyl groups (or polymer chain) form a four-membered ring that is opened up at the Ti-C bond when an olefin coordinates with the titanium, forming

a six-membered configuration. This allows for the insertion of the olefin before reverting back to the four-membered ring.

2.2.2.3 Monometallic mechanisms

Cossee^[35] proposed a monometallic mechanism for Ziegler-Natta olefin polymerization in the 1960s and the following concepts of this proposal have been generally accepted:^[17, 36]

1. The active centre in Ziegler-Natta catalysts is the transition metal-carbon bond of the transition metal complex, which is formed by the interaction between two components of the catalytic system. The active complex has to contain at least one transition metal-carbon bond or transition metal-hydrogen bond. Further, an open coordination position must be present or formed during reaction.
2. Polymerization takes place through two steps: First, complexation of the monomer to the transition metal atom of the active centre and second, migratory insertion of the complexed monomer to the bond between the transition metal atom and the first carbon atom of the polymer chain. Repetition of this process is responsible for chain growth.

In the Cossee mechanism (shown in Figure 2.1 below) a vacant coordination site is generated initially, followed by olefin complexation. Formal migration of the polymer chain and the formation of the metal-carbon bond occur jointly through a four-membered transition state. This recreates a vacant coordination site at the site originally occupied by the polymer chain and the process continues. In order to explain the formation of isotactic polyolefins from these (heterogeneous) types of catalysts, migration of the (new) alkyl group is required in the last step to restore the original configuration of the active site.

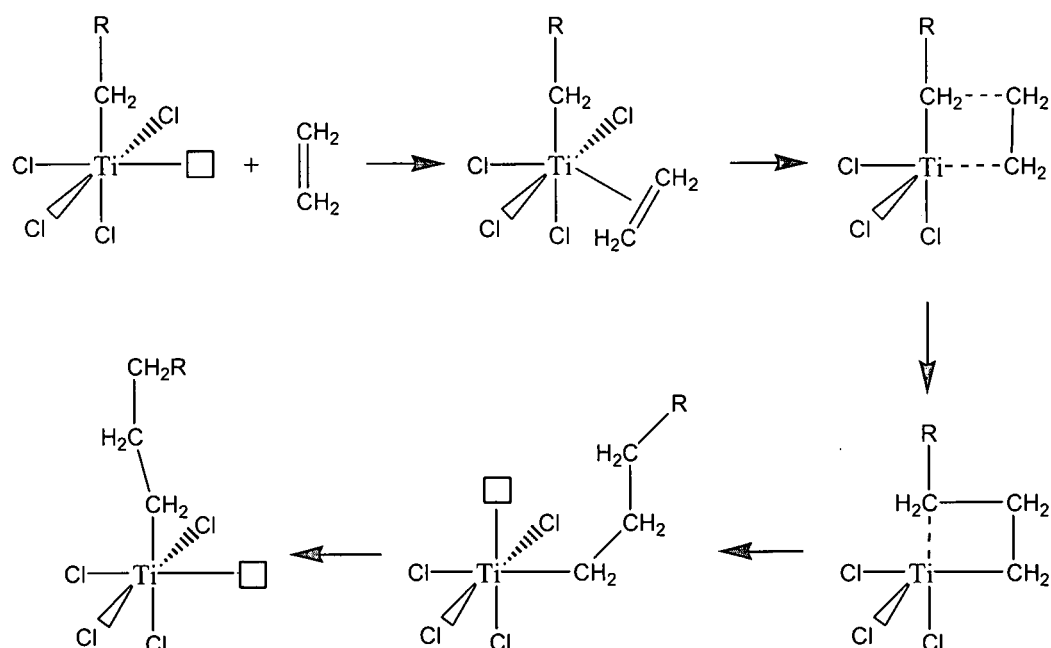


Figure 2.1 The Cossee mechanism for Ziegler-Natta olefin polymerization.

2.2.2.4 The Trigger mechanism

Although the Cossee mechanism has been widely accepted, there are some problems which are very difficult to explain through this mechanism:

- why the free, acidic coordination site is not attacked by Lewis bases,
- why the polymerization rate order relative to the monomer concentration is higher than 1,
- why the isospecific propagation rate is higher than the aspecific propagation rate, and
- why the stereoregularity of the first inserted monomer is lower than the subsequent insertions.

The trigger mechanism was proposed by Ystenes^[37] where the insertion of a complexed monomer molecule is triggered by an incoming monomer. According to this mechanism the main characteristics for the propagation step are:

1. The coordination site is never a free site, it is always occupied by a monomer.

2. The complexed monomer will be inserted if and only if a new monomer is ready to complex. Hence the monomer site is protected from attack by Lewis bases.
3. Two monomers are associated with the active metal complex in the transition state.

2.2.2.5 Mechanism of stereoregulation in α -olefin polymerization

The driving force for stereoregulation is steric by nature. In other words, the stereospecificity of a catalyst is determined by the difference in activation energy of the two coordination positions caused by steric interaction of the transition metal complex including the growing polymer chain with the incoming monomer.^[38] Two types of stereoregulation exist:

1. Catalytic site control occurs mostly in heterogeneous catalyst systems. Here, the asymmetric nature of each active centre forces the monomer to always add in the *si* or in the *re* configuration. Thus, isotactic chains are formed.
2. Chain end control results in the switching of the side group from one side to the other side of the chain. This can happen if the placement of the next monomer unit is controlled by the chirality of the last inserted monomer. If the last inserted monomer was erroneously placed with its side-group on the opposite side of the chain, placement of subsequent monomer units continue with this trend.

These two types of stereoregulation with primary or 1,2 insertion are shown in Figure 2.2.

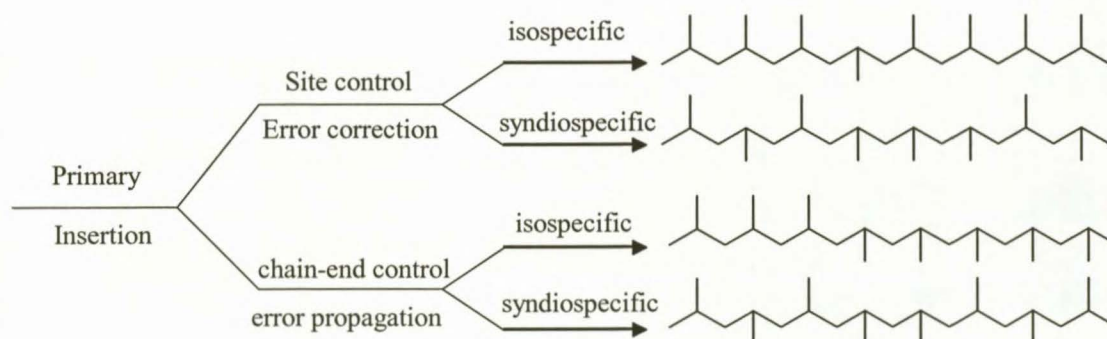


Figure 2.2 Stereoregulation mechanisms in α -olefin polymerization.

2.3 Polypropylenes

According to Moore,^[39] PP is defined as “the materials and related businesses that grew out of the Ziegler-Natta discovery of catalysts capable of producing stereoregular PP”.

PP homopolymer consists of three discernibly different types of polymer, namely isotactic, syndiotactic and atactic. The schematic illustrations of these different types of stereoregularity are shown in Figure 2.3. Of these three, isotactic PP (i-PP) is contained as a significant fraction in almost all types of PP.

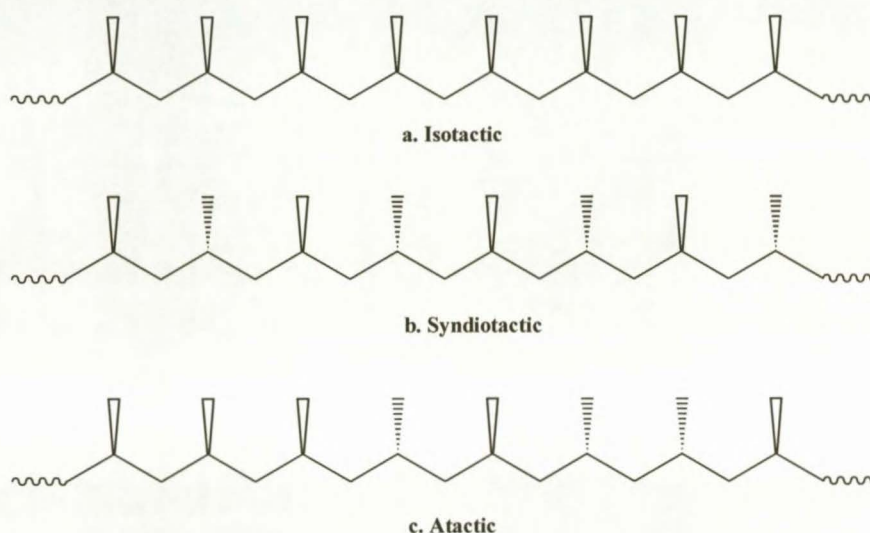


Figure 2.3 The schematic illustrations of isotactic (a), syndiotactic (b) and atactic (c) PP.

The degree of stereoregularity amongst PPs varies considerably. Xylene extractables in PP homopolymers is an indication of the atactic PP content, and as such varies from 1 % to about 20 %. As a result the degree of crystallinity can differ considerably. These variations are mainly due to the effectiveness of the catalyst, resulting in continual development in the PP industry to improve the catalyst performance.

Apart from PP homopolymers, there exists a wide range of PP copolymers, random and impact, as well as terpolymers, where the comonomers usually comprise ethylene and butene. Random PP copolymers typically contain up to 6 weight % of ethylene or other comonomers inserted at random along the polymer backbone. The comonomer in the polymer chain lowers crystallinity and the melting point. Impact PP copolymers contain up to 40 weight % ethylene-propylene rubber (EPR) interspersed in the PP homopolymer

matrix. These impact PP copolymers have better impact properties than the homopolymers or the random copolymers, especially at low temperature. The composition, morphology, molecular weight and amount of the dispersed EPR and PP homopolymer matrices are very important parameters in the impact properties of these materials. Section 2.4 will deal with these issues in more detail.

2.3.1 Polypropylene production processes

2.3.1.1 Early processes

The early catalysts used for PP polymerization typically had low activities and polymers containing high amounts of the atactic fraction were produced. The α -form of the early TiCl_3 catalysts yields PP with isotacticities between 80 and 90 %^[40] which made the development, by Montecatini, of the first industrial process for the production of PP possible. This process utilized slurry technology in where the isotactic fraction was kept in suspension while the atactic fraction was in solution. The slurry was then filtered to separate the two fractions. High molecular weight homopolymers, random copolymers containing small amounts of ethylene and impact polymers with low EPR content were typical products obtained from this technology.

Rexall^[41] and Phillips^[42] pioneered liquid monomer polymerization. The Rexall process used a stirred vessel and in the Phillips process a loop reactor containing the rapidly circulating polymer/monomer suspension. Polymer separation from the gaseous monomer takes place in a cyclone at ambient pressure resulting in the atactic fraction remaining in the polymer. The atactic polymer adversely affects the properties of the product and removal of the atactic material requires a further step. Solvay^[43] introduced a high activity catalyst which directed stereoregulation to a high degree. This catalyst was used in processes where polymerization in liquid monomer occurred without requiring removal of the atactic material. Montedison and Mitsui^[44] introduced a MgCl_2 -supported catalyst which decreased the amount of corrosive catalyst residues to such an extent that the post production removal of catalyst became unnecessary.

BASF^[45] pioneered gas-phase propylene polymerization processes through the introduction of the Novolen ® stirred-bed process. This process runs at temperatures

between 70 and 90 °C and pressures of about 30 bar. Unreacted monomer is condensed and recycled to provide additional heat transfer capability. The removal of atactic material was required, as it was not extracted as was done in the slurry process.

2.3.1.2 Current processes

Himont's Spheripol[®] process consists of two sections.^[46, 47] The first section contains one (or more) loop reactor(s) in which homo- or random copolymerization takes place in liquid monomer. Concentrated slurry is removed from the settling legs and fed to a cyclone where the polymer and gaseous monomer is separated. Condensed monomer is then fed back into the loop reactor(s) while the polymer is fed into (one or more) fluidized-bed gas-phase reactor(s) where ethylene and propylene is introduced for the formation of the desired rubber composition for impact polymers. The dense spherical polymer particles are steam-stripped from residual monomer and, at the same time, the catalyst is deactivated.

Mitsui's Hypol[®] process^[48] utilizes the Spheripol[®] catalyst technology. The Novolen[®] process of BASF has been rejuvenated through the use of SHAC. The Shell high activity catalyst as employed by Union Carbide uses a cascade reactor set-up where homopolymer and random copolymer are produced in a large fluidized-bed, gas-phase reactor. The product is then fed to a smaller reactor for the production of the rubber phase for impact polymers.

2.4 Impact polypropylenes

2.4.1 Introduction

Isotactic PP is a very versatile and useful product, finding wide application. Items such as fibres, films, pipes and injection moulded products can be produced.^[49] PP's relatively high melting temperature gives it good useability over a wide temperature range. In low temperature applications (below its glass transition temperature of 0 °C) however, the homopolymer is brittle. For certain applications the homopolymer is too rigid and displays poor transparency. Therefore, to broaden its application field, higher flexibility is required. A lower melting temperature for better weldability would be useful in certain

applications, whereas better impact resistance at low temperature combined with good stiffness would also be advantageous properties.

These desired properties can be attained through random copolymerization as well as through sequential copolymerization.^[47] Random copolymerization of propylene with another olefin, usually ethylene or butene, lowers the melting temperature and gives higher flexibility. Through sequential copolymerization, a material that is constituted of an elastomeric poly(propylene-co-ethylene), referred to as an EPR, well dispersed within a PP homopolymer matrix, shows improved stiffness together with an improvement in low temperature impact resistance.^[47] This type of material is known as an impact polypropylene copolymer.^[50] The next section will deal with the process of sequential copolymerization.

2.4.2 Sequential copolymerization

Sequential copolymerization is also referred to as in-situ polymerization.^[51] Sequential copolymerization is typically carried out in two steps. PP homopolymer is synthesized in the first step using a suitable transition metal catalyst. The PP homopolymer particles are then transferred to gas phase fluidized reactor, along with a mixture of ethylene and propylene, where the elastomeric phase (EPR) is produced within the homopolymer matrix.^[52] The resultant product is a complex mixture of PP homopolymer, EPR, semi-crystallized ethylene-propylene copolymer (EPC) and ethylene homopolymer.^[50]

Although this process of sequential copolymerization is a commercial success, the process is poorly understood, largely due to a lack of a thorough characterization of the resulting product. McKenna *et al.*^[53] proposed that the EPR which is formed on the active sites located on the surface of the catalyst crystallites underneath the layer of PP homopolymer creates stresses in the viscoelastic PP homopolymer, leading to crack formation in the PP. The EPR flows through the cracks, into the micro- and macropores, onto the surface of the polymer particle. Cecchin *et al.*^[54] proposed that after the first stage of polymerization the PP particle is composed of numerous polymer mesoparticles. The catalyst fragments segregates to the surface of the polymer mesoparticles during homopolymerization. EPR then formed in the second stage is located at the surfaces of these mesoparticles filling the pores between them, creating a continuous EPR network.

Various other authors also proposed different mechanisms for the growth and morphology of these impact PP particles.^[55-57]

2.4.3 Polypropylene blends

PP blends (i.e. post-reactor blending) have received considerable attention over the past few decades.^[58-62] The properties of these blends, for example mechanical strength, surface bonding and impact resistance are a function of the blend morphology. This morphology and associated phase behaviour depend heavily on the miscibility of the components in the blend.^[63] In order to improve the toughness of PP, different polymers, such as ethylene copolymers and elastomers, have been blended with PP. However, PP has bad miscibility with these materials and difficulty in controlling the morphology of these blends is encountered due to the crystallizability of PP.^[64] Blends of immiscible polymers generally exhibit poorer ultimate properties than that of their individual components due to strong phase separation leading to low interfacial adhesion.^[65] Post-reactor blending with butyl rubber,^[66] styrene butadiene-styrene (SBS) copolymer^[67] and EPDM copolymer^[68,69] have been widely investigated to improve the impact and tensile properties of PP.

2.4.4 Structure/property relationships of impact polypropylene copolymers

Impact PP produced through sequential copolymerization exhibit good impact-resistant properties due to the unique morphology and microstructure present. Galli^[70] showed that, since the elastomeric phase grows on the crystals which originated from the homopolymeric phase produced in the first reactor, an ideal morphology of impact polypropylenes can be attained through this polymerization method.

Hongjun *et al.*^[71] studied the chain structure of impact polypropylene copolymers prepared via sequential polymerization. These polymers were fractionated into four fractions and analysed by Fourier transform infrared (FTIR) and ¹³C Nuclear Magnetic Resonance (¹³C NMR) spectroscopy. The four fractions were identified as: EPR, ethylene-propylene segmented copolymer, ethylene-propylene block copolymer and PP homopolymer with a few ethylene monomers in the chain.

Zacur *et al.*^[72] investigated the effects of the blend composition in three impact polypropylene copolymers. The copolymers were fractionated. The fractions were analysed by differential scanning calorimetry (DSC), size exclusion chromatography (SEC) and FTIR. The morphology was examined by Scanning Electron Microscopy (SEM). The impact PPs were reported to consist of PP homopolymer, amorphous EPR, and crystallizable EPC. Particle size and shape of the dispersed phase for the different copolymers were correlated to the blend components and composition.

Fan *et al.*^[73] studied the structure and properties of impact PP in-situ copolymers synthesized by a spherical Ziegler-Natta catalyst. The polymers were fractionated by temperature-gradient extraction fractionation and characterized by FTIR, ¹³C NMR, DSC and wide-angle X-ray diffraction (WAXD). The copolymer was found to comprise of three portions: ethylene-propylene random copolymer, a series of segmented copolymer with PE and PP segments of different length and PP homopolymer. Impact PPs with higher amounts of segmented copolymer increased the impact strength correspondingly. Further study of the impact strength of the copolymers with and without the random copolymer section showed an increase in room temperature impact strength. Low temperature impact strength was markedly enhanced when both the random and segmented copolymer sections were present. Similar results were obtained by Fu *et al.*^[74]

Recently, Urdampilleta *et al.*^[52] studied the morphology of impact PP and showed that the PP particles are formed by a relatively small number (around 100) of mesoparticles. These mesoparticles had an average size one-fifth that of the particle diameter. The copolymerization of ethylene and propylene in the second stage fluidized bed leads to the formation of EPR around the catalyst fragments, which are well dispersed within the matrix, yielding a morphology consisting of finely dispersed EPR particles in the PP matrix.

Tan *et al.*^[65] compared two impact PP copolymers to study the proposal that ethylene-propylene segmented copolymers, with long ethylene sequences, act as compatibilizer that enhance the interfacial adhesion between the EPR disperse phase and the PP matrix. The two impact polypropylenes were produced by the Spheripol process, with one

copolymer being a testing product produced with a different spherical Ziegler-Natta catalyst.

2.5 Fractionation and characterization of polyolefins

As mentioned earlier, impact PP is a complex mixture consisting of PP homopolymer and ethylene-propylene copolymers, including EPR. In the words of Mirabella^[50], while analyzing and characterizing impact PP copolymers, “The molecular structure analysis of the resulting complex mixture is a formidable task”. A technique that enables the separation of this complex mixture which is, as all polyolefins, heterogeneous in nature would significantly aid in off-line analysis. In other words, a technique such as Prep-TREF can be employed to separate the complex mixture into discrete fractions, which can then be analyzed individually. This would then yield the identification of the individual components of such a complex polymer.^[75]

Different types of fractionation include: Prep-TREF, CRYSTAF and HT-GPC. The separation mechanisms of fractionation differ from technique to technique. HT-GPC fractionates according to molecular weight, Prep-TREF and CRYSTAF according to crystallizability. The crystallization of polyolefins is influenced by molecular properties such as, molecular weight (MW), molecular weight distribution (MWD), and the amount, type and distribution of comonomer in the case of copolymers.

The term “temperature rising elution fractionation” (TREF) was first coined by Shirayama *et al.*^[76] in 1965 to describe the method used to fractionate low density polyethylene according to crystallinity. The actual fractionation technique used was described in 1950 by Desreux and Spiegels^[77] who first recognized the potential of eluting at different temperatures to achieve a crystallization separation. Although elution of amorphous material under conditions of increasing temperature will also lead to fractionation, it will be on the basis of molecular weight.^[78] GPC can be employed for fractionation of amorphous polymers, leaving little interest in the fractionation of amorphous polymers by TREF. TREF has become known as a technique for analyzing semi-crystalline polymers by separating the molecular species according to their ability to crystallize. With the Prep-TREF technique, sufficient quantities of polymer fractions can be obtained in order to study the mechanical and physical properties.

Most of the earlier studies using Prep-TREF gave little attention to the cooling step and deposited polymer onto the column by natural or fast cooling. The later studies focused more on subjecting the hot polymer solution to a slow programmed cooling rate.^[78] According to Wild and Ryle,^[79] a 2 °C/hour cooling rate is needed for optimal separation. The benchmark article in the field of TREF was written by Wild *et al.*^[78] in 1990, wherein the application and apparatus of TREF is fully discussed. Various other authors have written good reviews of the TREF technique. Monrabal^[80] focused more on the analytical TREF technique itself. Xu *et al.*^[81] also reviewed the application of TREF in polyolefins. The fact that TREF has been limited to only polyolefins is highlighted, but TREF was successfully applied to other crystallizable polymers, such as metallocene-catalyzed styrene copolymers by Mulhaupt *et al.*^[82] A critical reason why TREF is applied to polyolefins is the fact that the polymer is dissolved in the solvent at high temperatures and can be eluted over a wide temperature range, typically from ambient to 130 °C. Other polymers, though, are soluble at room temperature and the extension of TREF below ambient temperatures is possible.

2.5.1 Separation mechanisms of fractionation

Desreux and Spiegels^[77] were the first to describe fractionation of a polyolefin by using an extraction technique with a single solvent system at increasing temperatures. They recognized that both the molecular weight and crystallinity separation come into effect in the case of PE, depending on whether the solvent composition or the temperature is varied in fractionation.

In the following years, the main objective of polymer fractionation was to establish molecular weight distributions. The emphasis fell on the development of strategies for achieving solubility separations using different solvent/non-solvent compositions. Later on, the elution of polymer supported on packed columns instead of approaches involving step-wise precipitation, evolved. The main advantages of the use of columns were described by Schneider,^[83] and include experimental convenience with the opportunity for automation, smaller volumes of solvent are required while the necessary condition of using dilute solutions are maintained, and fractionation takes less time, particularly in comparison to fractionation by precipitation.

MWD information on the polyolefins can be obtained by SEC.^[84] With the MWD data readily available, it became clear that this alone did not provide all the answers for the behaviour observed for these polymers. Attention was therefore focused on structural features controlling the solid-state properties. Here fractionation could play an important role.

The separation mechanism of Prep-TREF consists of two basic steps: a crystallization and an elution step. The actual step-by-step separation mechanism of Prep-TREF is explained, and illustrated, in Chapter 3.

2.5.2 Theory of fractionation

The principles of polymer fractionation or crystallization in solution can be explained by the use of the Flory-Huggins equation, which takes into account melting point depression in the presence of solvents. This is expressed by the equation 2.1.:

$$\frac{1}{T_m} - \frac{1}{T_m^0} = \frac{R}{\Delta H_u} \frac{V_u}{V_1} (\nu_1 - \chi_1 \nu_1^2) \quad (2.1)$$

where T_m is the equilibrium melting temperature of the polymer-solvent mixtures, T_m^0 is the melting temperature of the pure polymer, ΔH_u is the heat of fusion of each polymer repeat unit, V_u and V_1 are the molar volumes of the polymer repeat unit and diluent, respectively, ν_1 is the volume fraction of the diluent, and χ_1 is the Flory-Huggins thermodynamic interaction parameter.

For random copolymers the classical Flory equation applies, as shown in equation 2.2.:

$$\frac{1}{T_m} - \frac{1}{T_m^0} = \frac{R}{\Delta H_u} \ln(p) \quad (2.2)$$

where p is the molar fraction of the crystallizing unit. Flory^[85] proved that equation 2.1 reduces to the same form as equation 2.2. Therefore, when the concentration of the non-crystallizing comonomer units, diluents and polymer chain end groups are low, and they do not enter into the crystal lattice, they have equivalent effects on melting point depression.

When the term p is replaced with $(1 - N_2)$ in equation 2.2, where N_2 is the molar fraction of comonomer incorporated (non-crystallizing unit), equation 2.2 can be simplified when, for low values of N_2 , the following term is valid:

$$\ln(1 - N_2) \approx -N_2$$

which leads to equation 2.3:

$$\frac{1}{T_m} - \frac{1}{T_m^0} \approx \frac{R}{\Delta H_u} N_2 \quad (2.3)$$

Through experimental work, various authors have found a straight-line correlation between temperature and comonomer composition utilizing TREF, DSC and CRYSTAF.^[86-88] These correlations are independent of molecular weight.

2.5.3 Application of the TREF technique

TREF has been successfully applied to the characterization of mainly PEs, PPs and their copolymers. The evaluation of cocrystallization in polymer blends has also been reported by Wild *et al.*^[89] and shown to be negligible due to the fact that crystallization takes place from a dilute solution.

Wild and Ryle^[79] in 1977 showed how the principles of increasing temperature fractionation could be adapted to an analytical technique in order to determine the short chain branching (SCB) of LLDPE. Fractions of a narrow SCB distribution, which has different SCB averages, through the use of prep-TREF, were obtained and used to construct a calibration curve of the SCB as a function of elution temperature. Nakano and Goto^[90] combined analytical TREF and GPC for an automated composition fractionation/MWD measurement utilizing four LDPEs and a HDPE. Usami *et al.*^[91] compared four LLDPE samples with one high-pressure low-density polyethylene (HP-LDPE). It was shown that the HP-LDPE had a relatively narrow, low elution-temperature range, while all four LLDPE samples showed much broader and bimodal TREF profiles.

Wijga *et al.*^[92] made one of the first attempts to fractionate i-PP by an increasing temperature fractionation technique. This method was compared to the fractionation of PP through the elution gradient method, where fractionation is accomplished by increasing the fraction of solvent in a solvent/non-solvent mixture at constant temperature. Kamatah and Wild^[93] showed, through the fractionation of PP from dilute solution, that fractional crystallization was mainly dependant on stereoregularity and almost independent of molecular weight. Kioka *et al.*^[94] fractionated i-PP produced by a $\text{TiCl}_4/\text{MgCl}_2$ catalyst, with and without electron donors, over a wide temperature range. Isotactic PP produced without electron donors showed much broader distributions of molecular weight and isotacticity. Although the molecular weights of the fractions increased with elution temperature, it was not enough to suggest that fractionation is influenced by molecular weight effects.

Prep-TREF was used by Kakugo *et al.*^[95] to investigate the active catalytic sites during the formation of ethylene-propylene and propylene-1-butene copolymers. The fractions

were analysed by ^{13}C NMR spectroscopy. Kakugo *et al.*^[96] analysed ethylene-1-hexene copolymers using TREF and determined a trimodal composition distribution. Three different types of catalytic sites were identified with the most common site producing 1-hexene-rich random copolymer, the intermediate producing ethylene-rich random copolymer, while the least numerous catalytic site produced a copolymer containing long sequences of ethylene. Combining prep-TREF and ^{13}C NMR, Cheng and Kakugo^[97] were able to characterize compositional heterogeneity in ethylene-propylene copolymers produced by a Ti-based heterogeneous Ziegler-Natta catalyst.

Mirabella^[50, 98] was the first to fractionate impact PP by using TREF. In the characterization of this copolymer, three zones were clearly identified. The first zone is a rubbery ethylene-propylene copolymer, EPR, which is soluble at room temperature. Zone two, at somewhat higher temperatures, comprised of crystallizable ethylene-propylene copolymer fractions. A fraction consisting of an ethylene-rich copolymer was found at higher temperatures. Finally, i-PP fractions are recovered at the end of the fractionation. Usami *et al.*^[99] reported similar results to Mirabella. Xu and Feng^[100] studied the microstructure of two commercially obtained impact PPs by using prep-TREF. The fractions recovered were analysed by ^{13}C NMR and DSC. Xu and Feng identified the four main components as ethylene-propylene random copolymer, a block-type copolymer, a transition copolymer and propylene homopolymer. Pires *et al.*^[51] investigated five different impact PPs using prep-TREF and found that the relative amount of each component present in the polymer depended on the ethylene/propylene ratio used in the copolymerization step. For higher ethylene concentration present in the feed, a richer ethylene rubber is formed as well as a higher amount of crystallizable ethylene-propylene copolymer. Further, the amount of rubber present has an impact on the crystallization of the PP and EPC.

This study will investigate 5 different impact polypropylenes, and see if batch and composition differences can be identified and quantified by using prep-TREF as fractionation tool.

2.6 References

1. Berzelius, J., Jahresber. Fortsch. Phys. Wissensch., 1832. **11**: 44.
2. Berthelot, M., Ann. Chem. Phys., 1858. **3**(53): 158.
3. Berthelot, M., Soc. Chem. Paris, 1866. **148**: 18.
4. Mark, H., *Preface to History of Polyolefins*, ed. R.B. Seymour, Cheng, T. 1985, Dordrecht, The Netherlands: Reidel, D.
5. Berthelot, M., Bull. Soc. Chim. Fr., 1869. **1**(11): 4.
6. Butlerov, A., Annalen, 1876. **180**: 247.
7. Goryainov, V., and Butlerov, A., Annalen, 1873. **169**: 146.
8. Fontana, C.M., Kidder, G.A. and Herold, R.J., Ind. Eng. Chem., 1952. **44**: 1688.
9. Buterlov, A.M., Goryainov, V., J. Russ Chem. Soc., 1873. **5**: 302.
10. Thomas, R.M., Sparks, W.J., *U.S. Patent 2,356,128*, 1944.
11. Natta, G., Valvassor, A., Satori, G., *Polymer Chemistry and Synthetic Elastomers, Part II*, ed. J.P. Kennedy, Tornquist, E.G.M. 1969, New York: Wiley-Interscience.
12. Fawcett, E.W., and Gibson, R.O., J. Chem. Soc., 1934. 386.
13. Fawcett, E.W., Gibson, R.O., Perrin, M.W., Patten, J.G., and Williams, E.G., *British Patent 471,590*, 1937.
14. Ziegler, K., Holzkamp, E., Breil, H., and Martin, H., *German Patent 973,626*, 1960.
15. Hogan, J.P., Banks, R.L., *U.S. Patent 2,825,721*, 1958.
16. Sailors, H.R., Hogan, J.P., Macromol. Sci. Chem., 1981. **A15**: 1377.
17. Boor, J., *Ziegler-Natta Catalysts and Polymerization*. 1979, New York: Academic Press.
18. Natta, G., Pino, P., Farina, M., *Ricerca Sci.*, 1955. **25A**: 120.

19. Natta, G., *J. Polym. Sci*, 1955. **16**: 143.
20. Lieberman, R.B., Barbe, P.C., *Propylene Polymers*, in *Encyclopedia of Polymer Science and Engineering*, J.I. Kroschwitz, Exec. Ed. John Wiley & Sons, Editor. 1988: New York. 464.
21. Welch, M.B., Hsieh, H.L., *Olefin Polymerization Catalyst Technology*, in *Handbook of Polyolefins*, C. Vasile, Seymour, R.B., Editor. 1993, Marcel Dekker: New York.
22. Solvay, *German Patent 2,213,086*, 1972.
23. Albizzati, E., Giannini, U., Collina, G., Noristi, L., and Resconi, L., *Catalysts and Polymerizations*, in *Polypropylene Handbook*, E.P. Moore, Editor. 1996, Hanser Verlag: Munich.
24. Montedison, *British Patent 1,286,867*, 1968.
25. Pasquon, I., Giannini, U., *Catalysis Science and Technology*, ed. J.R. Anderson, Boudart, M., Vol. 6, Chapter 2. 1984, Berlin: Springer Verlag.
26. Montedison, *Belgian Patent 785,332*, 1972.
27. Galli, P., Barbe, P.C., Noristi, L., *Angew. Makromol. Chem.*, 1984. **120**: 73.
28. Ziegler, K., Gellert, H., Holzkamp, E., Wilke, G., Duck, E., Kroll, W., *Ann.*, 1960. **629**: 172.
29. Natta, G., *Macromol. Chem.*, 1955. **16**: 213.
30. Nenitzescu, C.D., Huch, C., Huch, A., *Angew. Chem.*, 1956. **68**: 438.
31. Friedlander, H.N., Oita, K., *Ind. Eng. Chem.*, 1957. **49**: 1885.
32. Gilchrist, A., *J. Polym. Sci*, 1959. **34**: 49.
33. Uelzmann, H., *J. Org. Chem.*, 1960. **25**: 671.
34. Natta, G., Mazzanti, G., *Tetrahedron*, 1960. **8**: 86.
35. Cossee, P., *Tetrahedron Lett.*, 1960. **17**: 12.
36. Sinn, H., Kaminsky, W., *Adv. Organomet. Chem.*, 1980. **18**: 99.

37. Ystenes, W., *Macromol. Chem. Macromol. Symp.*, 1993. **66**: 71.
38. Huang, J., Rempel, G.L., *Prog. Polym. Sci.*, 1995. **20**: 467.
39. Moore, E.P., *Introduction*, in *Polypropylene Handbook*, E.P. Moore, Editor. 1996, Hanser Verlag: Munich.
40. Natta, G., Corradini, P., Allegra, G., *J. Polym. Sci.*, 1961. **51**: 399.
41. *British Patent 1,044,811*, Rexall Drug and Chemical Co., 1962.
42. Smith, D.E., Keeler, R.M., Guenther, E., *U.S. Patent 3,476,729*, Phillips Petroleum Co., 1969.
43. Hermans, J.P., Henriouille, P., *U.S. Patent 3,769,233*, Solvay & Cie, 1973.
44. *German Patent Application 2,643,143*, Montedison and Mitsui Petrochemicals, 1975.
45. Ross, J.F., Bowles, W.A., *Ind. Eng. Chem. Prod. Res. Dev.*, 1985. **24**: 149.
46. Galli, P., Haylock, J.C., *Macromol. Chem., Macromol. Symp.*, 1992. **63**: 19.
47. Galli, P., Haylock, J.C., *Prog. Polym. Sci.*, 1991. **16**: 443.
48. *Hydrocarbon Process*, 1993. **72**(3): 204.
49. Moore, E.P., *Catalysts and Polymerizations*, in *Polypropylene Handbook*, E.P. Moore, Editor. 1996, Hanser Verlag: Munich.
50. Mirabella, F.M., *Polymer*, 1993. **34**(8): 1729.
51. Pires, M., Mauler, R.S., Liberman, S.A., *J. Appl. Polym. Sci.*, 2004. **92**: 2155.
52. Urdampilleta, I., Gonzalez, A., Iruin, J.J., de la Cal, J.C., Asua, J.M., *Macromolecules*, 2005. **38**(7): 2795.
53. McKenna, T., Bouzid, D., Matsunami, S., Sugano, T., *Polymer React. Eng.*, 2003. **11**: 177-197.
54. Cecchin, G., Marchetti, E., Baruzzi, G., *Macromol. Chem.*, 2001. **202**: 1978.
55. Kakugo, M., Sadatoshi, H., Sakai, J., Yokohama, M., *Macromolecules*, 1989. **22**: 551.

56. Kakugo, M., Sadatoshi, H., Sakai, J., Yokohama, M., *Macromolecules*, 1989. **22**: 3172.
57. Debling, J.A., Ray, W.H., *J. Appl. Polym. Sci.*, 2001. **81**: 3085.
58. Blom, H.P., Teh, J.W., Rudin, A., *J. Appl. Polym. Sci.*, 1996. **61**: 959.
59. Li, J., Shanks, R.A., Long, Y., *J. Appl. Polym. Sci.*, 2001. **82**: 628.
60. Li, J., Shanks, R.A., Long, Y., *Polymer*, 2001. **42**: 1941.
61. Kukaleva, N., Cser, F., Jollands, M., Kosior, E., *J. Appl. Polym. Sci.*, 2000. **77**: 1591.
62. Zacur, R., Goizueta, G., Capiati, N., *Polym. Eng. Sci.*, 1999. **39**(5): 921.
63. Lo, C., Seifert, S., Thiyagarajan, P., Narasimhan, B., *Polymer*, 2004. **45**: 3671.
64. Xu, J., Fu, Z., Fan, Z., Feng, L., *Eur. Polym. J.*, 2002. **38**: 1739.
65. Tan, H., Li, L., Chen, Z., Song, Y., Zheng, Q., *Polymer*, 2005. **46**: 3522.
66. Van Gisbergen, J.G.M., Meijer, H.E.H., Lemstra, P.J., *Polymer*, 1989. **30**: 2153.
67. Choudhary, V., Varma, H.S., Varma, I.K., *Polymer*, 1991. **32**: 2534.
68. Bartczak, Z., Galeski, A., Martuscelli, E., Janik, H., *Polymer*, 1985. **26**: 1843.
69. D'Orazio, L., Mancarella, C., Martuscelli, E., *Polymer*, 1991. **32**: 1186.
70. Galli, P., *Prog. Polym. Sci.*, 1994. **19**: 959.
71. Hongjun, C., Xiaolie, L., Dezhu, M., Jianmin, W., Hongsheng, T., *J. Appl. Polym. Sci.*, 1999. **71**: 93.
72. Zacur, R., Goizueta, G., Capiati, N., *Polym. Eng. Sci.*, 2000. **40**: 1921.
73. Fan, Z., Zhang, Y., Xu, J., Wang, H., Feng, L., *Polymer*, 2001. **42**: 5559.
74. Fu, Z., Fan, Z., Zhang, Y., Feng, L., *Eur. Polym. J.*, 2003. **39**: 795.
75. Wild, L., Ryle, T., Knobloch, D., and Peat, I., *J. Polym. Sci., Polym. Phys. Edn.*, 1982. **20**: 441.
76. Shirayama, K., Okada, T., Kita, S.I., *J. Polym. Sci., Part 2A*, 1965. **3**: 907.

77. Desreux, V., Spiegels, M.L., Bull. Soc. Chim. Belg., 1950. **59**: 476.
78. Wild, L., Adv. Polym. Sci., 1990. **98**(1): 1-47.
79. Wild, L., Ryle, T., Polym. Preprint Am. Chem. Soc., 1977. **18**: 182.
80. Monrabal, B., *Temperature rising elution fractionation and crystallization analysis fractionation*, in *Encyclopaedia of Analytical Chemistry*. 2000, John Wiley and Sons Ltd.: Chichester. 8074-8084.
81. Xu, J., Feng, L., Eur. Polym. J., 2000. **36**: 867-878.
82. Thomann, Y., Sernetz, F.G., Thomann, R., Kressler, J., Mulhaupt, R., Macromol. Chem. Phys., 1997. **198**: 739.
83. Schneider, N.S., J. Polym. Sci. C, 1965. **8**: 179.
84. Moore, J.C., J. Polym. Sci., Pt. 2A, 1964: 835.
85. Flory, P.J., *Principles of Polymer Chemistry*. Ithaca ed. 1953, New York: Cornell University Press.
86. Alamo, R., Mandelkern, L., Macromolecules, 1989. **22**: 1273.
87. Monrabal, B., J. Appl. Polym. Sci., 1994. **52**: 491.
88. Wild, L., Blatz, C., *New Advances in Polyolefins*, ed. T. Chung. 1993, New York: Plenum Press.
89. Wild, L., Knobeloch, D.C. *SPE Polyolefins IV Conference Prepr.* 427. 1984.
90. Nakano, S., Goto, Y., J. Appl. Polym. Sci., 1981. **26**: 4217.
91. Usami, T., Gotoh, Y., Takayama, S., Macromolecules, 1986. **19**: 2722.
92. Wijga, P.W.O., Van Schooten, J., Boerma, J., Macromol. Chem., 1960. **36**: 115.
93. Kamatah, P.M., Wild, L., Polym. Eng. Sci., 1966. **6**: 213.
94. Kioka, M., Makio, H., Mizuno, A., Kashiwa, N., Polymer, 1994. **35**: 580.
95. Kakugo, M., Miyatake, T., Mizunuma, K., Kawai, Y., Macromolecules, 1988. **21**: 2309.
96. Kakugo, M., Miyatake, T., Mizunuma, K., Macromolecules, 1991. **24**: 1469.

97. Cheng, H.N., Kakugo, M., *Macromolecules*, 1991. **24**: 1724.
98. Mirabella, F.M., *J. Appl. Polym. Sci. Appl. Polym. Symp.*, 1992. **51**: 117.
99. Usami, T., Gotoh, Y., Umemoto, H., Takayama, S., *J. Appl. Polym. Sci. Appl. Polym. Symp.*, 1993. **52**: 145.
100. Xu, J., Feng, L., *Polym. Int.*, 1998. **47**: 433.

Chapter 3

Experimental

3.1 Materials

3.1.1 Impact polypropylene copolymers

Three impact polypropylene copolymers with different ethylene contents were kindly donated by SASOL for the purposes of this study. For two impact polypropylene copolymers, two batches of each were received to study batch consistency.

3.1.2 Sand

The sand, white quartz (-50+70 mesh), was obtained from Aldrich and used as received.

3.1.3 Glass wool

The glass wool, which is low in lead, was obtained from Merck and used as received.

3.1.4 Solvents

3.1.4.1 Xylene

Xylene uniVAR was obtained from Merck and used as received.

3.1.4.2 Deuterated solvents

Deuterated benzene and tetrachloroethane were obtained from Aldrich and used as received.

3.2 Equipment

3.2.1 Temperature Rising Elution Fractionation (TREF)

The preparative-TREF equipment was built in-house.^[1] The technique is composed of two basic steps. In the first step, the polymer is subjected to slow crystallization onto a support. This separates the molecular species into layers from low to high crystallizability. In the second step, the polymer, crystallized on the support, is packed into a stainless steel column and a suitable solvent is passed through as the temperature is

increased. This increase in temperature dissolves the different molecular species at their respective solution temperatures and the fractions are thus collected.^[2]

3.2.1.1 Crystallization step

Typically 3 g polymer and stabilizer (2 wt% Ciba[®] Irganox[®] 1010) was dissolved in 300 mL xylene at 130 °C in a glass reactor, equipped with a Teflon-coated magnetic follower, on a magnetic heater/stirrer. The reactor was transferred to an oil bath kept constant at 130 °C. Preheated sand (heated to 130 °C to prevent premature crystallization) was added to the solution and the oil bath was then cooled to room temperature at 1 °C/hour. During this slow cooling, polymer fractionation occurs by the deposition of layers of decreasing crystallinity onto the support. At this stage the polymer is already segregated in layers of different composition.^[3] The crystallization setup is illustrated in Figure 3.1.

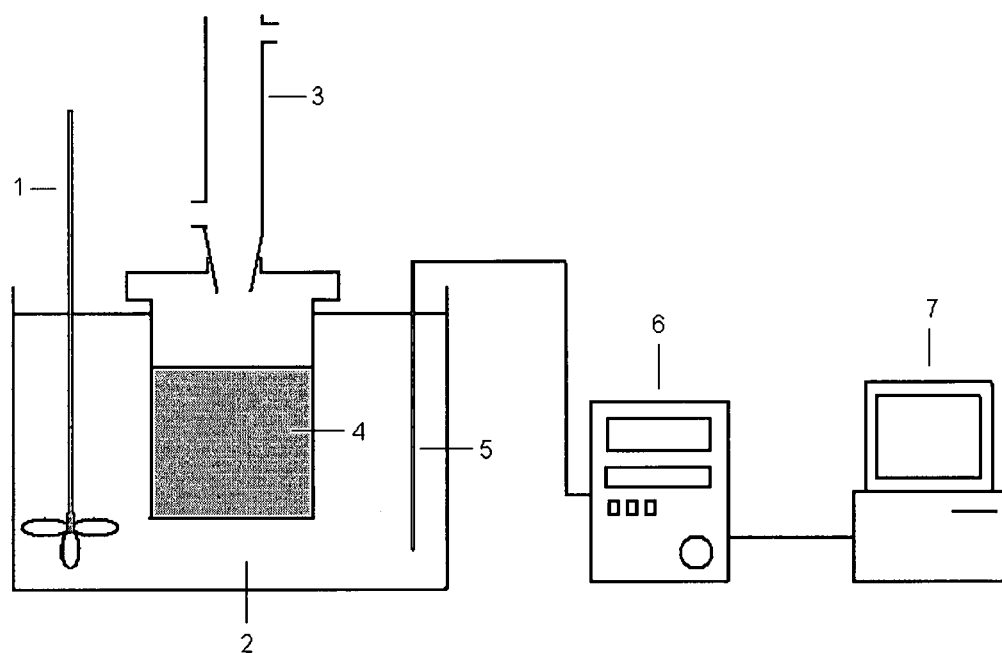


Figure 3.1 Crystallization step setup showing stirrer (1), oil bath (2), reflux condenser (3), the glass reactor with dissolved polymer and sand (4), thermosensor (5), temperature controller (6) and processor (7).

3.2.1.2 Elution step

The stainless steel elution column was packed with a layer of glass wool, ceramic beads and, once again, glass wool. The polymer, crystallized on the support material, was packed on top of these layers followed by a final layer of glass wool. The column is shown in Figure 3.2.

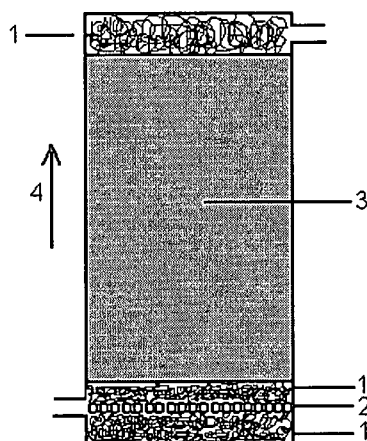


Figure 3.2 The elution column with glass wool (1), ceramic beads (2), polymer on support (3) and the Xylene flow direction (4).

The column was then fitted into a modified GC oven. Xylene was passed through the column by applying nitrogen pressure and fractions were collected at selected temperature intervals. The solvent dissolves the fractions of increasing crystallinity as the temperature rises.^[3] The elution setup is illustrated in Figure 3.3.

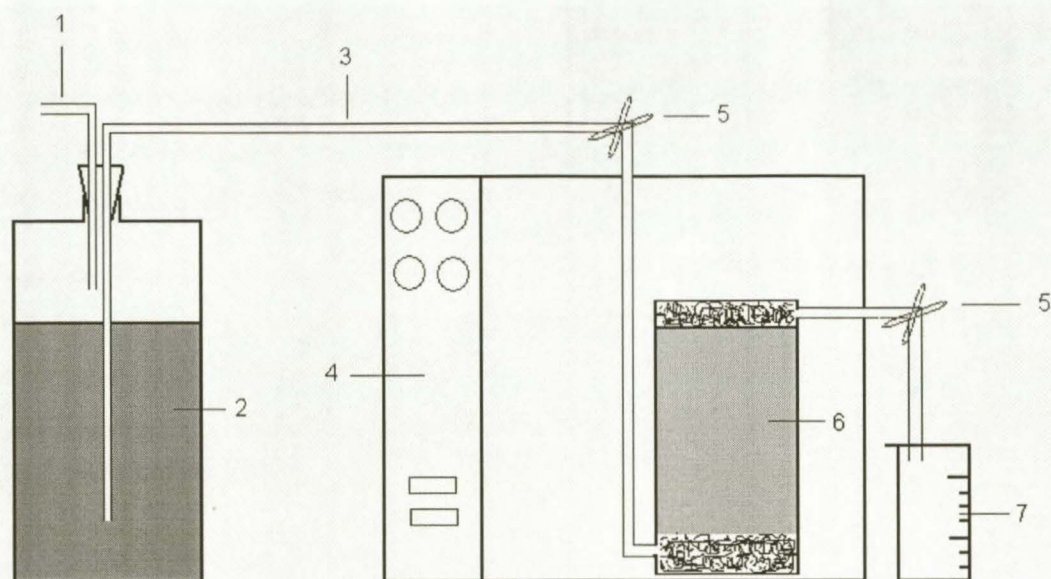


Figure 3.3 Elution step setup, indicating nitrogen flow (1), the Xylene reservoir (2), copper tubing (3), the GC oven (4), control valve (5), elution column (6) and the collection beaker.

3.3 Polymer characterization

3.3.1 Differential scanning calorimetry (DSC)

Melting and crystallization behaviour was determined on a TA Instruments Q100 DSC system calibrated with indium metal according to standard procedures. A typical analysis sequence is as follows: the samples were heated from 25 to 220 °C at 10 °C/min, held isothermally at 220 °C for 1 minute, cooled to -30 °C at a rate of 10 °C/min during which time the crystallization curve was recorded. At -30 °C, the temperature was kept constant for 1 minute after which the melting curve was recorded between -30 and 190 °C at a heating rate of 10 °C/min. All DSC analyses were done in a nitrogen atmosphere, and at a purge gas flow rate of 50 mL/min.

3.3.2 Crystallization analysis fractionation (CRYSTAF)

Crystallization analysis fractionation was carried out using a commercial CRYSTAF apparatus, model 200 manufactured by Polymer Char S.A. (Valencia, Spain). The crystallization was carried out in stirred, stainless steel reactors, each with a volume of 60

mL. Dissolution and filtration took place automatically in the reactors. Approximately 20 mg of sample was dissolved in 30 mL 1,2,4-trichlorobenzene. The temperature was decreased at a rate of 0.10 °C/min from 100 °C to 30 °C. The fractions eluted at lower temperatures during prep-TREF were analysed using the same cooling rate but over a lower temperature range (90 °C to 10 °C). Fractions were taken automatically and the polymer concentration from solution was determined by an infrared detector, using 3.5 μm as the chosen wavelength.

3.3.3 High temperature gel permeation chromatography (HT – GPC)

Molecular weights were determined using high-temperature gel permeation chromatography. A flow rate of 1 mL/min on a PL-GPC 220 high temperature chromatograph (Polymer Laboratories) was used and the measurements were performed at 160 °C. Three mixed bed columns in series were used (PL gel MIXED-B [9003-53-6] from Polymer Laboratories). The column length was 300 mm and the diameter was 7.5 mm. Average particle size radius was 10 μm (polystyrene/divinylbenzene copolymer). The sample concentration was 2 mg/mL and the solvent used was 1,2,4-trichlorobenzene, stabilized with 0.0125 % 2,6-di-tert-butyl-4-methylphenol (BHT). BHT was used as a flow rate marker. Calibration of the instrument was done with monodisperse polystyrene standards (EasiCal from Polymer Laboratories). A differential refractive index detector was used.

3.3.4 ^{13}C Nuclear magnetic resonance (^{13}C NMR) spectroscopy

^{13}C NMR spectra were recorded at 120 °C on a Varian VXR 300 MHz spectrometer in a 9:1 mixture of 1,2,4-trichlorobenzene/ C_6D_6 , using C_6D_6 at δ 128.02 as internal secondary reference. The pulse angle was 45 degrees and the acquisition time was 0.82 seconds. Additional spectra were recorded at 120 °C on a Varian Unity-Inova 600 MHz spectrometer in deuterated tetrachloroethane, using δ 75.00 as internal reference. The pulse width was 90 degrees, with a pulse delay of 15 seconds. The acquisition time was 1.8 seconds.

3.4 References

1. Rabie, A.J., *M.Sc Thesis, Blends with low-density polyethylene (LDPE) and plastomers*, University of Stellenbosch, Stellenbosch, 2004.
2. Mirabella, F.M., *J. Liq. Chrom.*, 1994. **17**(14&15): 3201.
3. Monrabal, B., *Temperature rising elution fractionation and crystallization analysis fractionation*, in *Encyclopaedia of Analytical Chemistry*. 2000, John Wiley & sons Ltd. pp. 8074-8094.

Chapter 4

Results and discussion

Summary

The chapter has been divided into four parts. First, the analysis and properties of the original, unfractionated impact PP copolymers are discussed. This is done in order to provide insight into the complex nature of these impact copolymers. Second, the development of the optimal number of Prep-TREF samples collected per elution run is explained. In the third section, the results of only one of these impact copolymers are shown and discussed. This is done in order to avoid repetition. Finally, comparisons are made between the properties of the fractions obtained from Prep-TREF of the different batches. Differences as well as similarities are discussed. The copolymers with different ethylene content are also compared to each other.

4.1 Impact polypropylene copolymers

4.1.1 Introduction

Impact PP is a copolymer of propylene and ethylene made through a two-reactor, sequential copolymerization system. In the first reactor, PP homopolymer is produced. The PP is then transferred to a second reactor where additional catalyst and ethylene gas are added. This yields a complex blend of PP homopolymer, EPR as well as semi-crystallizable ethylene-propylene copolymer.^[1] Some ethylene homopolymer might also be present. This is discussed in Chapter 2.

The nomenclature used for the polymers studied is as follows: polymers A and B have similar ethylene content but are from different batches. Likewise, polymers C and D have similar ethylene content and are also from different batches. Polymer E has lower ethylene content than polymers A and C. These code assignments were made from data

sheets supplied by the manufacturer. In this section the analyses of the unfractionated polymers will be discussed.

4.1.2 ^{13}C NMR analysis

Peak assignments were made by the use of literature where possible. These values were then correlated with the chemical shift assignments predicted by the additivity rules described by Grant and Paul.^[2] The chemical shift prediction for a specific carbon, according to the rules of Grant and Paul, is made by determining the combined effects of the neighbouring carbons. The number of carbon atoms in the positions α , β , γ , δ and ϵ relative to the carbon atom in question, are counted and multiplied by the respective constants. These constants are given in Table 4.1.

Table 4.1 The parameters for calculating the chemical shifts of alkanes using the empirical additivity relationships.

Carbon position	A_i (ppm)
α	8.61
β	9.78
γ	-2.88
δ	0.37
ϵ	0.06

The branching of the carbon chain also affects the chemical shift values. The following correction factors, shown in Table 4.2, must be taken into account during the calculation of the chemical shift of a specific carbon.

Table 4.2 The correction term S_i for calculating the chemical shifts of branched alkanes using the chemical shift relationship.

	S_i (ppm)
$1^\circ(3^\circ)$	-1.40
$1^\circ(4^\circ)$	-3.35 ± 0.35
$2^\circ(3^\circ)$	-2.45
$2^\circ(4^\circ)$	-7.50
$3^\circ(2^\circ)$	-2.65
$3^\circ(3^\circ)$	-9.45
$4^\circ(1^\circ)$	-1.50 ± 0.10
$4^\circ(2^\circ)$	-8.35

Here, $1^\circ(3^\circ)$ represents a methyl group attached to a tertiary carbon, $2^\circ(3^\circ)$ represents a secondary carbon attached to a tertiary carbon and $3^\circ(2^\circ)$ represents a tertiary carbon attached to a secondary carbon. The following equation was proposed for determining the chemical shifts:

$$\delta_c = B + \sum A_i n_i + \sum S_i \quad (4.1)$$

where

B = regression constant given by the chemical shift of methane (-1.87),

A_i = additive shift due to carbon i ,

S_i = corrective term included to account for branching, and

n_i = number of carbons at position i away from carbon in question.

4.1.2.1 Microstructure determination of unfractionated polymers

The comonomer composition of the impact PPs (ethylene content) was determined by determining the ratios of the integrals of characteristic peaks of the different monomers in the ^{13}C NMR spectrum of the unfractionated polymers. In Figure 4.1 a sequence of ethylene-propylene in the polymer backbone is depicted, and the relevant carbons used for the ^{13}C NMR analyses are shown.

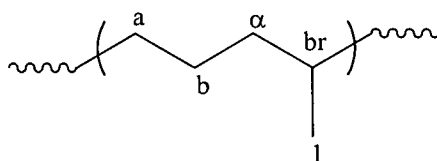


Figure 4.1 The backbone structure of polymer containing ethylene and propylene.

The ethylene content is calculated using the following equation:

$$\% \text{ Ethylene} = \frac{(\frac{1}{2}(a + \alpha) + b)}{(a + b + \alpha + br)} \times 100$$

where a , α , b and br in the equation represents the integrals of the ^{13}C NMR peaks representing the carbons denoted by the same letters in Figure 4.1.

In this case, the a and α carbons for ethylene and propylene, respectively, have identical chemical shifts.

In Figure 4.2 the ^{13}C NMR spectra of the unfractionated polymers (A-E) are shown. From the spectra it is clearly evident that the molecular architecture of these polymers is highly complex.

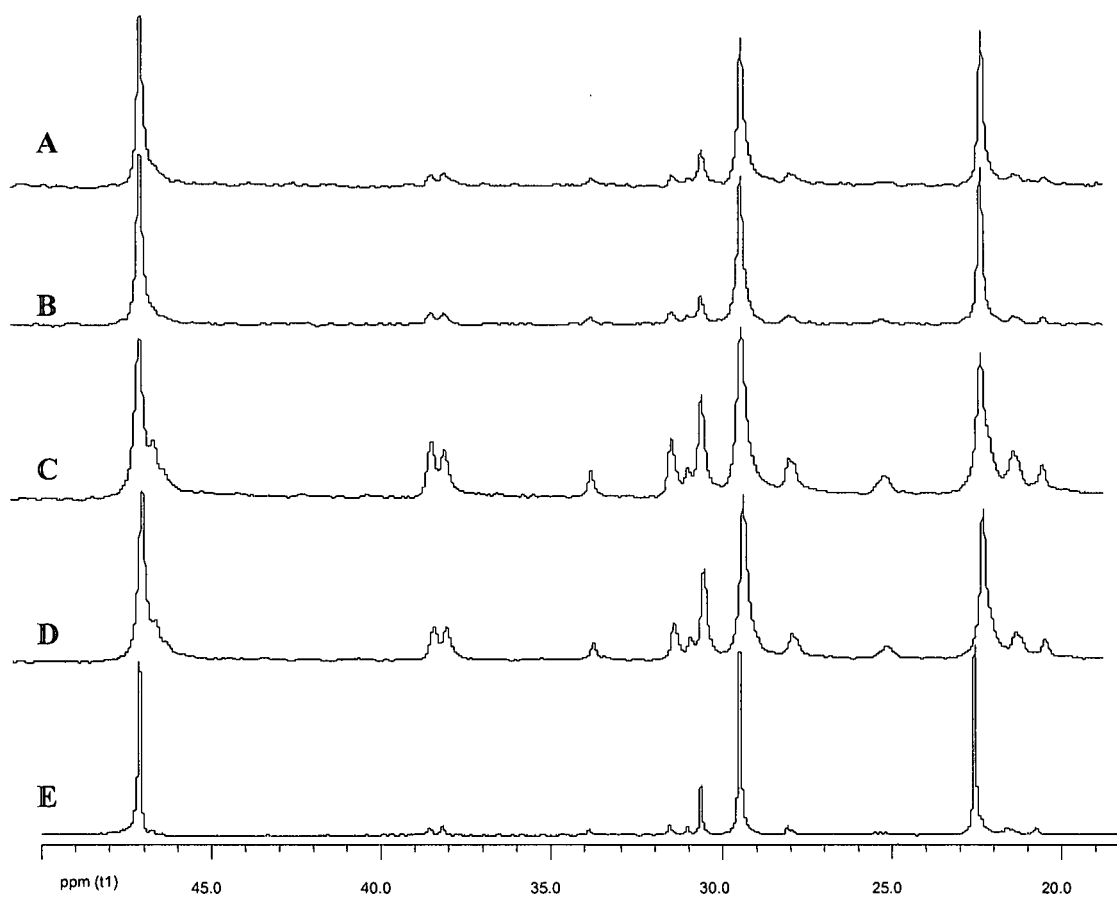


Figure 4.2 ^{13}C NMR spectra of the unfractionated polymers (A-E).

As an illustration, unfractionated polymer C is chosen to show the possible chain structures present, and to illustrate the complexity of the polymer. The ^{13}C NMR spectrum of unfractionated polymer C is shown in Figure 4.3. The peak assignments made in Figure 4.3 are based on the possible chain structures as shown in Figure 4.4.

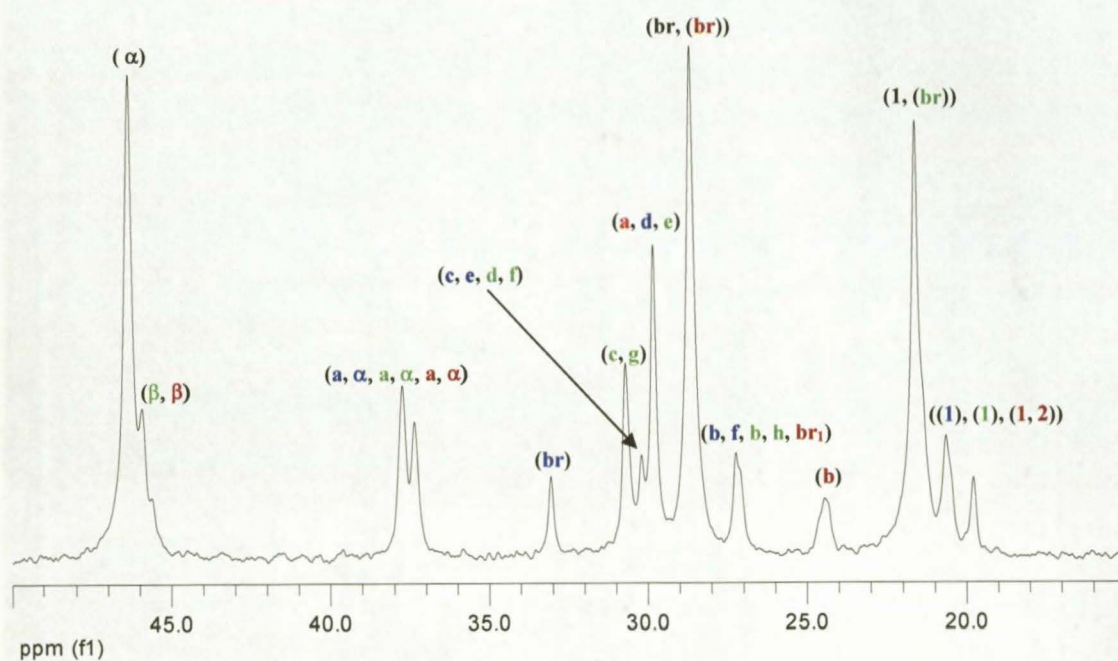


Figure 4.3 ^{13}C NMR spectrum of unfractionated polymer C.

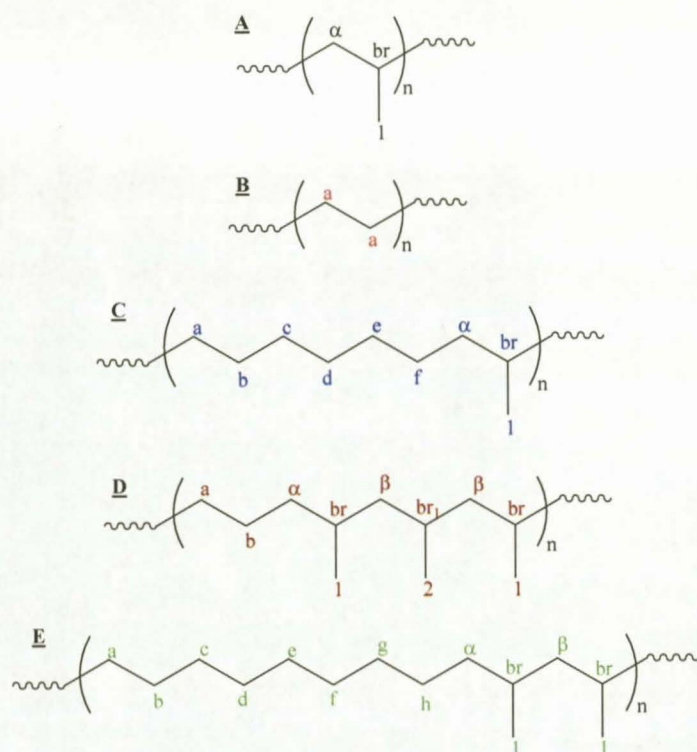


Figure 4.4. Possible repeat units present in unfractionated polymer C.

Here, it is possible to identify the resonance peaks that resulted from the polypropylene homopolymer produced in the first reactor. The carbon (C) relaxation peaks at 46.32 ppm, 28.64 ppm and 21.59 ppm are due to the methylene, methine and methyl carbons of isotactic propylene homopolymer sequences. The peak representative of polyethylene homopolymer or long ethylene sequences in the copolymer, is observed at 29.80 ppm.

The numerous smaller peaks are due to different configurational distributions of the ethylene and propylene repeat units in the copolymer structures present. This can be seen in Figure 4.4 C to E. It is interesting to note that where there is a single propylene insertion into the growing ethylene chain (Figure 4.4 C), a methine carbon, (br) peak appears downfield (33.05 ppm). It can also be seen that where more than one propylene repeat unit is consecutively inserted into the growing chain (Figure 4.4 D and E), a peak for the methylene carbon, (β), of propylene appears downfield. In this fashion we can clearly differentiate between single and consecutive insertions of ethylene and propylene in the polymer chain.

From Figure 4.3 it is clear that polymer C consists mainly of polypropylene homopolymer and little copolymer (based on the relative integrals of the different peaks), but that the copolymer present is a varied mixture. In other words, combinations of copolymer structures are present. From the ^{13}C NMR spectra all of the possible structures can be seen as shown in Figure 4.4. The ^{13}C NMR spectra of polymers A, B, D and E show similar complex structures, but it is also clear that the composition of these polymers are fundamentally different. At first glance, A and B are similar, but different from C and D (which are similar), and these polymers are all different from polymer E.

Table 4.3 shows the comparison of the ethylene content in the copolymers between the supplier's product data sheets and as calculated from ^{13}C NMR.

Table 4.3 Mole% ethylene in the copolymers as supplied and as calculated from ^{13}C NMR.

Impact PP	Ethylene in copolymer (mole%) ^a	Ethylene in copolymer (mole%) ^b
A	13.6	17.5
B	13.6	16.2
C	17.0	31.8
D	17.0	28.5
E	9.4	18.0

^a supplier product data sheets^b calculated from ^{13}C NMR (see section 4.1.2.1)

4.1.3 CRYSTAF analysis

Figure 4.5 shows the CRYSTAF traces for the five unfractionated polymers. Although polymers A and B have similar ethylene content there are marked differences in their CRYSTAF traces. Polymer A has a crystallization peak maximum at 80.5 °C while polymer B has a peak maximum at 76.9 °C. Polymer B also has a much broader crystallization peak than polymer A. Similarly, there are also differences between polymers C and D. Polymer C has a higher crystallization peak maximum than D (80.2 °C for polymer C as opposed to 77.9 °C for polymer D), as well as a slightly narrower crystallization peak. Polymer E has a peak maximum at 78.7 °C. It had been expected, based on the ethylene content from the supplier's product data sheets, that polymer E would have a higher crystallization temperature than polymers A and B, which in turn should have higher crystallization temperatures than those of polymers C and D. Solution crystallization analyses indicate that these materials, that appear chemically similar when ^{13}C NMR spectra are compared, seem to be different in their molecular make-up when crystallization data is compared. Also interesting is the apparent differences in soluble content for polymers with apparently similar ethylene content (for example B and E). This indicates that the distribution of the ethylene within the copolymers varies from polymer to polymer.

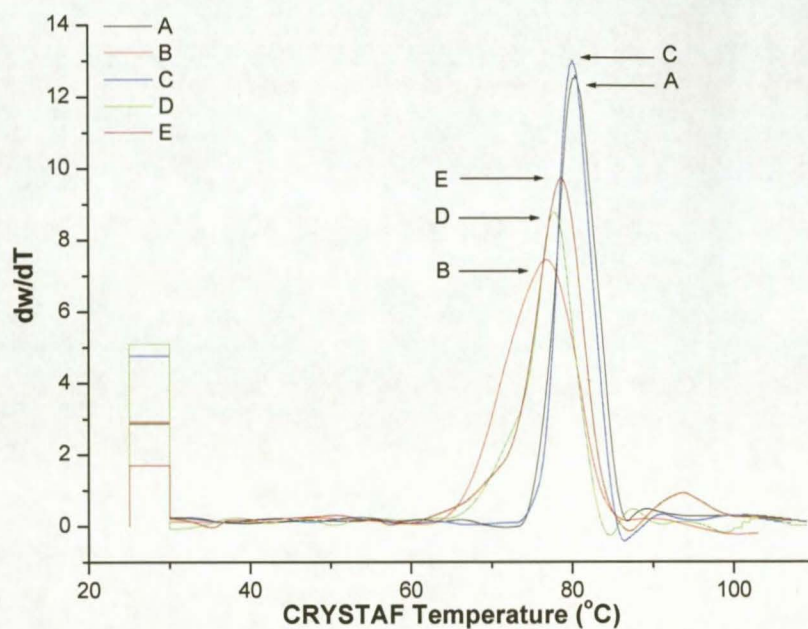


Figure 4.5 CRYSTAF traces for the unfractionated polymers (A-E).

4.1.4 DSC analysis

Figures 4.6 and 4.7 show the DSC crystallization exotherms and the DSC melting endotherms for the unfractionated polymers, respectively. As can be seen from Figure 4.6 the crystallization peak maxima temperatures (T_c) for the different polymers are about 123 °C. A single, sharp crystallization peak is observed for all the polymers. The melting peak maxima temperatures (T_m) of the unfractionated polymers, A through E, in Figure 4.7 are about 165 °C and also observed to be single peaks. Significant ‘tailing’ is seen to the left of each peak maximum, suggesting the melting of crystallizable material of different chain lengths. DSC data indicates very similar melting and crystallization behaviour for all the polymers, despite NMR showing clear differences between the three types of polymer, and CRYSTAF showing differences in polymers that, from NMR analyses, seem similar.

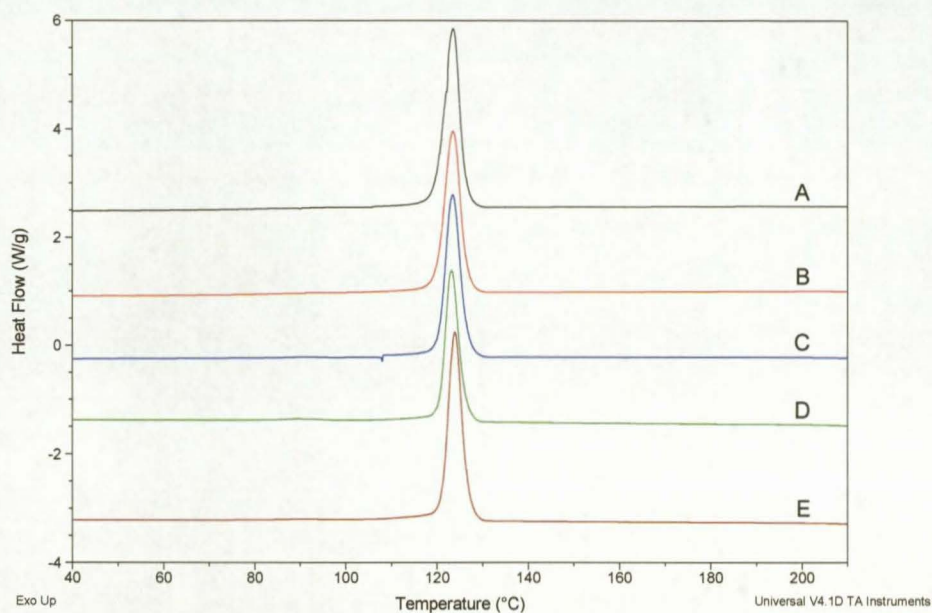


Figure 4.6 DSC crystallization exotherms of the unfractionated polymers (A-E).

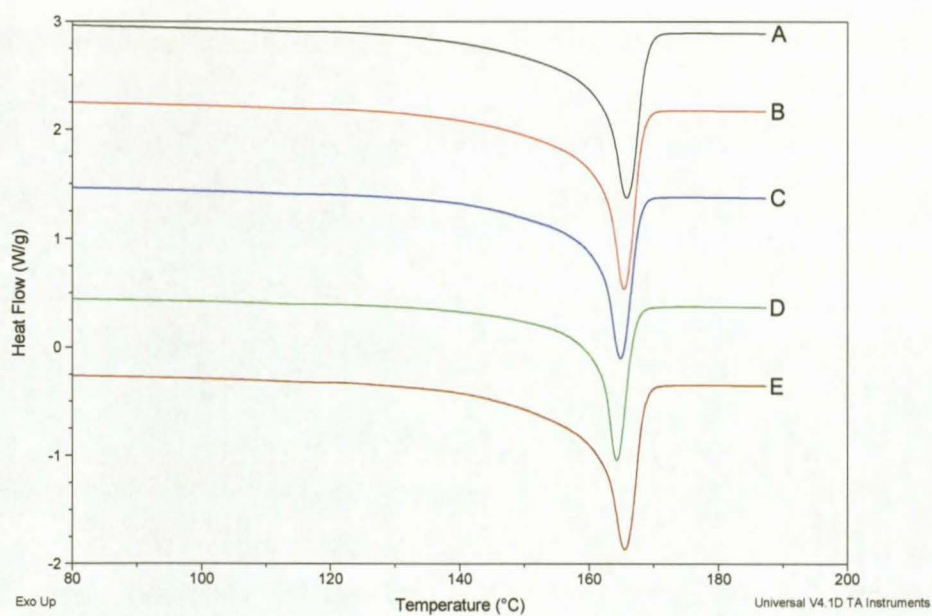


Figure 4.7 DSC melting endotherms of the unfractionated polymers (A-E).

4.1.5 HT-GPC analysis

Figure 4.8 shows the HT-GPC curves for the unfractionated polymers. There is a single, broad peak for each of the polymers at a retention time of about 1100 s. This broad distribution is expected for a polymer produced with a Ziegler-Natta catalyst, which is heterogeneous by nature.^[3, 4]

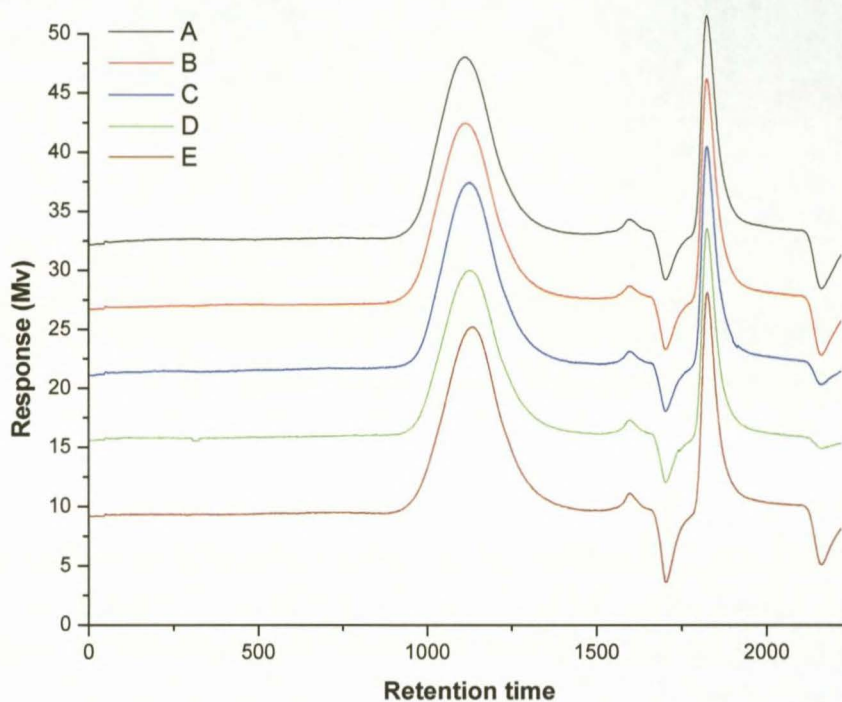


Figure 4.8 HT-GPC curves of the response vs. retention time (s) of the unfractionated polymers (A-E).

4.1.6 Characterization of the impact polypropylene copolymers: A summary

The results of the characterization experiments of the unfractionated polymers are summarized in Table 4.4.

Table 4.4 Summary of properties for the unfractionated polymers (A-E).

Polymer code	Ethylene in copolymer (mole%) ^a	T _m DSC (°C)	T _c DSC (°C)	T _c CRYSTAF (°C)	\overline{M}_n (g/mol)	\overline{M}_w (g/mol)	PD
A	17.5	165.8	123.6	80.5	98 400	556 800	5.7
B	16.2	165.4	123.6	76.9	94 000	585 100	6.2
C	31.8	164.9	123.5	80.2	85 900	453 800	5.3
D	28.5	164.2	123.2	77.9	73 400	458 100	6.2
E	18.0	165.5	123.9	78.7	73 900	482 300	6.5

^a calculated from ¹³C NMR (see Section 4.1.2.1).

As expected, polymers A and B have similar ethylene content (about 17 %) as well as polymers C and D (about 30 %). According to the supplier, polymer E should have the lowest ethylene content but it does not (ethylene content of 18 %). This is quite similar in ethylene content to that of polymers A and B although there are differences as shown by CRYSTAF. Similar melting and crystallization temperatures are shown for the polymers from DSC analysis. Polymers A and B, with the lowest ethylene content, have the highest weight average molecular weight (\overline{M}_w). Polymers C and D, with highest ethylene content, have the lowest \overline{M}_w . Polymer E with intermediate ethylene content has a \overline{M}_w in between that of polymers A and B and polymers C and D.

Differences between batches can also be identified at this early stage through consideration of the crystallization peak temperatures from CRYSTAF analyses. Polymers A and B have a 3 °C difference, while polymers C and D have a 2 °C difference in their respective maximum peak temperatures. It is also observed that the broadness of the crystallization curves from the CRYSTAF analyses were different for polymers with similar ethylene content. Differences are also seen in the polydispersities by HT-GPC of the polymers with similar ethylene content.

4.2 Fractionation of impact polypropylene copolymers

4.2.1 Introduction

Prep-TREF was used to fractionate the copolymers according to crystallizability. Prep-TREF is defined as a fractionation technique in which fractions are recovered for further analysis.^[5] This allows the characterization of the individual components of a complex mixture.

In this section the development of the optimal number of fractions collected will be highlighted. This will be followed by a detailed discussion of the impact polypropylene copolymers and their fractions obtained using prep-TREF. Fractions were analyzed by ¹³C NMR, DSC, CRYSTAF and HT-GPC.

4.2.2 Optimization of prep-TREF

Figure 4.9 shows the curves of the cumulative weight of the fractions recovered ($\Sigma W_i\%$) and the differential weight fraction to temperature ($W_i\%/\Delta T_i$) against elution temperature for polymer C. During the first prep-TREF experiments nine fractions were collected, at regular temperature intervals. In Figure 4.9 it can be seen that there is a peak at 120 °C for the $W_i\%/\Delta T_i$ against elution temperature curve. The curve of cumulative fraction weight ($\Sigma W_i\%$ against elution temperature) indicates that at elution temperatures between 50-100 °C, the weight of each fraction is relatively low.

The data of the fractionation process for polymer C (nine fractions) are summarized in Table 4.5, including elution temperature (T_e , °C), the weight of the fraction (W_i , g), the cumulative weight of the fractions recovered ($\Sigma W_i\%$) and the differential weight fraction to temperature ($W_i\%/\Delta T_i$). The major weight fractions are the 25 °C fraction, ($W_i\% = 19.31\%$), and the 120 °C fraction, ($W_i\% = 53.99\%$). From this data it was evident that the 120 °C fraction could be split into more fractions. It was decided to increase the number of fractions taken to twelve. Instead of taking only 3 fractions from 100-140 °C,

five fractions would now be collected. A final fraction at 150 °C was also collected in order to ensure that most of the polymer is collected. Although only results for polymer C are shown in Figure 4.9 and results for polymer D are shown in Figure 4.10, it should be pointed out that similar curves for all the other polymers were obtained. These are given in Appendix A.

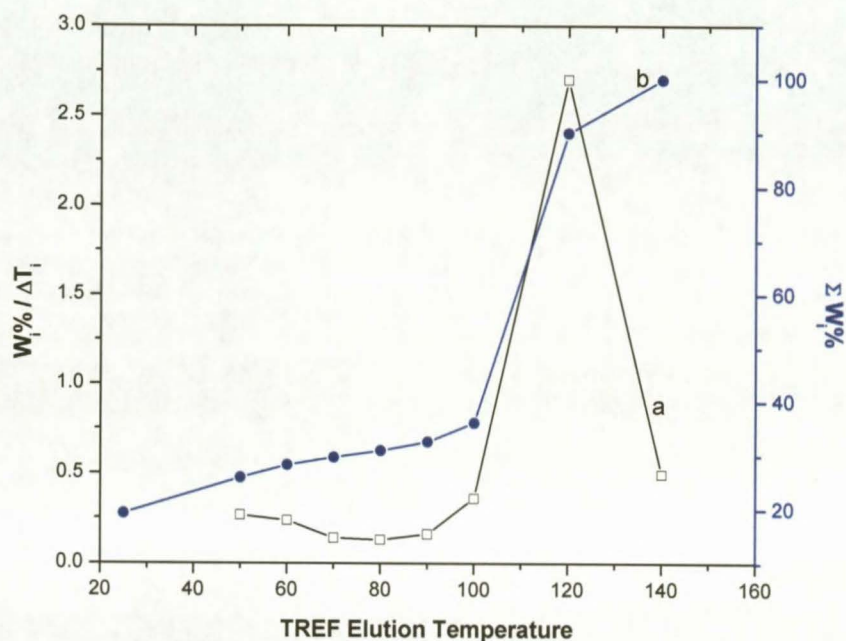


Figure 4.9 The curves of TREF for polymer C (9 fractions). The weight of the fractions as a function of the elution temperature (°C), (a) the differential weight fraction to temperature, $W_i\% / \Delta T_i$, (b) accumulative weight fraction, $\Sigma W_i\%$.

Table 4.5 Fractionation data of polymer C (9 fractions).

Fraction no.	T_e (°C)	W_i (g)	W_i (%)	ΣW_i (%)	$W_i/\Delta T$
1	25	0.600	19.31	19.31	n/a
2	50	0.206	6.64	25.94	0.27
3	60	0.073	2.35	28.30	0.24
4	70	0.043	1.39	29.68	0.14
5	80	0.040	1.29	30.97	0.13
6	90	0.050	1.60	32.57	0.16
7	100	0.112	3.59	36.16	0.36
8	120	1.679	53.99	90.16	2.70
9	140	0.306	9.84	100	0.49

In Figure 4.10 the curves of the cumulative weight of the fractions recovered and the differential weight fraction to temperature against elution temperature for polymer D are shown. From Figure 4.10, curve (a), it is clearly visible that the peak has now shifted to 110 °C. In Figure 4.10, curve (b), low mass for each fraction between 50-100 °C is also seen (similar to results in Figure 4.9, curve (b)).

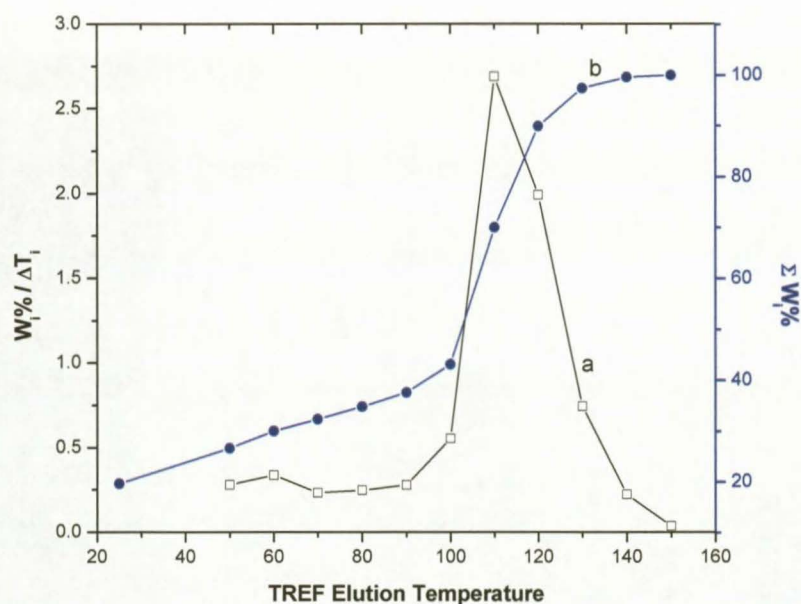


Figure 4.10 The curves of TREF for polymer D (12 fractions). The weight of the fractions as a function of the elution temperature (°C), (a) the differential weight fraction to temperature, $W_i\%/\Delta T_i$, (b) accumulative weight fraction, $\Sigma W_i\%$.

Table 4.6 shows the data obtained for the fractionation of polymer D (twelve fractions). It is now possible to identify three major weight fractions, namely the 25 °C ($W_i\%$ = 19.65 %), 110 °C ($W_i\%$ = 26.89 %), and 120 °C ($W_i\%$ = 19.92 %) fractions.

At this point, I thought there might still be material, with different degrees of crystallizability, co-eluting between temperatures of 100 and 110 °C and between temperatures between 110 and 120 °C. It was then decided to decrease the elution temperature interval from 10 °C to 5 °C in these temperature regions. Sixteen fractions, as opposed to twelve fractions, were collected. Better separation between materials with different crystallizability was thus achieved. This is illustrated in Figure 4.11.

Table 4.6 Fractionation data of polymer D (12 fractions).

Fraction no.	T_c (°C)	W_i (g)	W_i (%)	ΣW_i (%)	$W_i/\Delta T$
1	25	0.657	19.65	19.65	n/a
2	50	0.235	7.02	26.67	0.28
3	60	0.113	3.38	30.05	0.34
4	70	0.078	2.32	32.37	0.23
5	80	0.083	2.47	34.84	0.25
6	90	0.093	2.79	37.63	0.28
7	100	0.185	5.53	43.16	0.55
8	110	0.898	26.89	70.05	2.69
9	120	0.666	19.92	89.97	1.99
10	130	0.249	7.46	97.43	0.75
11	140	0.074	2.22	99.65	0.22
12	150	0.012	0.35	100	0.04

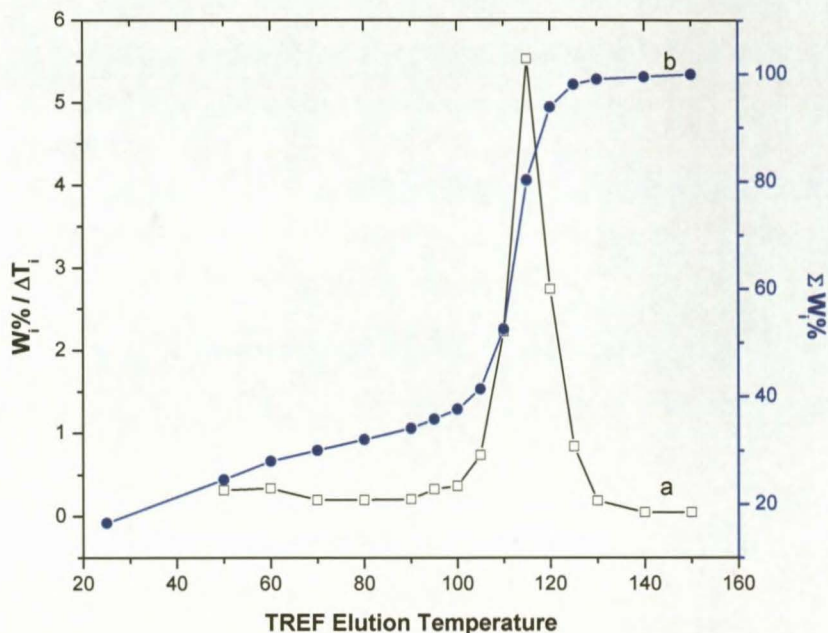


Figure 4.11 The curves of TREF for polymer D (16 fractions). The weight of the fractions as a function of the elution temperature (°C), (a) the differential weight fraction to temperature, $W_i\% / \Delta T_i$, (b) accumulative weight fraction, $\Sigma W_i\%$.

From Figure 4.11, curve (a), the peak is now at 115 °C (as opposed to 120 °C for nine fractions and 110 °C for twelve fractions). In table 4.7 (Section 4.2.3) the fractionation data for polymer D (sixteen fractions) together with the data for the other four impact polypropylenes. Now, four major fractions can be identified for polymer D, namely the 25 °C ($W_i\% = 16.48\%$), 110 °C ($W_i\% = 11.14\%$), 115 °C ($W_i\% = 27.65\%$), and 120 °C ($W_i\% = 13.69\%$) fractions.

Prep-TREF fractionation of the copolymers thus involved collecting sixteen fractions of each polymer for off-line analyses. It is important to point out that in order to fully characterize the fractions, only fractions where enough material was collected in order to carry out all of the different analysis techniques, were chosen. Most of the techniques used required very little sample for analysis, but ^{13}C NMR is a relatively sensitive technique that required about 60 mg of sample. Therefore, seven samples were chosen

for full analysis. These seven fractions constitute the bulk of the copolymer, and as such give rise to the properties of the copolymer.

4.2.3 Prep-TREF results of the five copolymers

Figure 4.12 shows the curves of the weight per fraction, W_i (g), as a function of the elution temperature ($^{\circ}\text{C}$), for all five impact polypropylene copolymers. As mentioned in Section 4.2.2, sixteen fractions were collected per prep-TREF elution for these five copolymers. A peak at 115 $^{\circ}\text{C}$ is seen for the five copolymers. The seven fractions chosen for full analysis were as follows: the 25-, 50-, 105-, 110-, 115-, 120- and 125 $^{\circ}\text{C}$ fractions.

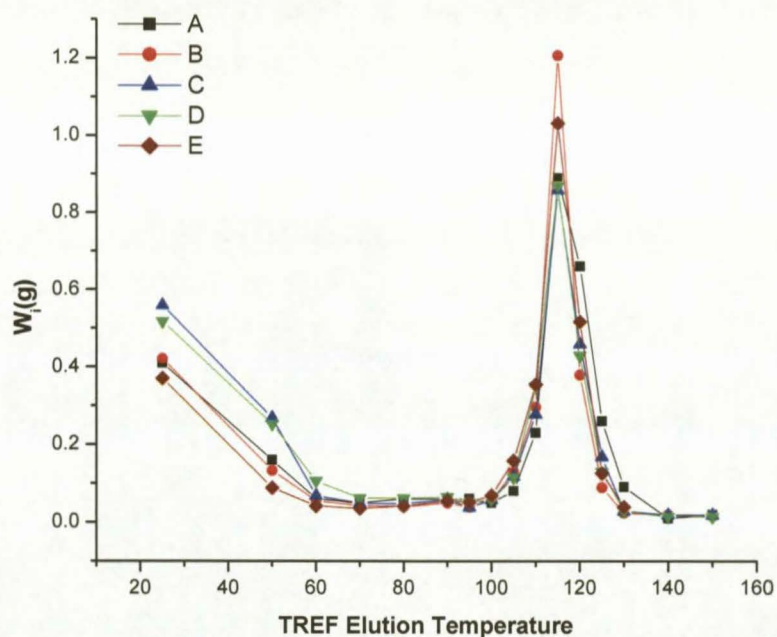


Figure 4.12 The curves of TREF for all five polymers. The weight per fraction, W_i (g), as a function of the elution temperature, ($^{\circ}\text{C}$).

The data of the fractionation process seen in Figure 4.12 for the copolymers will be discussed in detail in Section 4.4.3. The different ethylene content copolymers will be

compared and discussed. The data of the fractionation process for the five copolymers are included in Table 4.7.

Table 4.7 Fractionation data for the five copolymers.

Polymer	Fraction no.	T_c (°C)	W_i (g)	W_i (%)	ΣW_i (%)	$W_i\%/\Delta T$
A	1	25	0.415	13.21	13.21	n/a
	2	50	0.158	5.03	18.24	0.20
	3	60	0.055	1.75	19.99	0.18
	4	70	0.050	1.60	21.60	0.16
	5	80	0.056	1.78	23.38	0.18
	6	90	0.061	1.95	25.33	0.19
	7	95	0.056	1.77	27.10	0.35
	8	100	0.048	1.53	28.63	0.31
	9	105	0.081	2.57	31.20	0.51
	10	110	0.230	7.33	38.54	1.47
	11	115	0.892	28.40	66.94	5.68
	12	120	0.656	20.90	87.84	4.18
	13	125	0.265	8.44	96.28	1.69
	14	130	0.088	2.82	99.09	0.56
	15	140	0.013	0.41	99.50	0.04
	16	150	0.016	0.50	100	0.05
B	1	25	0.421	14.00	14.00	n/a
	2	50	0.134	4.44	18.44	0.18
	3	60	0.056	1.86	20.30	0.19
	4	70	0.043	1.44	21.74	0.14
	5	80	0.041	1.37	23.11	0.14
	6	90	0.050	1.68	24.79	0.17
	7	95	0.040	1.32	26.11	0.26
	8	100	0.058	1.93	28.03	0.39
	9	105	0.130	4.32	32.35	0.86
	10	110	0.297	9.88	42.23	1.98
	11	115	1.206	40.10	82.33	8.02
	12	120	0.380	12.63	94.96	2.53
	13	125	0.090	3.01	97.97	0.60
	14	130	0.025	0.82	98.79	0.16
	15	140	0.020	0.67	99.46	0.07
	16	150	0.016	0.54	100	0.05

Table 4.7 (continued). Fractionation data for the five copolymers.

Polymer	Fraction no.	T_e (°C)	W_i (g)	W_i (%)	ΣW_i (%)	$W_i\%/\Delta T$
C	1	25	0.562	18.01	18.01	n/a
	2	50	0.266	8.54	26.55	0.34
	3	60	0.071	2.27	28.82	0.23
	4	70	0.048	1.54	30.35	0.15
	5	80	0.050	1.61	31.96	0.16
	6	90	0.058	1.87	33.83	0.19
	7	95	0.043	1.39	35.23	0.28
	8	100	0.061	1.97	37.19	0.39
	9	105	0.122	3.92	41.11	0.78
	10	110	0.278	8.93	50.04	1.79
	11	115	0.860	27.58	77.62	5.52
	12	120	0.459	14.72	92.34	2.94
	13	125	0.167	5.36	97.70	1.07
	14	130	0.031	0.99	98.69	0.20
	15	140	0.022	0.71	99.40	0.07
	16	150	0.019	0.60	100	0.06
D	1	25	0.519	16.48	16.48	n/a
	2	50	0.254	8.08	24.56	0.32
	3	60	0.108	3.43	27.99	0.34
	4	70	0.064	2.02	30.01	0.20
	5	80	0.064	2.03	32.04	0.20
	6	90	0.067	2.12	34.15	0.21
	7	95	0.052	1.66	35.82	0.33
	8	100	0.059	1.86	37.68	0.37
	9	105	0.117	3.71	41.38	0.74
	10	110	0.351	11.14	52.52	2.23
	11	115	0.871	27.65	80.17	5.53
	12	120	0.431	13.69	93.86	2.74
	13	125	0.132	4.19	98.06	0.84
	14	130	0.030	0.96	99.02	0.19
	15	140	0.016	0.49	99.51	0.05
	16	150	0.016	0.49	100	0.05

Table 4.7 (continued). Fractionation data for the five copolymers.

Polymer	Fraction no.	T_c (°C)	W_i (g)	W_i (%)	ΣW_i (%)	$W_i\%/\Delta T$
E	1	25	0.371	12.29	12.29	n/a
	2	50	0.089	2.96	15.25	0.12
	3	60	0.042	1.41	16.66	0.14
	4	70	0.036	1.21	17.86	0.12
	5	80	0.042	1.38	19.24	0.14
	6	90	0.056	1.86	21.10	0.19
	7	95	0.052	1.72	22.82	0.34
	8	100	0.070	2.32	25.13	0.46
	9	105	0.159	5.26	30.39	1.05
	10	110	0.355	11.75	42.15	2.35
	11	115	1.031	34.18	76.33	6.84
	12	120	0.517	17.15	93.48	3.43
	13	125	0.126	4.17	97.65	0.83
	14	130	0.040	1.32	98.97	0.26
	15	140	0.015	0.50	99.47	0.05
	16	150	0.016	0.53	100	0.05

There is also a difference between the batches. The weight of the fraction eluted at the peak temperature, 115 °C, for copolymers A and B differ significantly. This difference, together with other differences, will be discussed later in this chapter when the batches are compared to each other.

For now, though, the preparative fractionation of only one polymer, namely polymer C, and the characterization of its fractions will be discussed in detail while the characterization data for polymers A, B, D and E are given in Appendix B. This is to avoid repetition.

4.3 Results and discussion of fractionated polymer C

4.3.1 Introduction

Figure 4.13 shows the curves of the cumulative fraction weight and the weight fraction per temperature interval plotted against elution temperature for polymer C. In the curve

of the weight fraction per temperature interval ($W_i\%/\Delta T_i$), the peak lies at 115 °C. From the curve of cumulative fraction weight ($\Sigma W_i\%$), in Figure 4.13, as well as from Table 4.7, it can be seen that the seven main fractions identified constitutes about 85 % of the copolymer. The seven fractions chosen are, once again, the 25 °C, 50 °C, 105 °C, 110 °C, 115 °C, 120 °C and 125 °C fractions. This result is similar for the other four copolymers (see Table 4.7).

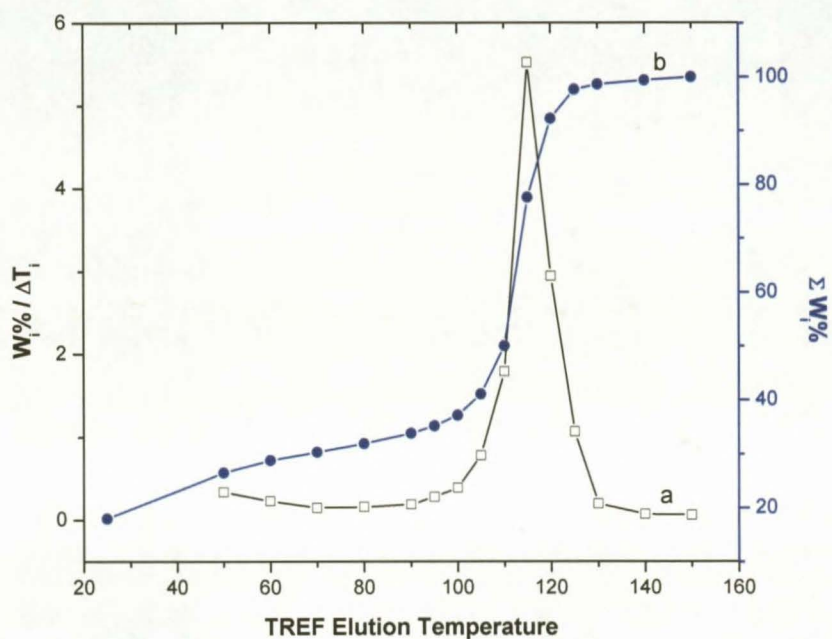


Figure 4.13 The curves of TREF for polymer C. The weight of the fractions as a function of the elution temperature (°C), (a) $W_i\%/\Delta T_i$, (b) $\Sigma W_i\%$

4.3.2 CRYSTAF results

Figure 4.14 shows the curves of the crystallization temperature distribution for the unfractionated, and fractions, of polymer C. In CRYSTAF, the concentration of the corresponding fraction in solution is determined as a function of temperature. The Y-axis is offset for the purpose of clarity.

The curve for the 25 °C fraction, as well as the 50 °C fraction, has no solution crystallization peak. This indicates clearly that these two fractions are composed of only non-crystallizable material. The curves for other five fractions, 105-125 °C, all have similar crystallization temperatures of about 80 °C. The five high elution temperature fractions have similar or narrower distributions than that of the unfractionated polymer. This seems to indicate that the fractionation process was successful.^[6]

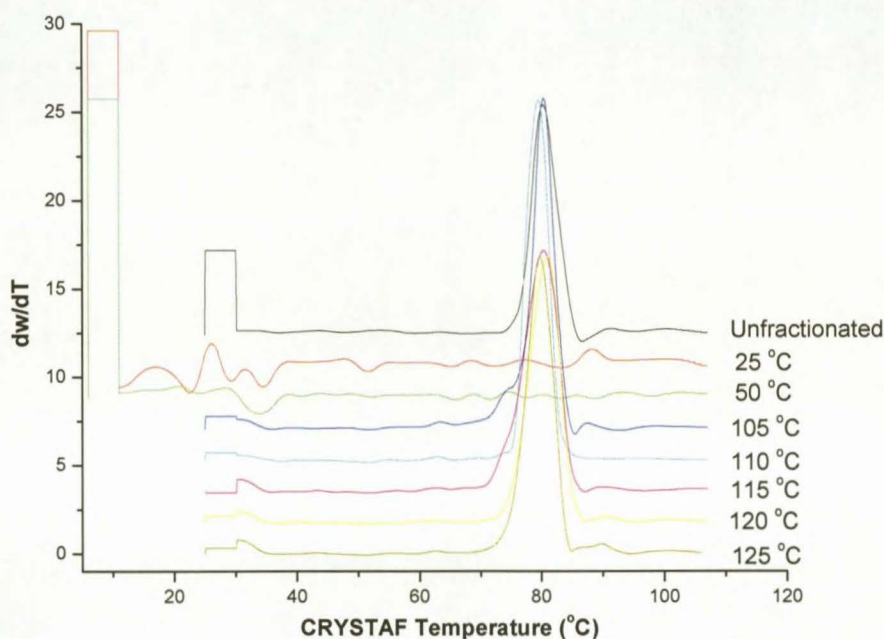


Figure 4.14 The concentration in solution, determined by CRYSTAF, for the unfractionated, and fractions, of polymer C as a function of temperature.

In Figure 4.15 the ‘undercooling’ effect is illustrated between CRYSTAF and prep-TREF for polymer C. The curves shown are (a) the crystallization temperature distribution for the unfractionated polymer C and (b) the curve of the differential weight fraction to temperature, $W_i\%/\Delta T_i$.

From Figure 4.15, curve (a), it can be seen that the crystallization curve obtained from CRYSTAF has a peak maximum at 80.2 °C. In curve (b), from prep-TREF, a peak maximum is observed at 115 °C. This higher value for the prep-TREF peak is attributed

to the 'undercooling' effect, as described by Monrabel.^[7] Monrabel states that both CRYSTAF and TREF share the same principles and separates according to crystallizability. A slow cooling process is involved in both these techniques. Prep-TREF involves two complete temperature cycles, namely, crystallization and elution, while in CRYSTAF the analysis is done in a single step, namely the crystallization step. It is this extra elution step involved with prep-TREF, which does not occur in CRYSTAF that is responsible for the temperature difference. However, a solvent effect cannot be ruled out since trichlorobenzene is used in CRYSTAF and xylene in Prep-TREF.

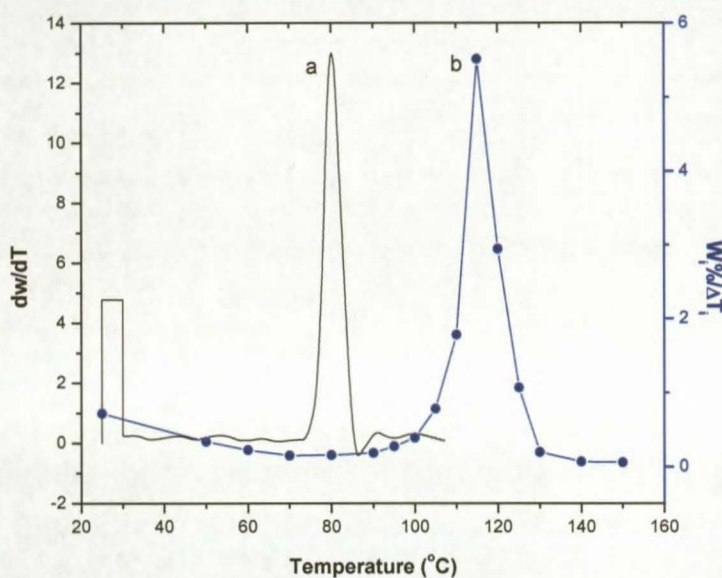


Figure 4.15 The 'undercooling' effect as demonstrated by comparing (a) the CRYSTAF crystallization temperature distribution curve and (b) the prep-TREF curve of the differential weight fraction to temperature, $W_i\%/\Delta T_i$, as a function of temperature.

4.3.3 DSC results

Figure 4.16 shows the DSC melting, (T_m), and crystallization, (T_c), peak maxima temperatures for most of the Prep-TREF fractions of polymer C. The two fractions eluted at 25 °C and 50 °C, are not included as they are non-crystalline. The melting and crystallization values of the fractions, other than the seven main fractions identified, are included purely to illustrate a trend.

Curve (a) in Figure 4.16 represents the DSC melting peak maxima (T_m); curve (b) represents the DSC crystallization peak maxima (T_c). Curve (c) represents the case where temperature values for melting or crystallization equals the TREF elution temperatures.

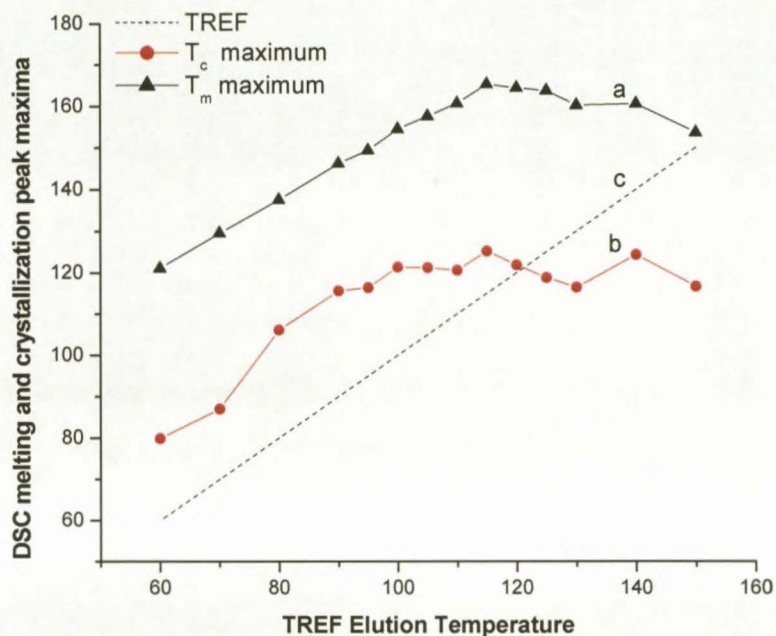


Figure 4.16 The DSC melting and crystallization peak maxima as a function of the TREF elution temperature for the fractions from polymer C, (a) DSC melting peak maxima, T_m , (b) DSC crystallization peak maxima, T_c , (c) represents the situation where T_m or $T_c =$ TREF elution temperature.

Figure 4.16 shows that the DSC melting peak maximum temperatures for fractions eluted between 60-115 °C increases almost linearly with an increase in TREF elution temperature (curve (a)). The maximum melting temperature ($T_m = 165.26$ °C), is for the fraction eluted at 115 °C, which is also the biggest fraction ($W_i\%/\Delta T_i$) (Figure 4.13). The DSC melting temperature maxima of the fractions eluted at temperatures higher than 115 °C decreases. A similar decrease is also seen in the corresponding DSC crystallization peak maxima (Figure 4.16, curve (b)).

In Figure 4.16, curve (b), a general increase in the DSC crystallization peak maxima for the 60-115 °C fractions is observed. Thereafter, slight decreases in the DSC crystallization peak maxima are seen. The DSC maximum crystallization temperature, at $T_c = 125.12$ °C, is for the 115 °C fraction.

Figures 4.17 and 4.18 show the DSC melting (endothermic) and crystallization (exothermic) curves for the prep-TREF fractions of polymer C. The two low elution temperature fractions, at 25 °C and 50 °C, have no melting peaks. This is in agreement with the CRYSTAF results (Section 4.3.2), that these two fractions are indeed composed of non-crystallizable material. The five higher elution temperature fractions all have melting peaks at about 160 °C. These melting peak temperatures are close to the melting peak temperature expected for i-PP homopolymer (168-172 °C^[8]). There might be many reasons why the melting peaks observed here are lower than that of i-PP. One explanation is that the isotacticity index of the polymer might be low due to catalyst effects.

Some differences are also observed between these fractions in Figure 4.17. The 105 °C fraction has a shoulder at 163 °C while the main melting peak temperature value is lower than for the other fractions. A small peak is visible at about 150 °C on the melting curves for the fractions eluted at 115 °C, 120 °C and 125 °C. This might be due to a small amount of propylene-rich copolymer being present. In relation to the main peaks at around 160 °C, these smaller peaks are smaller, yet significant.

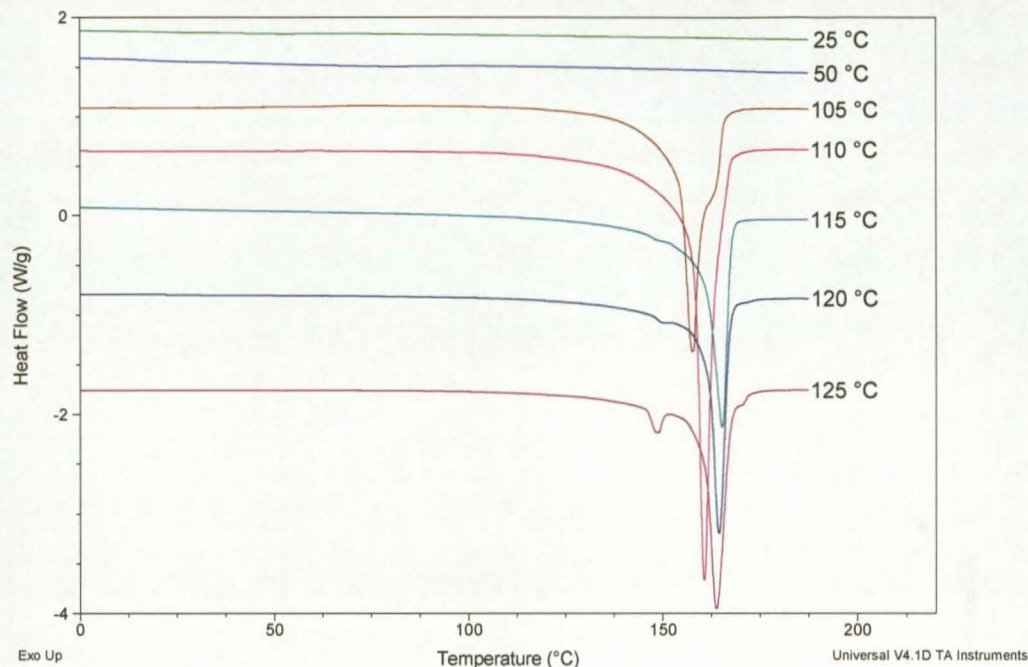


Figure 4.17 DSC melting curves (2nd heating cycle) of the fractions obtained from polymer C.

In Figure 4.18 the two lower elution temperature fractions show no crystallization peaks. This is what is expected for non-crystallizable material. The other five fractions have slightly different crystallization peak temperatures. The crystallization peaks of the three fractions eluted at 115 °C, 120 °C and 125 °C differ by about 7 °C. As shown in Figure 4.16, there is a decrease in the DSC crystallization peak temperatures after the fraction at 115 °C. Interestingly, the appearance of a secondary melting peak in the heating cycle of some of these materials (Figure 4.17) is not reflected in the crystallization behaviour of these materials.

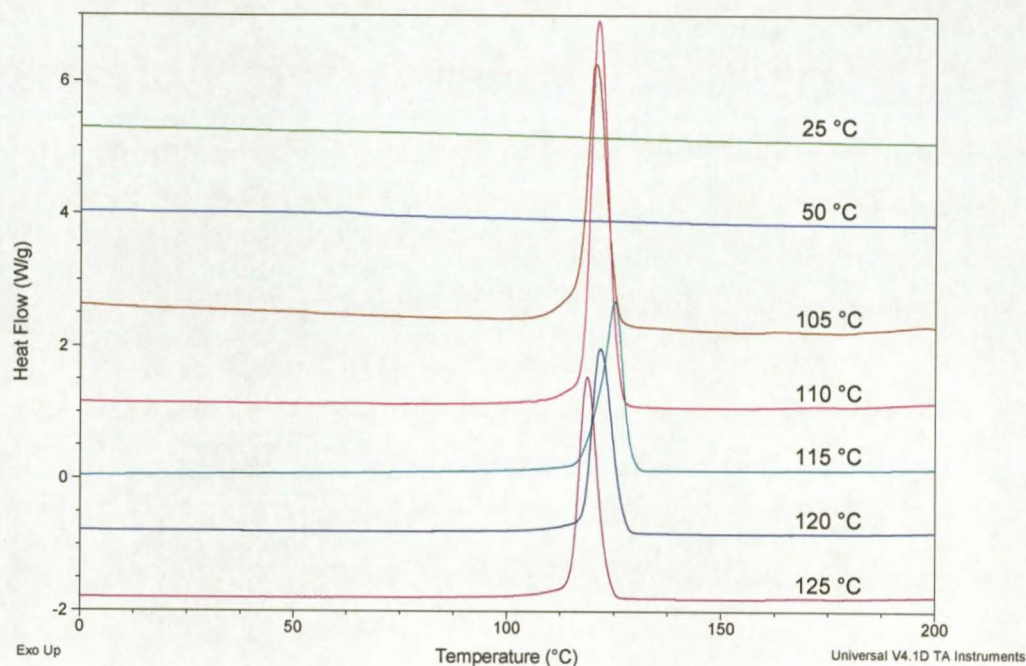


Figure 4.18 DSC crystallization curves of the fractions from polymer C.

4.3.4 HT-GPC results

Figure 4.19 shows the HT-GPC results for the seven fractions from polymer C as recovered from the prep-TREF fractionation. In Figure 4.19 a single, relatively narrow peak is seen for each of the fractions between 1 000 and 1 500 seconds. The sharp, narrow peak seen in each trace between 1 800 and 1 950 seconds is the BHT peak used as a flow rate marker.

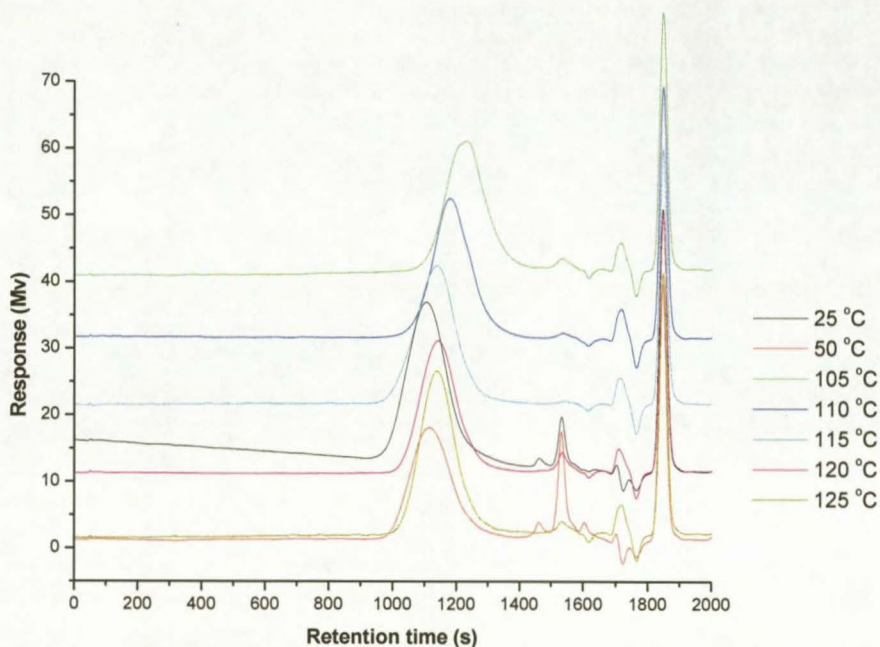


Figure 4.19 HT-GPC results for the fractions from polymer C.

Figures 4.20 and 4.21 illustrates the average molecular weights, weight average (\overline{M}_w) as well as number average (\overline{M}_n), of the fractions from polymer C against the Prep-TREF elution temperature, respectively. The two lower temperature fractions, 25 °C and 50 °C, have the highest average molecular weights of the seven fractions. The 25 °C fraction has $\overline{M}_w = 400\,400$ and $\overline{M}_n = 134\,200$ while the 50 °C fraction has $\overline{M}_w = 326\,000$ and $\overline{M}_n = 120\,000$. There is a big decrease in molecular weight to the 105 °C fraction, with $\overline{M}_w = 66\,100$ and $\overline{M}_n = 27\,700$. From the 105 °C fraction there is an almost linear increase in molecular weight up to the 115 °C fraction (which is the peak fraction in the Prep-TREF elution, see Figure 4.13), with $\overline{M}_w = 295\,600$ and $\overline{M}_n = 101\,500$. There is decrease in molecular weight for the final two fractions. The polydispersities, ($PD = \frac{\overline{M}_w}{\overline{M}_n}$), for the fractions are quite narrow, ranging between 2.4 to 3.0. These values for the PD of the fractions are all below that of the unfractionated polymer C ($PD = 5.3$).

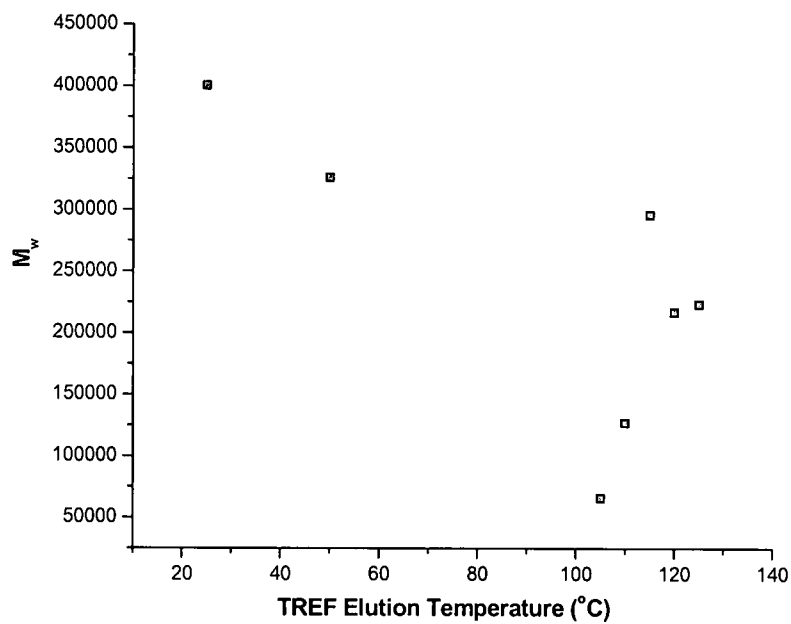


Figure 4.20 The weight average molecular weight, of the fractions from polymer C as a function of elution temperature.

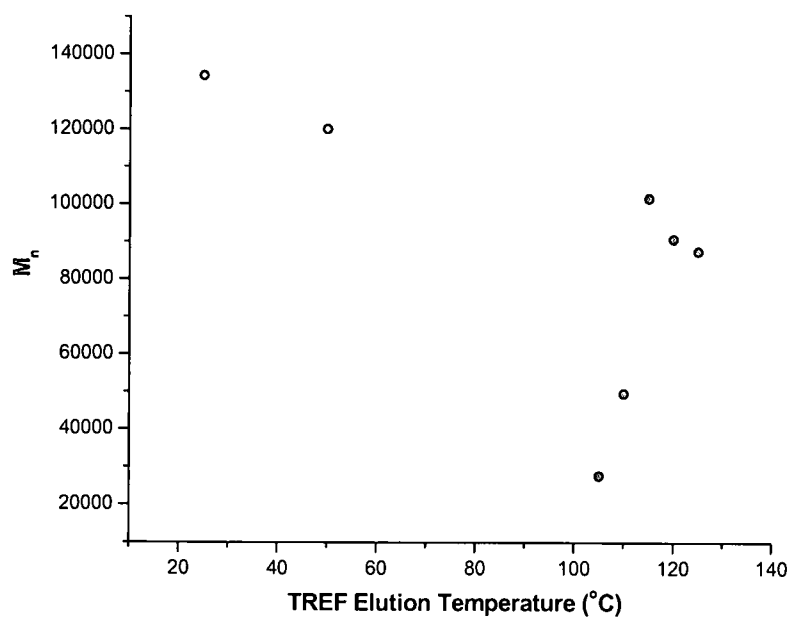


Figure 4.21 The number average molecular weight of the fractions from polymer C as a function of elution temperature.

The non-crystalline fractions is therefore composed of high molecular weight material, while the crystalline fractions appear to increase in molecular weight as the elution temperature increases. In conjunction with the composition analyses (see Section 4.3.5) the molecular weight data will complete the picture of the molecular make-up of the crystalline fractions

4.3.5 ^{13}C NMR results

Figure 4.22 shows the ^{13}C NMR spectra of the fractions for polymer C. It is known from CRYSTAF and DSC analysis that the first two fractions, namely, the 25 °C and 50 °C fractions, are composed of non-crystalline material. This includes a major ethylene propylene rubber (EPR) component as well as a minor atactic PP component. The ethylene content of the 25 °C and 50 °C fractions are 58.0 and 55.6 mole %, respectively, as calculated from ^{13}C NMR. From Figure 4.3 (The ^{13}C NMR of unfractionated polymer C) the numerous smaller peaks were attributed to different configurational distributions of the ethylene and propylene repeat units in the copolymer structures as presented in Figure 4.4. The higher temperature fractions, 105 – 125 °C, are composed of mainly highly crystalline polypropylene homopolymer with a small amount of ethylene interspersed in some of the fractions. This is illustrated in Figure 4.23, which highlights the methine carbon area of the 105 °C fraction from polymer C. The peak associated with multiple $-\text{CH}_2-$ units or blocks thereof is seen at about 30.6 ppm (arrow in Figure 4.23). These amounts of ethylene present ranged from about 0.2-2.5 %.

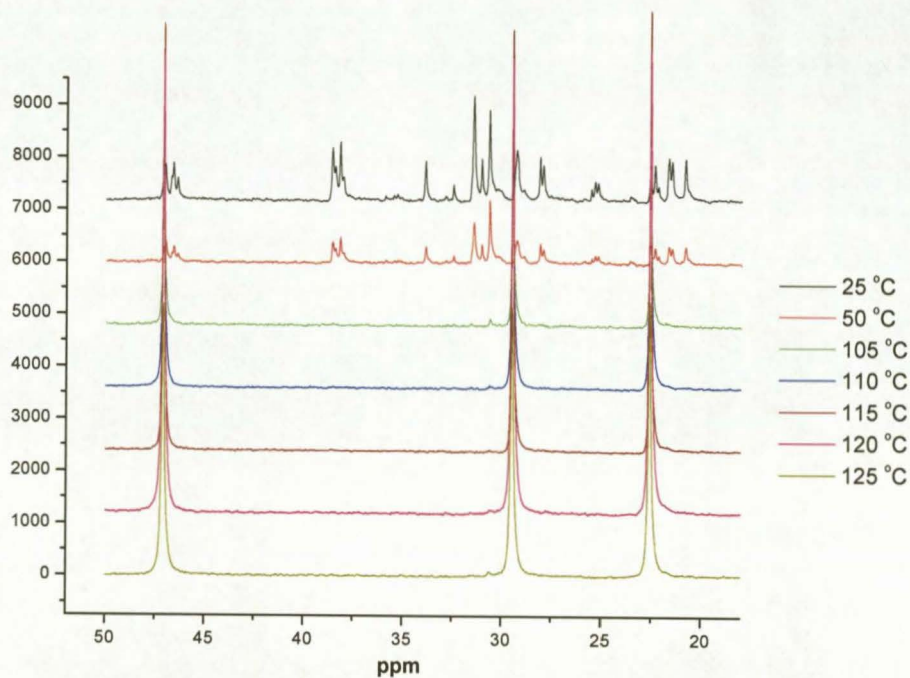


Figure 4.22 The ^{13}C NMR spectra of the fractions from polymer C.

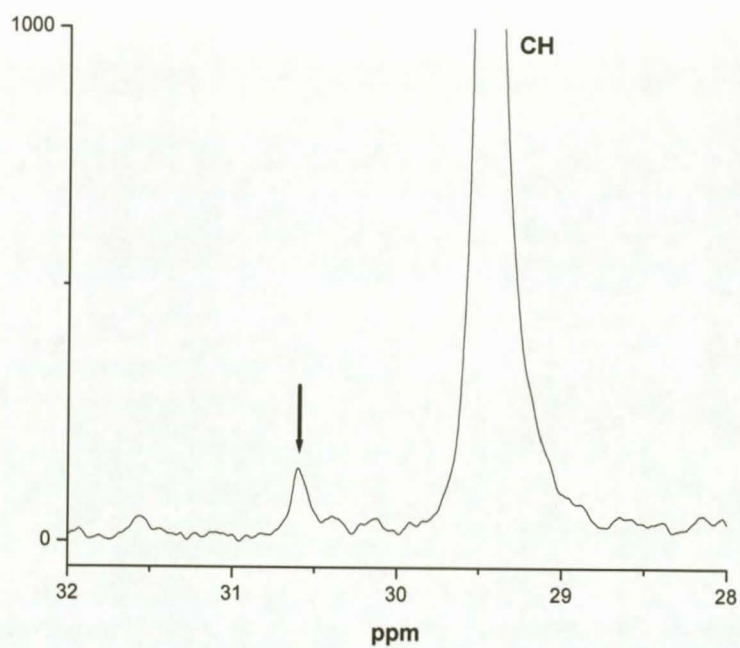


Figure 4.23. The ^{13}C NMR spectrum of the 105 °C fraction from polymer C, showing the methine area.

If one examines the ^{13}C NMR spectra of the fractions eluted at 105 °C and above, these materials appear to be chemically similar, with small differences in ethylene content. Taken in conjunction with the molecular weight data, it appears as if separation on crystallizability is not solely dependent on molecular make-up, but that chain length does play a role.

4.3.6 Summary of characterization results for the fractions from polymer C

Table 4.8 summarizes the characterization results for the main fractions from polymer C.

Table 4.8 Summary of properties for the fractions from polymer C.

Fraction no.	T_e (°C)	Ethylene content (mole%)	T_m DSC (°C)	T_c DSC (°C)	T_c CRYSTAF (°C)	M_n (g/mol)	M_w (g/mol)	PD
1	25	58.0	- ^a	- ^a	- ^a	130 100	417 100	3.2
2	50	55.6	- ^a	- ^a	- ^a	113 800	330 600	2.9
9	105	2.3	157.6	121.2	80.2	26 700	63 600	2.4
10	110	0.6	160.7	120.5	79.4	47 900	127 200	2.7
11	115	0.2	165.3	125.1	80.2	99 000	308 000	3.1
12	120	0.4	149.9/164.4	121.8	80.9	88 100	222 200	2.5
13	125	0.8	148.6/163.8	118.7	79.6	85 000	229 100	2.7

^a non-crystallizable material, no values.

It can be seen from Table 4.8 that as the ethylene content of the fractions decreases, there is a corresponding increase in the melting peak temperatures (for the 105 °C, 110 °C and 115 °C fractions). Results given in Section 4.3.3 show a decrease in the melting peak temperatures for the fractions eluted at 120 °C and 125 °C. This could be attributed to the increase in ethylene content seen for these two fractions, or the decrease in molecular weight compared to the foregoing fractions.

Table 4.9 summarizes the different components of the fractions from polymer C.

Table 4.9 Components of the fractions from polymer C.

Fraction no.	T_e (°C)	W_i %	Component		
			Major	Minor	Trace
1	25	18.01	EPR	atactic PP	
2	50	8.54	EPR	atactic PP	
9	105	3.92	PP ^a		PE ^c
10	110	8.93	PP ^a		PE ^c
11	115	27.58	PP ^a		PE ^c
12	120	14.72	PP ^a	PE ^b	
13	125	5.36	PP ^a	PE ^b	

^a highly isotactic PP^b linear PE^c ethylene-rich material

4.4 Comparing batch consistency and copolymers with differing ethylene content

4.4.1 Introduction

In the first section a closer look will be taken at the differences present between the polymers with similar ethylene content, but which come from different batches. Therefore, polymers A and B as well as polymers C and D will be compared to each other, respectively. The difference in weights used per Prep-TREF elution does not exceed 0.7 % between the two polymers analyzed. Differences, as well as similarities, will be pointed out. Then, in the second section, the five copolymers will be compared to each other.

4.4.2 Differences between polymer batches

4.4.2.1 Polymers A and B

Table 4.10 highlights the properties for the fractions of polymers A and B. From previous analyses it is known that the 25 °C and 50 °C fractions consist primarily of ethylene-propylene copolymers. Double melting peaks are observed for the three higher temperature fractions (no. 11, 12 and 13) of polymer A. A single melting peak is

observed for the three similar higher temperature fractions of polymer B. Higher \overline{M}_w for the 25 °C and 50 °C fractions (no. 1 and 2) for polymer A is also recorded. The polydispersities of both polymers are also lower than the PD of the corresponding unfractionated polymers (for polymer A, PD = 5.7 and for polymer B, PD = 6.2). Although no determination of ethylene content was done for the 25 °C fraction of Polymer B, the overall percentage of ethylene in the copolymer seems similar. This does not, however, take into consideration the differences in fraction weights that might exist. This will influence the distribution of ethylene in the copolymer, something which will be discussed in the next section.

Table 4.10 Summary of properties for the fractions of both polymers A and B (run 2).

Polymer	Fraction no.	T _c (°C)	Ethylene content (%)	T _m DSC (°C)	T _c DSC (°C)	T _c CRYSTAF (°C)	M _n (g/mol)	M _w (g/mol)	PD
A	1	25	57.4	-	-	-	151 700	555 400	3.7
	2	50	60.6	-	-	-	116 100	503 000	4.3
	9	105	- ^a	157.7	122.9	- ^a	31 400	86 500	2.8
	10	110	0.6	160.8	121.9	76.1	43 500	100 700	2.3
	11	115	0.4	148.2/163.7	119.2	80.2	120 600	309 000	2.6
	12	120	0.1	147.3/163.0	119.0	79.5	150 300	401 000	2.7
	13	125	1.6	148.4/163.2	119.4	79.5	84 600	199 000	2.4
B	1	25	- ^b	-	-	-	122 000	422 800	3.5
	2	50	61.8	-	-	-	117 700	389 500	3.3
	9	105	1.2	160.5	124.3	78.6	32 700	74 600	2.3
	10	110	0.4	160.9	119.3	79.7	46 600	117 100	2.5
	11	115	0.1	166.1	124.1	79.7	150 800	381 600	2.5
	12	120	0.6	164.7	122.1	79.6	115 700	287 300	2.5
	13	125	1.6	161	116.5	80	102 200	368 200	3.6

^a Insufficient sample of 105 °C fraction

^b No ¹³C NMR result for the 25 °C fraction

Table 4.11 compares the ethylene content for the fractions of both polymers A and B. No ¹³C NMR data is available for the 25 °C fraction of polymer B, but it is seen that the majority of ethylene is contained in the 25 °C and 50 °C fractions of polymer A (about 63

%, when calculated as a percentage of the total sample ethylene content). The higher temperature fractions all contain relatively small amounts of ethylene.

In order to get an idea of the distribution of ethylene, the percentage of ethylene in each fraction, based on the total amount of ethylene in the copolymer, was calculated. The seven fractions comprise 2.70 g or 90% of the total sample of polymer A and 2.66 g or 88.7% of sample of polymer B, respectively. The original ethylene content of the two materials were 17.5 and 16.2 mole% respectively. Based on the fact that the polymers comprise only ethylene and propylene, it is a fairly simple matter to calculate (a) the mass of ethylene in each fraction, and (b) the percentage of the total ethylene originally present. Results are presented in Table 4.11.

Table 4.11 Ethylene content comparisons for the fractions of both polymers A and B (run 2).

Polymer	Fraction no.	T _c (°C)	Ethylene content (mole%)	W _i (g)	W _i (Ethylene content)(g)	Fraction Ethylene content as % of total sample ethylene content ^a
A	1	25	57.4	0.415	0.1960	58.68
	2	50	60.6	0.158	0.0780	23.35
	9	105	- ^b	0.081		0.00
	10	110	0.6	0.230	0.0009	0.27
	11	115	0.4	0.892	0.0024	0.72
	12	120	0.1	0.656	0.0004	0.12
	13	125	1.6	0.265	0.0028	0.84
B	1	25	- ^c	0.421	-	-
	2	50	61.8	0.134	0.0695	22.94
	9	105	1.2	0.130	0.0010	0.33
	10	110	0.4	0.297	0.0079	2.62
	11	115	0.1	1.206	0.0008	0.26
	12	120	0.6	0.380	0.0015	0.50
	13	125	1.6	0.090	0.0010	0.33

^a Total sample ethylene content: Polymer A = 0.5285 g, Polymer B = 0.4852 g.

^b Insufficient sample of 105 °C fraction

^c No ¹³C NMR result for the 25 °C fraction

As the majority of the ethylene is in the soluble fractions, it becomes interesting to examine subtle differences in the crystalline fractions. This is illustrated in Figure 4.24.

Here it is shown that the fractions do contain slightly different amounts of ethylene. This is particularly evident in the 110 °C fractions.

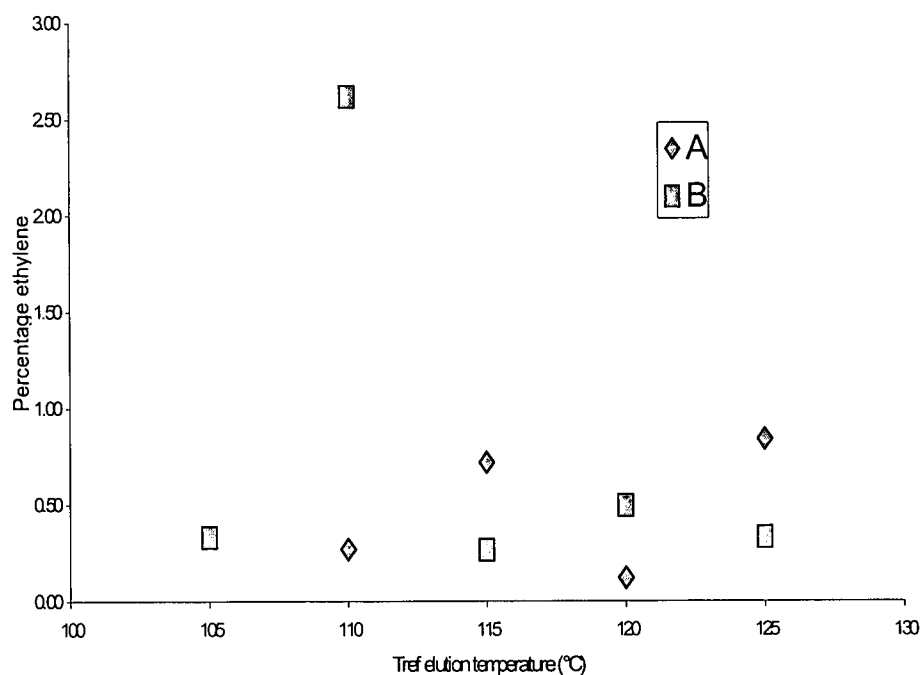


Figure 4.24. The ethylene content of the fractions of polymers A and B as a percentage of the total sample ethylene content vs. the elution temperature

When comparing the unfractionated polymers A and B, no major differences could be seen. Both polymers have similar DSC melting and crystallization peak temperatures, similar molecular weights and polydispersities. Differences are noted when the results of the fractions obtained through Prep-TREF are compared. Figure 4.25 shows the weight per fraction data from TREF for polymers A and B as a function of the elution temperature (°C). The seven main fractions identified earlier are plotted here. Similar weights (in gram) are collected per fraction for both polymers up to 110 °C. However, significant differences are seen in the weight per fraction collected for the 115 – 125 °C fractions.

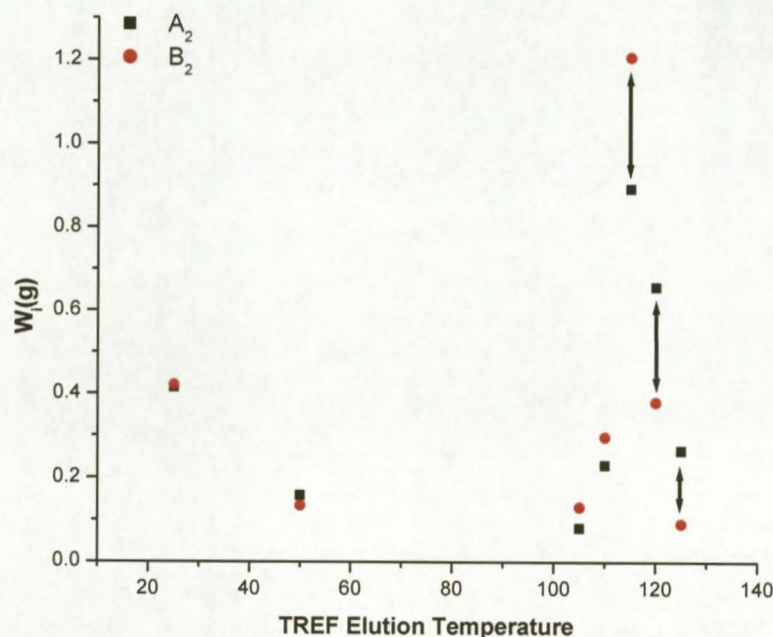


Figure 4.25 The data from TREF for polymers A and B (run 2). The weight per fraction, W_i (g), as a function of the elution temperature.

These differences can further be illustrated in Figure 4.26, which show the DSC exotherms, (T_c), and endotherms, (T_m), for the 115 °C fractions of both polymers A and B. A 5 °C difference is seen between the DSC crystallization peak temperatures for polymers A and B, with polymer B having the higher T_c . Also, differences are seen in the T_m peak temperatures. Polymer B has a higher T_m than polymer A. From ^{13}C NMR the ethylene content for the 115 °C fractions of both polymers A and B can be calculated (see Tables 4.10 and 4.11). The 115 °C fraction of polymer A contains more ethylene than 115 °C fraction of polymer B if the ethylene content of the fraction is calculated as a percentage of the total sample ethylene content. Polymer A has an additional melting peak at about 150 °C that polymer B does not have. This additional melting peak is thus attributed to an ethylene-containing copolymer species which is absent from polymer B. The heat of fusion for 100 % crystalline polypropylene is 209 J/g. From this it was calculated that the 115 °C fraction of polymer A has 32.5 % crystallinity as opposed to 54.9 % for the same fraction of polymer B. It can be concluded that the 115 °C fraction of polymer B has more crystalline polypropylene homopolymer than polymer A.

Consequently, less material is collected for the subsequent two fractions of polymer B, namely the 120 °C and 125 °C fractions.

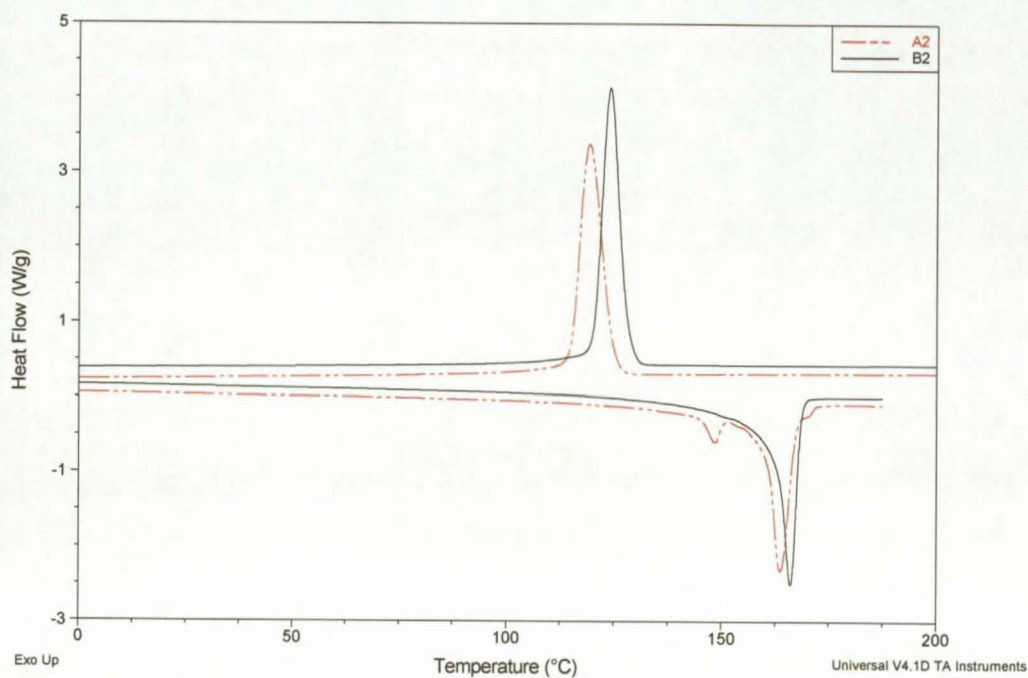


Figure 4.26 The DSC exotherms, (T_c), and endotherms, (T_m), for the 115 °C fractions of both polymers, A and B (run 2)

Figure 4.27 clearly illustrates the differences in \overline{M}_w of the fractions between polymers A and B. Major differences are seen between all the different temperature fractions (in excess of 100 000 g/mol), except between the 105 °C and 110 °C fractions. The biggest difference in \overline{M}_w is observed in the 125 °C fractions, where a difference of about 170 000 g/mol is seen.

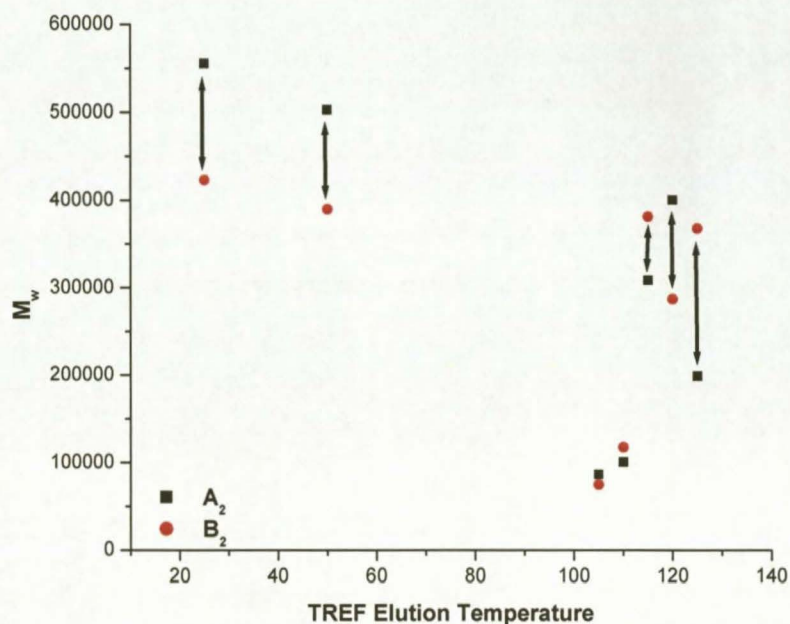


Figure 4.27 The weight average molecular weights for the fractions of both polymers A and B as a function of TREF elution temperature (°C) (run 2).

As an unfractionated polymer, no major differences can be pointed out between polymers A and B. Batch consistency between polymers A and B is not very good if the properties of the fractions are compared. Differences were seen in the distribution of ethylene, the amounts of crystallizable material, and the molecular weight of the fractions. TREF clearly can be used to illustrate batch variations in seemingly similar polymers.

4.4.2.2 Polymers C and D

Figure 4.28 shows the weight per fraction data from TREF for polymers C and D as a function of the elution temperature. The seven main fractions are plotted here. Similar weights (in gram) are collected for all of the fractions.

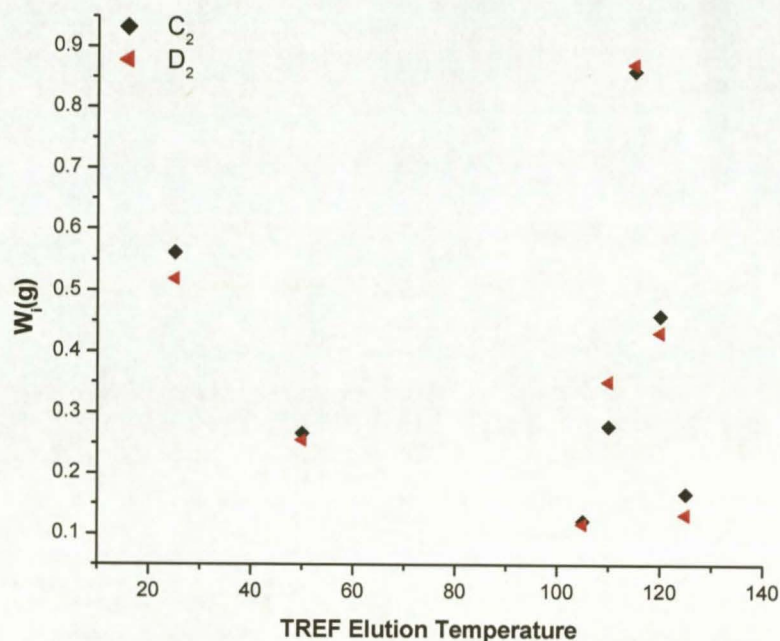


Figure 4.28 The data from TREF for polymers C and D (run 2). The weight per fraction, W_i (g), as a function of the elution temperature.

Table 4.12 shows the properties for the fractions of both polymers C and D. From previous results it is known that the ethylene content for the unfractionated polymers C and D was about 30 %. Similar values for DSC T_m and T_c , CRYSTAF T_c and molecular weights are obtained for the different fractions of polymers C and D. Double melting peaks are observed for the three higher temperature fractions (no. 11, 12 and 13) for both polymers. The polydispersities of both polymers are also lower than that of the corresponding unfractionated polymers (for polymer C, $PD = 5.3$ and for polymer D, $PD = 6.2$).

Table 4.12 Summary of properties for the fractions of both polymers C and D.

Polymer	Fraction no.	T _c (°C)	Ethylene content (%)	T _m DSC (°C)	T _c DSC (°C)	T _c CRYSTAF (°C)	\overline{M}_n (g/mol)	\overline{M}_w (g/mol)	PD
C	1	25	58.0	-	-	-	130 100	417 100	3.2
	2	50	55.6	-	-	-	113 800	330 600	2.9
	9	105	2.3	157.6	121.2	80.2	26 700	63 600	2.4
	10	110	0.6	160.7	120.5	79.4	47 900	127 200	2.7
	11	115	0.2	148.5/165.3	125.1	80.2	99 000	308 000	3.1
	12	120	0.4	149.9/164.4	121.8	80.9	88 100	222 200	2.5
	13	125	0.8	148.6/163.8	118.7	79.6	85 000	229 100	2.7
D	1	25	- ^a	-	-	-	129 300	420 300	3.3
	2	50	- ^a	-	-	-	127 000	388 600	3.1
	9	105	- ^a	157.8	117.7	78.6	26 700	65 900	2.5
	10	110	- ^a	162.3	122.3	79.7	44 900	112 900	2.5
	11	115	- ^a	150.8/165.8	125.5	80.7	94 200	257 300	2.7
	12	120	- ^a	149.8/164.9	121.1	80.4	96 900	239 700	2.5
	13	125	- ^a	150.2/165.1	121.6	80.4	97 500	265 200	2.7

^a No ¹³C NMR result for polymer D

Figure 4.29 illustrates the similarities in \overline{M}_w of the fractions of polymers C and D. Similar \overline{M}_w values are seen for all the fractions except for that of the 50 °C fractions for polymers C and D. This difference is less than 60 000 g/mol. On average, the difference in \overline{M}_w is less than 50 000 g/mol, with about 2 000 g/mol the smallest difference.

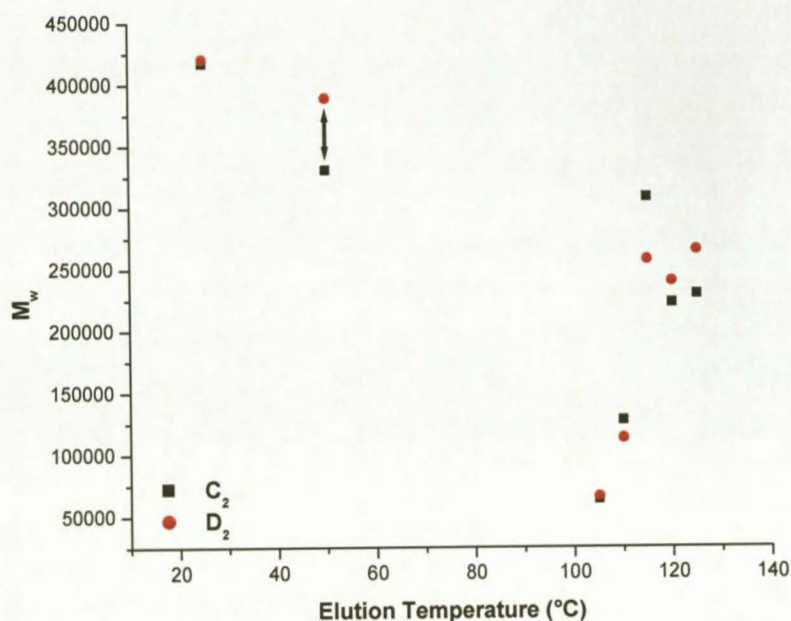


Figure 4.29. The weight average molecular weights for the fractions of both polymers C and D as a function of TREF elution temperature (°C) (run 2).

The consistency between the batches here is very good. Similar fraction weights, DSC melting and crystallization temperatures, CRYSTAF crystallization temperatures, molecular weights and polydispersities are seen.

4.4.3 Comparing copolymers with different ethylene content

Differences can be highlighted between the copolymers if the results of the weight per fraction, W_i (g), is shown as a function of elution temperature, °C, in Figure 4.30. The room temperature fraction and the 50 °C fraction of each copolymer clearly shows that as the ethylene content increases for each copolymer ($A, B \approx E < C, D$), the weight of those specific fractions eluted increases as well. These two fractions eluting at room temperature and 50 °C are the xylene soluble fractions, i.e., non-crystallizable material. This suggests that an increase in ethylene added during the polymerization process results in the incorporation of the extra ethylene into this atactic material. This suggestion is further strengthened by the fact that an increase in ethylene content has no major impact

on the DSC T_m and T_c peak values of the different copolymers (see Table 4.4, Summary of properties for the unfractionated polymers (A-E)). An elution temperature peak is seen at 115 °C for all five copolymers.

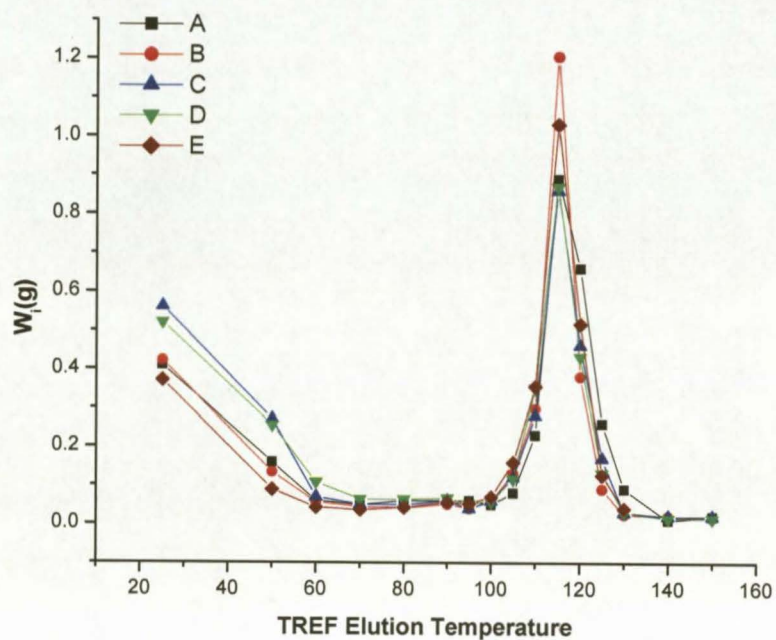


Figure 4.30 The curves of TREF for all five polymers. The weight per fraction, W_i (g), as a function of the elution temperature.

Table 4.13 Summary of properties for the fractions of both polymers A and C (run 2).

Polymer	Fraction no.	T _c (°C)	Ethylene content (%)	T _m DSC (°C)	T _c DSC (°C)	T _c CRYSTAF (°C)	M _n (g/mol)	M _w (g/mol)	PD
A	1	25	57.4	-	-	-	151 700	555 400	3.7
	2	50	60.6	-	-	-	116 100	503 000	4.3
	9	105	- ^a	157.7	122.9	- ^a	31 400	86 500	2.8
	10	110	0.6	160.8	121.9	76.1	43 500	100 700	2.3
	11	115	0.4	148.2/163.7	119.2	80.2	120 600	309 000	2.6
	12	120	0.1	147.3/163.0	119.0	79.5	150 300	401 000	2.7
	13	125	1.6	148.4/163.2	119.4	79.5	84 600	199 000	2.4
C	1	25	58.0	-	-	-	130 100	417 100	3.2
	2	50	55.6	-	-	-	113 800	330 600	2.9
	9	105	2.3	157.6	121.2	80.2	26 700	63 600	2.4
	10	110	0.6	160.7	120.5	79.4	47 900	127 200	2.7
	11	115	0.2	148.5/165.3	125.1	80.2	99 000	308 000	3.1
	12	120	0.4	149.9/164.4	121.8	80.9	88 100	222 200	2.5
	13	125	0.8	148.6/163.8	118.7	79.6	85 000	229 100	2.7

^a Insufficient sample of 105 °C fraction

Table 4.13 highlights the properties for the fractions of both polymers A and C. Polymers A and C have similar melting and crystallization temperatures for the 105 °C and 110 °C fractions. The three higher temperature fractions from 115 °C to 125 °C for both these polymers have double melting peaks. Polymer C has higher melting and crystallization temperatures than polymer A for these three higher temperatures. When comparing the 115 °C fractions of both these polymers it is seen that polymer C has a 6 °C higher crystallization temperature than polymer A. This suggests that polymer C contains less ethylene in the 115 °C fraction than polymer A, and from Table 4.13 it can be seen that polymer C contains half the amount of ethylene than polymer A in this 115 °C fraction (0.2 % ethylene vs. 0.4 % ethylene). This can be put in perspective when the ethylene content of the fraction is expressed as a percentage of the total sample ethylene content. This is illustrated in Table 4.14.

It is seen that polymer C, in fact, contains less ethylene than polymer A when the fraction ethylene content is calculated as a percentage of the total sample ethylene content. This confirms that the 115 °C fraction of polymer C contains less ethylene than the 115 °C fraction of polymer A.

Table 4.14 Ethylene content comparisons for the fractions of both polymers A and C (run 2).

Polymer	Fraction no.	T _e (°C)	Ethylene content (%)	W _i (g)	W _i (Ethylene content)(g)	Fraction Ethylene content as % of total sample ethylene content ^a
A	1	25	57.4	0.415	0.196	58.68
	2	50	60.6	0.158	0.078	23.35
	9	105	- ^b	0.081		
	10	110	0.6	0.230	0.0009	0.27
	11	115	0.4	0.892	0.0024	0.72
	12	120	0.1	0.656	0.0004	0.12
	13	125	1.6	0.265	0.0028	0.84
C	1	25	58.0	0.562	0.2690	41.77
	2	50	55.6	0.266	0.1210	18.79
	9	105	2.3	0.122	0.0019	0.30
	10	110	0.6	0.278	0.0011	0.17
	11	115	0.2	0.860	0.0011	0.17
	12	120	0.4	0.459	0.0012	0.19
	13	125	0.8	0.167	0.0009	0.14

^a Total sample ethylene content: Polymer A = 0.5285 g, Polymer C = 0.9564 g.

^b Insufficient sample of 105 °C fraction

From Table 4.14 it can be seen that the 25 °C and 50°C fractions of both these polymers consist of between 55 % to 60 % ethylene, respectively. Only when the ethylene content is calculated as a percentage of the total sample ethylene content, can differences be seen. Figure 4.31 shows the differences in the fraction ethylene content as a percentage of the total ethylene contained in the seven fractions analyzed. It is clear that the distribution of ethylene in polymer C is much more even than in polymer A. Most of the ethylene is contained in the two low temperature fractions. The weight of these two low temperature fractions collected comprise approximately 19 % of the total sample weight for polymer A and approximately 28 % for polymer C. The five higher temperature fractions consist

of about 70 % of the total sample weight for polymer A as versus about 63 % for polymer C.

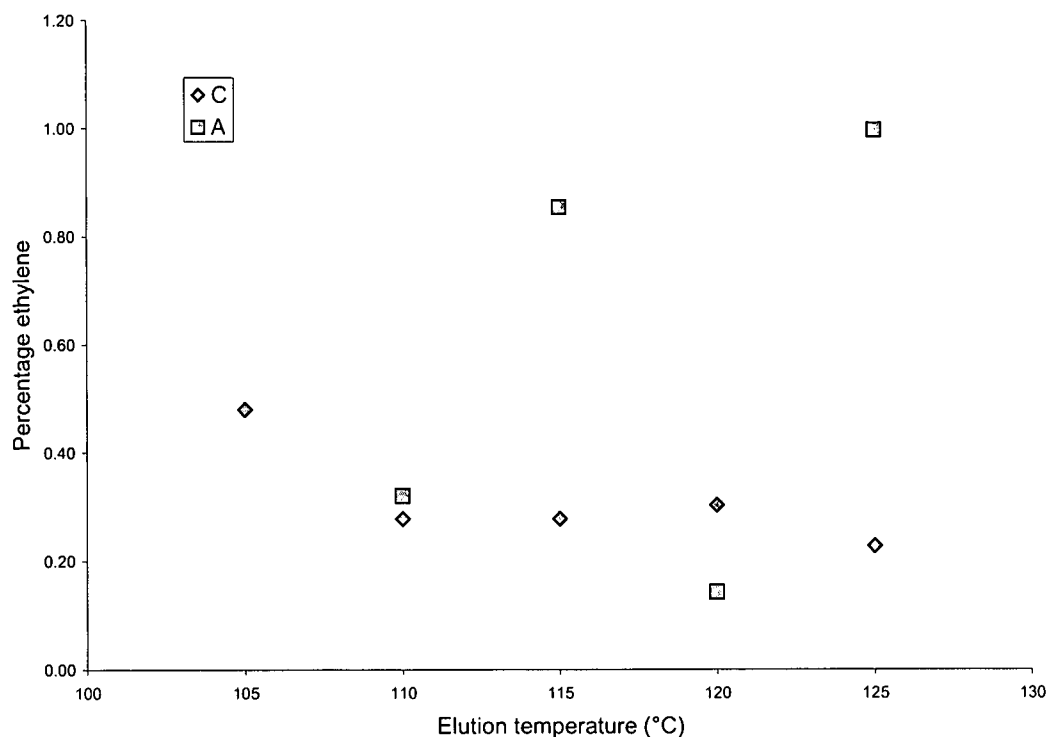


Figure 4.31 The ethylene content of the fractions of polymers A and C as a percentage of the total sample ethylene content vs. the elution temperature

Of the total ethylene contained in the seven fractions, about 97% is present in the two low temperature fractions. An increase in ethylene addition during the polymerization process apparently makes little difference in the distribution of ethylene; the majority ends up in the non-crystalline fractions. In Figure 4.32 the weight average molecular weights of polymers A and C are compared as a function of the TREF elution temperature. Polymer C has lower weight average molecular weights (difference > 100 000 g/mol) for the 25 °C and 50 °C fractions than polymer A.

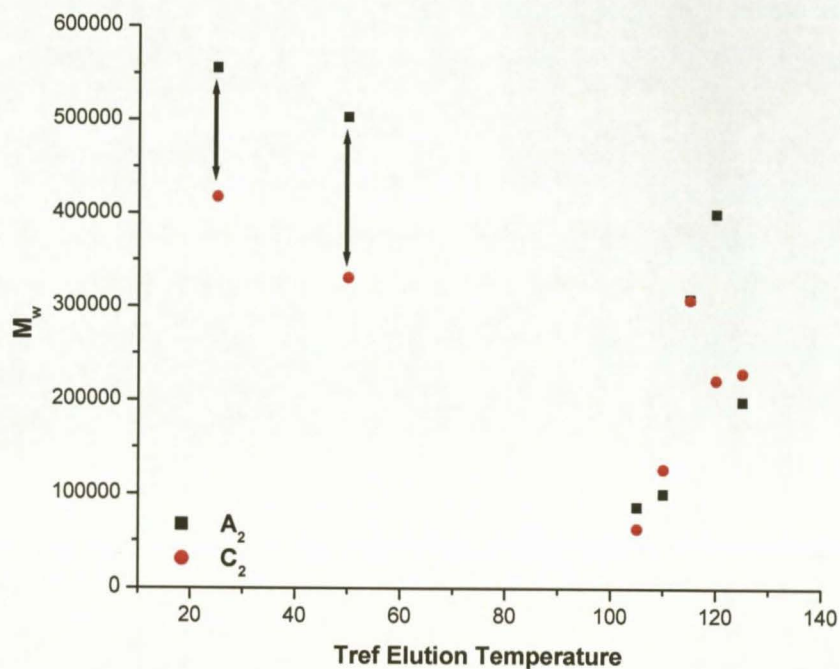


Figure 4.32 The weight average molecular weights for the fractions of both polymers A and C as a function of TREF elution temperature (°C) (run 2).

In conclusion, differences between these two polymers can readily be identified. Differences were seen in the DSC melting and crystallization temperatures, the weight average molecular weights and the fraction ethylene content of the different fractions. A maximum fraction ethylene content of about 60% is seen irrespective of the total sample ethylene content. Also, when the fraction ethylene content is calculated as a percentage of the total sample weight differences are observed.

4.5 References

1. Mirabella, F.M., *Polymer*, 1993. **34**(8): 1729.
2. Grant, D.M., Paul, E.G., *J. Am. Chem. Soc.*, 1964. **86**: 2984.
3. Busico, V., Cipullo, R., *Prog. Polym. Sci.*, 2001. **26**: 443.
4. Gahleitner, M., Bachner, C., Ratajski, E., Rohaczek, G., Neißl, W., *J. Appl. Polym. Sci.*, 1999. **73**: 2507.
5. Wild, L., *Adv. Polym. Sci.*, 1990. **98**(1): 1.
6. Zhang, Y., Wu, C.J., Zhu, S.N., *Polymer*, 2002. **34**(9): 700.
7. Monrabel, B., *Temperature rising elution fractionation and crystallization analysis fractionation*, in *Encyclopaedia of Analytical Chemistry*. 2000, John Wiley & sons Ltd. 8074-8094.
8. Jancar, J., *Adv. Polym. Sci.*, 1999. **139**: 1.

Chapter 5

Conclusions and recommendations

5.1 Introduction

In this chapter, some general conclusion about the study is drawn. This will summarize the results discussed in Chapter 4.

5.2 Conclusions

Five commercial “impact” polypropylene copolymers with varying ethylene content were obtained. These polymers comprised two sets of two polymers each, each set being supposedly similar but from different batches. A fifth copolymer was also obtained, with an ethylene content that was supposedly different from any of the other copolymers.

Original polymers

These polymers were first fully characterized.

- 1 The ethylene content determined by ^{13}C NMR was significantly different from that claimed by the manufacturers.
- 2 During solution crystallization analyses by CRYSTAF, differences could be seen in two seemingly similar polymers from different batches.
- 3 In other aspects (thermal properties and molecular weight), polymers from the two batches (designated polymers A and B in this study), the polymers appeared identical.

Fractionation

Polymers were then subjected to fractionation by prep-TREF, and fractions isolated and analyzed off-line.

- 1 The prep-TREF technique was optimized for these materials, particularly with respect to the elution temperatures and temperature intervals of the materials.

- 2 Up to 15 clearly identifiable different fractions were obtained for each of the polymers. These experiments were repeatable and recovery was typically quantitative.
- 3 Of the 15 fractions, 7 comprised about 90% of the total weight of the polymer (before fractionation). These seven fractions were full analyzed and the polymer compared.
- 4 Three major components were isolated from each of the polymers. These were ethylene-propylene rubber (50 – 60 mole% ethylene), propylene homopolymer and ethylene-rich copolymers. Small amounts of ethylene homopolymer and propylene-rich copolymer was also present. The EPR was non-crystalline and largely present in the fractions isolated at elution temperatures of 25 and 50 °C. These were also the fractions with the highest molecular weight.
- 5 Polymers A and B were shown to be different on a molecular level. This was reflected in the fractionation profile as well as the distribution of ethylene amongst the more crystalline fractions. Polymers C and D were virtually identical, indicating good batch consistency in the latter case.
- 6 A comparison of polymer C with A showed that the ethylene distribution in the former was more uniform than the latter. This comparison also showed that most of the ethylene in these copolymers is present as ethylene-propylene rubber. Increasing the ethylene content does correspondingly increases the rubbery, soluble part of the polymer.
- 7 Overall, prep-TREF was shown to be a useful technique to compare polymers of similar or different molecular make-up. This holds true even for very complex materials such as the propylene impact copolymers.

5.3 Recommendations

- 1 Selective removal of fractions and recombination of these materials and micromechanical analyses will allow for an understanding of the role of the various fractions in these complex polymers.

Appendix A

TREF curves and fractionation data for polymers A – E

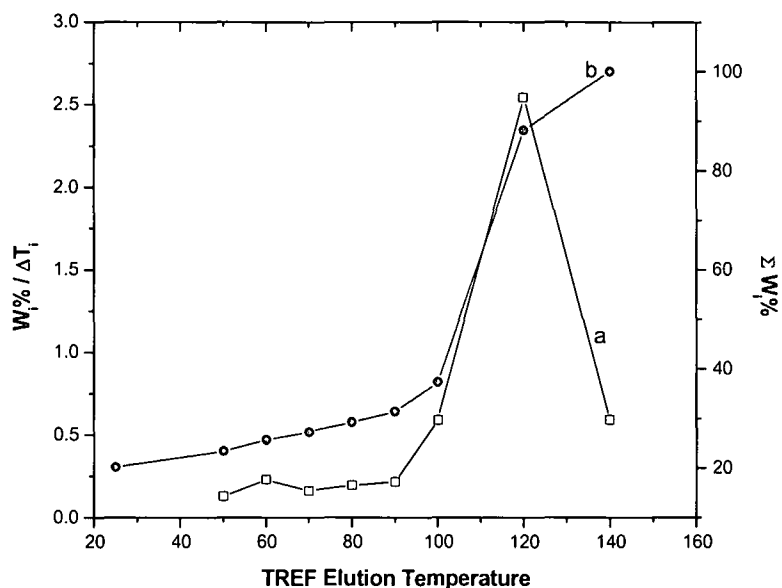


Figure A.1. The curves of TREF for polymer A₁. The weight of the fractions as a function of the elution temperature (°C), (a) the differential weight fraction to temperature, $W_i\%/\Delta T_i$, (b) accumulative weight fraction, $\Sigma W_i\%$.

Table A.1. Fractionation data of polymer A₁:

Fraction no.	T_e (°C)	W_i	W_i (%)	ΣW_i (%)	$W_i\%/\Delta T$
1	25	0.459	20.15	20.15	n/a
2	50	0.073	3.21	23.36	0.13
3	60	0.052	2.29	25.65	0.23
4	70	0.037	1.62	27.27	0.16
5	80	0.044	1.94	29.22	0.19
6	90	0.049	2.16	31.38	0.22
7	100	0.135	5.93	37.31	0.59
8	120	1.159	50.86	88.17	2.54
9	140	0.270	11.83	100.00	0.59

(Note: A₁ refers to the author's first fractionation run of polymer A; A₂ refers to the second fractionation run of polymer A, etc.)

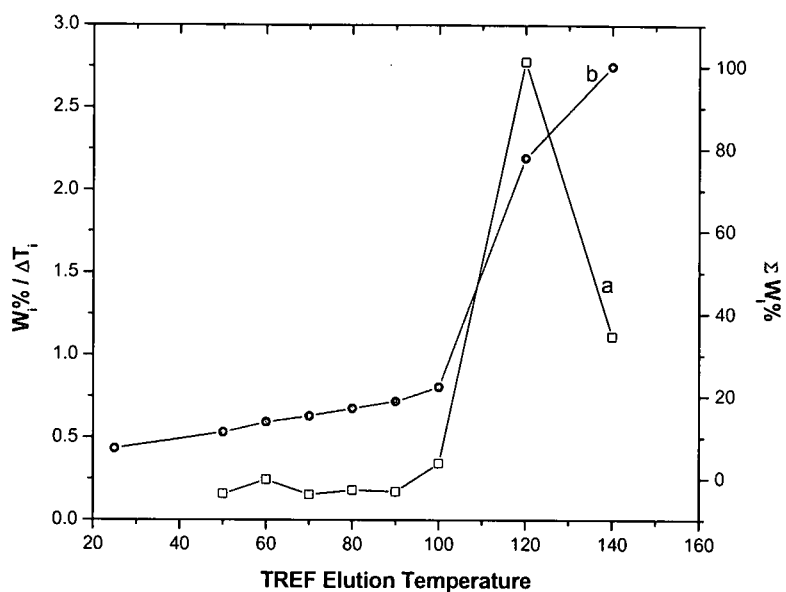


Figure A.2. The curves of TREF for polymer B₁. The weight of the fractions as a function of the elution temperature (°C), (a) the differential weight fraction to temperature, $W_i\%/\Delta T_i$, (b) accumulative weight fraction, $\Sigma W_i\%$.

Table A.2. Fractionation data of polymer B₁:

Fraction no.	T_e (°C)	W_i	W_i (%)	ΣW_i (%)	$W_i\%/\Delta T$
1	25	0.231	7.32	7.32	n/a
2	50	0.124	3.93	11.25	0.16
3	60	0.077	2.43	13.69	0.24
4	70	0.048	1.53	15.22	0.15
5	80	0.058	1.83	17.05	0.18
6	90	0.054	1.71	18.76	0.17
7	100	0.109	3.44	22.20	0.34
8	120	1.752	55.53	77.73	2.78
9	140	0.703	22.27	100.00	1.11

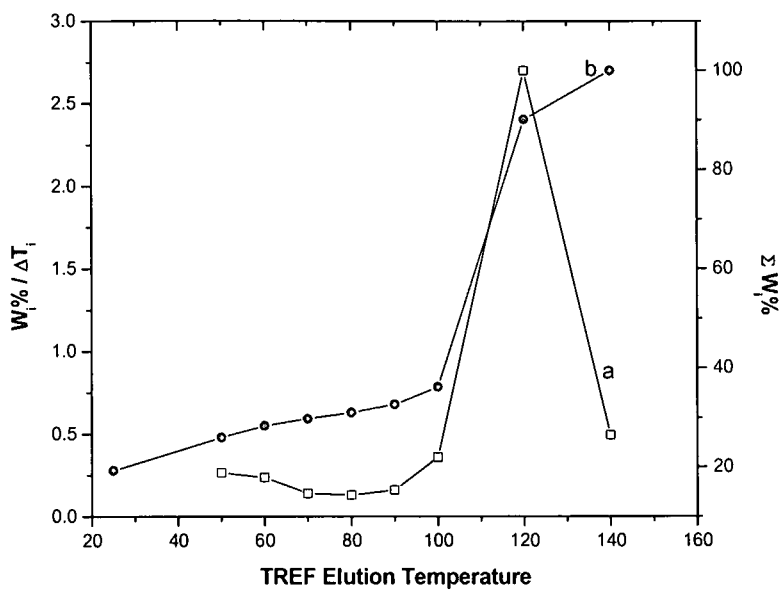


Figure A.3. The curves of TREF for polymer C₁. The weight of the fractions as a function of the elution temperature (°C), (a) the differential weight fraction to temperature, $W_i\%/\Delta T_i$, (b) accumulative weight fraction, $\Sigma W_i\%$.

Table A.3. Fractionation data of polymer C₁:

Fraction no.	T_e (°C)	W_i (g)	W_i (%)	SW_i (%)	$W_i\%/DT$
1	25	0.600	19.31	19.31	n/a
2	50	0.206	6.64	25.94	0.27
3	60	0.073	2.35	28.30	0.24
4	70	0.043	1.39	29.68	0.14
5	80	0.040	1.29	30.97	0.13
6	90	0.050	1.60	32.57	0.16
7	100	0.112	3.59	36.16	0.36
8	120	1.679	53.99	90.16	2.70
9	140	0.306	9.84	100	0.49

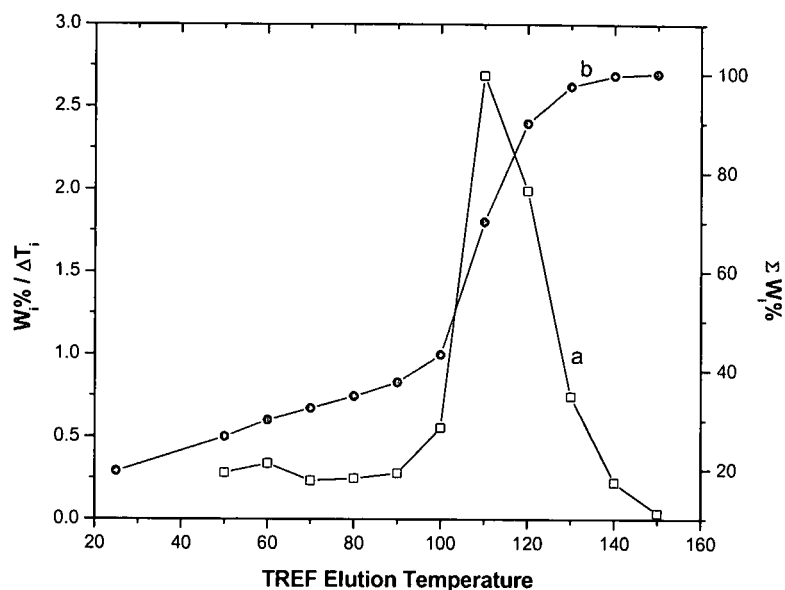


Figure A.4. The curves of TREF for polymer D₁. The weight of the fractions as a function of the elution temperature (°C), (a) the differential weight fraction to temperature, $W_i\%/\Delta T_i$, (b) accumulative weight fraction, $\Sigma W_i\%$.

Table A.4. Fractionation data of polymer D₁:

Fraction no.	T_e (°C)	W_i (g)	W_i (%)	ΣW_i (%)	$W_i\%/\Delta T$
1	25	0.657	19.65	19.65	n/a
2	50	0.235	7.02	26.67	0.28
3	60	0.113	3.38	30.05	0.34
4	70	0.078	2.32	32.37	0.23
5	80	0.083	2.47	34.84	0.25
6	90	0.093	2.79	37.63	0.28
7	100	0.185	5.53	43.16	0.55
8	110	0.898	26.89	70.05	2.69
9	120	0.666	19.92	89.97	1.99
10	130	0.249	7.46	97.43	0.75
11	140	0.074	2.22	99.65	0.22
12	150	0.012	0.35	100	0.04

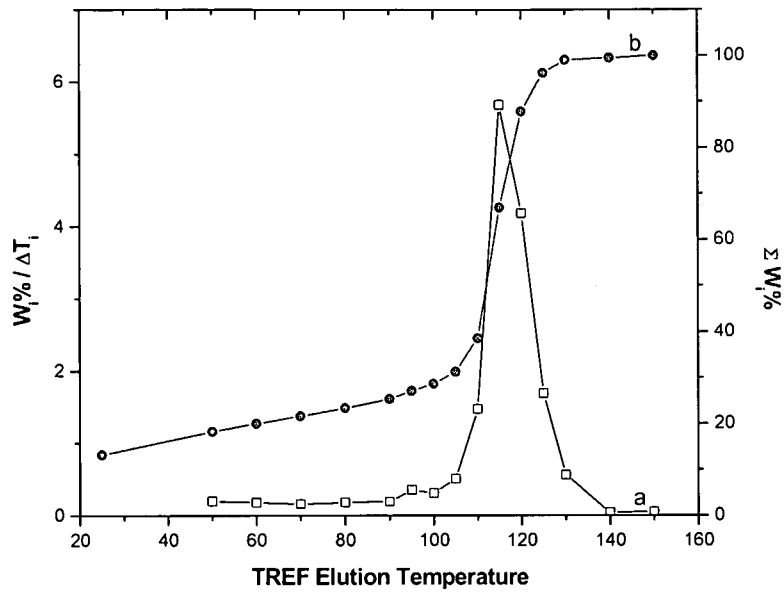


Figure A.5. The curves of TREF for polymer A₂. The weight of the fractions as a function of the elution temperature (°C), (a) the differential weight fraction to temperature, $W_i\%/\Delta T_i$, (b) accumulative weight fraction, $\Sigma W_i\%$.

Table A.5. Fractionation data of polymer A₂:

Fraction no.	T_e (°C)	W_i (g)	W_i (%)	ΣW_i (%)	$W_i\%/\Delta T$
1	25	0.415	13.21	13.21	n/a
2	50	0.158	5.03	18.24	0.20
3	60	0.055	1.75	19.99	0.18
4	70	0.050	1.60	21.60	0.16
5	80	0.056	1.78	23.38	0.18
6	90	0.061	1.95	25.33	0.19
7	95	0.056	1.77	27.10	0.35
8	100	0.048	1.53	28.63	0.31
9	105	0.081	2.57	31.20	0.51
10	110	0.230	7.33	38.54	1.47
11	115	0.892	28.40	66.94	5.68
12	120	0.656	20.90	87.84	4.18
13	125	0.265	8.44	96.28	1.69
14	130	0.088	2.82	99.09	0.56
15	140	0.013	0.41	99.50	0.04
16	150	0.016	0.50	100	0.05

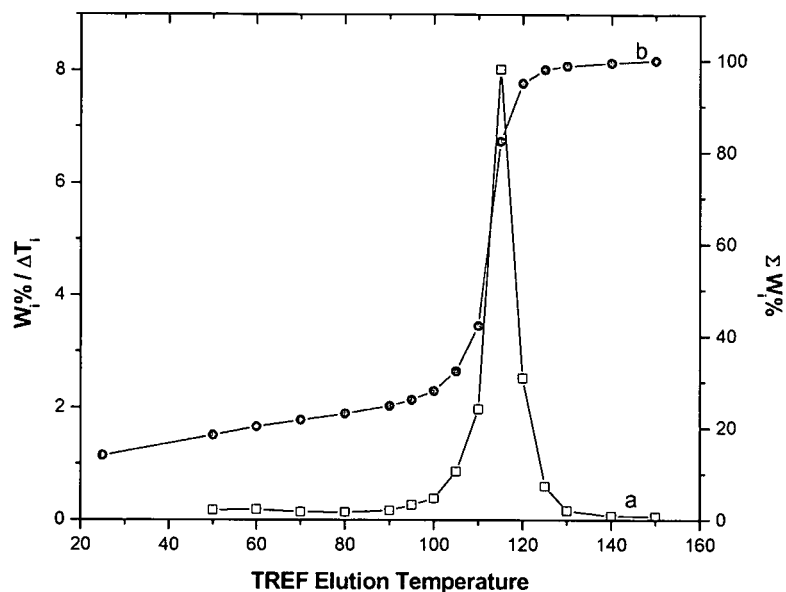


Figure A.6. The curves of TREF for polymer B₂. The weight of the fractions as a function of the elution temperature (°C), (a) the differential weight fraction to temperature, $W_i\%/\Delta T_i$, (b) accumulative weight fraction, $\Sigma W_i\%$.

Table A.6. Fractionation data of polymer B₂:

Fraction no.	T _e (°C)	W _i (g)	W _i (%)	ΣW _i (%)	W _i %/ΔT
1	25	0.421	14.00	14.00	n/a
2	50	0.134	4.44	18.44	0.18
3	60	0.056	1.86	20.30	0.19
4	70	0.043	1.44	21.74	0.14
5	80	0.041	1.37	23.11	0.14
6	90	0.050	1.68	24.79	0.17
7	95	0.040	1.32	26.11	0.26
8	100	0.058	1.93	28.03	0.39
9	105	0.130	4.32	32.35	0.86
10	110	0.297	9.88	42.23	1.98
11	115	1.206	40.10	82.33	8.02
12	120	0.380	12.63	94.96	2.53
13	125	0.090	3.01	97.97	0.60
14	130	0.025	0.82	98.79	0.16
15	140	0.020	0.67	99.46	0.07
16	150	0.016	0.54	100	0.05

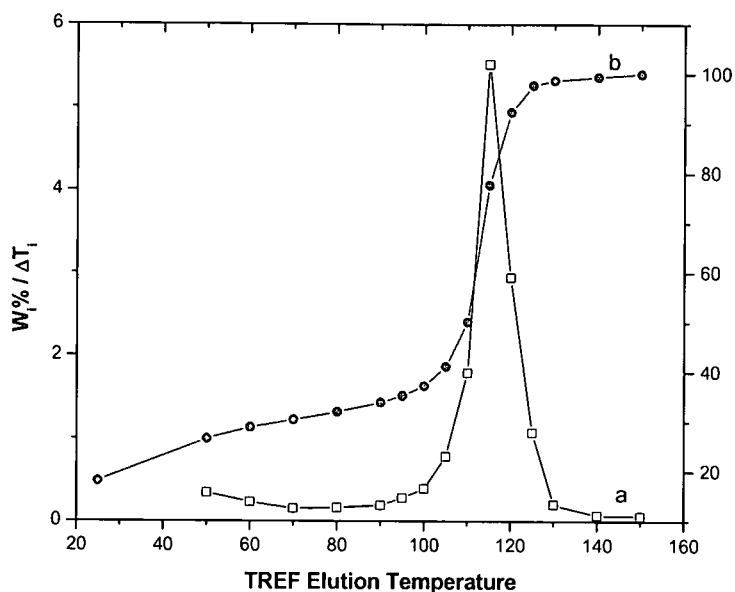


Figure A.7. The curves of TREF for polymer C₂. The weight of the fractions as a function of the elution temperature (°C), (a) the differential weight fraction to temperature, $W_i\%/\Delta T_i$, (b) accumulative weight fraction, $\Sigma W_i\%$.

Table A.7. Fractionation data of polymer C₂:

Fraction no.	T _c (°C)	W _i (g)	W _i (%)	ΣW _i (%)	W _i %/ΔT
1	25	0.562	18.01	18.01	n/a
2	50	0.266	8.54	26.55	0.34
3	60	0.071	2.27	28.82	0.23
4	70	0.048	1.54	30.35	0.15
5	80	0.050	1.61	31.96	0.16
6	90	0.058	1.87	33.83	0.19
7	95	0.043	1.39	35.23	0.28
8	100	0.061	1.97	37.19	0.39
9	105	0.122	3.92	41.11	0.78
10	110	0.278	8.93	50.04	1.79
11	115	0.860	27.58	77.62	5.52
12	120	0.459	14.72	92.34	2.94
13	125	0.167	5.36	97.70	1.07
14	130	0.031	0.99	98.69	0.20
15	140	0.022	0.71	99.40	0.07
16	150	0.019	0.60	100	0.06

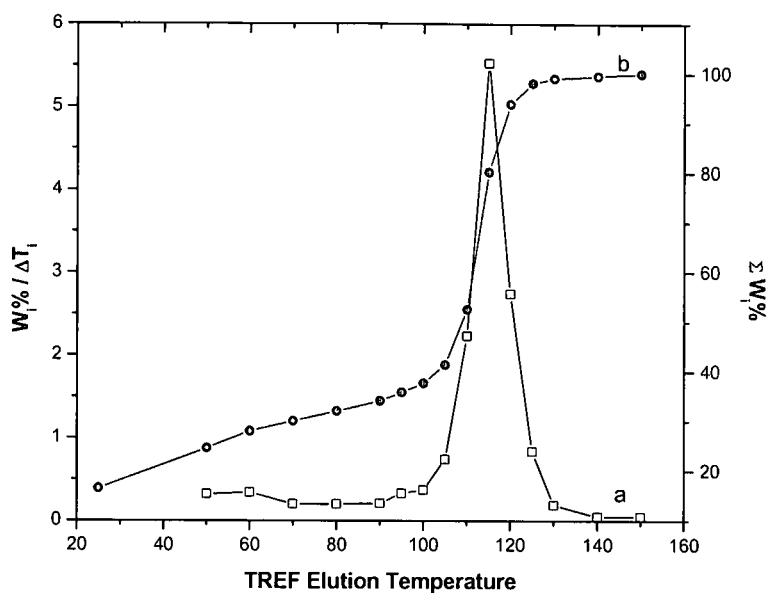


Figure A.8. The curves of TREF for polymer D₂. The weight of the fractions as a function of the elution temperature (°C), (a) the differential weight fraction to temperature, $W_i\%/\Delta T_i$, (b) accumulative weight fraction, $\Sigma W_i\%$.

Table A.8. Fractionation data of polymer D₂:

Fraction no.	T_e (°C)	W_i (g)	W_i (%)	ΣW_i (%)	$W_i\%/\Delta T$
1	25	0.519	16.48	16.48	n/a
2	50	0.254	8.08	24.56	0.32
3	60	0.108	3.43	27.99	0.34
4	70	0.064	2.02	30.01	0.20
5	80	0.064	2.03	32.04	0.20
6	90	0.067	2.12	34.15	0.21
7	95	0.052	1.66	35.82	0.33
8	100	0.059	1.86	37.68	0.37
9	105	0.117	3.71	41.38	0.74
10	110	0.351	11.14	52.52	2.23
11	115	0.871	27.65	80.17	5.53
12	120	0.431	13.69	93.86	2.74
13	125	0.132	4.19	98.06	0.84
14	130	0.030	0.96	99.02	0.19
15	140	0.016	0.49	99.51	0.05
16	150	0.016	0.49	100	0.05

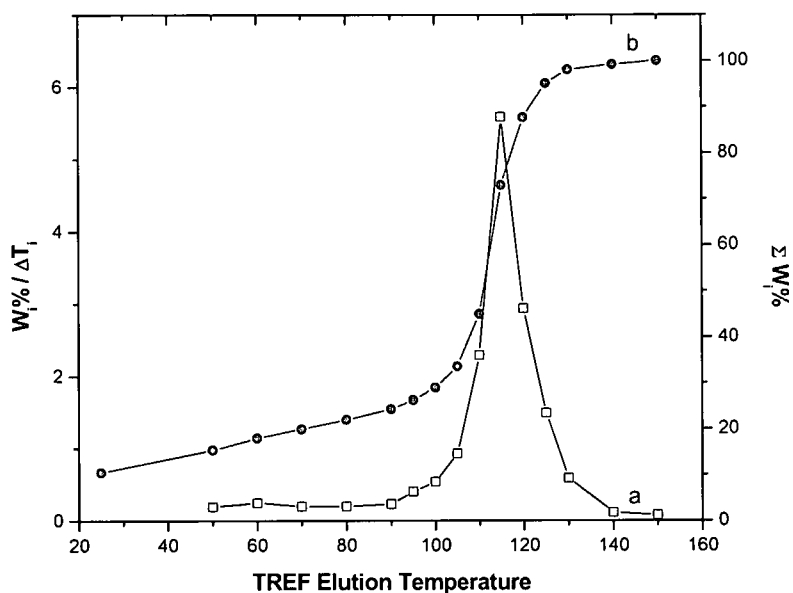


Figure A.9. The curves of TREF for polymer A₃. The weight of the fractions as a function of the elution temperature (°C), (a) the differential weight fraction to temperature, $W_i\%/\Delta T_i$, (b) accumulative weight fraction, $\Sigma W_i\%$.

Table A.9. Fractionation data of polymer A₃:

Fraction no.	T_e (°C)	W_i	W_i (%)	ΣW_i (%)	$W_i\%/\Delta T$
1	25	0.333	10.52	10.52	n/a
2	50	0.154	4.87	15.39	0.19
3	60	0.081	2.54	17.93	0.25
4	70	0.064	2.01	19.94	0.20
5	80	0.064	2.02	21.96	0.20
6	90	0.073	2.29	24.26	0.23
7	95	0.063	1.98	26.24	0.40
8	100	0.085	2.68	28.93	0.54
9	105	0.147	4.65	33.57	0.93
10	110	0.362	11.43	45.00	2.29
11	115	0.886	27.97	72.98	5.59
12	120	0.467	14.72	87.70	2.94
13	125	0.236	7.43	95.13	1.49
14	130	0.093	2.93	98.07	0.59
15	140	0.036	1.13	99.20	0.11
16	150	0.026	0.80	100.00	0.08

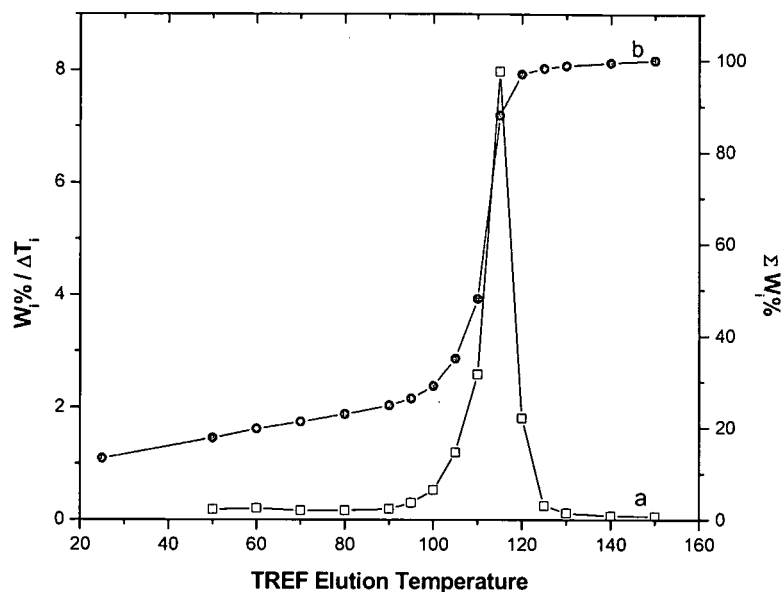


Figure A.10. The curves of TREF for polymer B₃. The weight of the fractions as a function of the elution temperature (°C), (a) the differential weight fraction to temperature, $W_i\%/\Delta T_i$, (b) accumulative weight fraction, $\Sigma W_i\%$.

Table A.10. Fractionation data of polymer B₃:

Fraction no.	T_e (°C)	W_i	W_i (%)	ΣW_i (%)	$W_i\%/\Delta T$
1	25	0.419	13.32	13.32	n/a
2	50	0.141	4.48	17.79	0.18
3	60	0.061	1.95	19.74	0.20
4	70	0.050	1.58	21.32	0.16
5	80	0.052	1.64	22.96	0.16
6	90	0.061	1.92	24.88	0.19
7	95	0.047	1.50	26.38	0.30
8	100	0.084	2.67	29.05	0.53
9	105	0.190	6.02	35.07	1.20
10	110	0.407	12.94	48.01	2.59
11	115	1.256	39.88	87.89	7.98
12	120	0.284	9.03	96.93	1.81
13	125	0.040	1.27	98.20	0.25
14	130	0.018	0.58	98.78	0.12
15	140	0.021	0.65	99.43	0.07
16	150	0.018	0.57	100.00	0.06

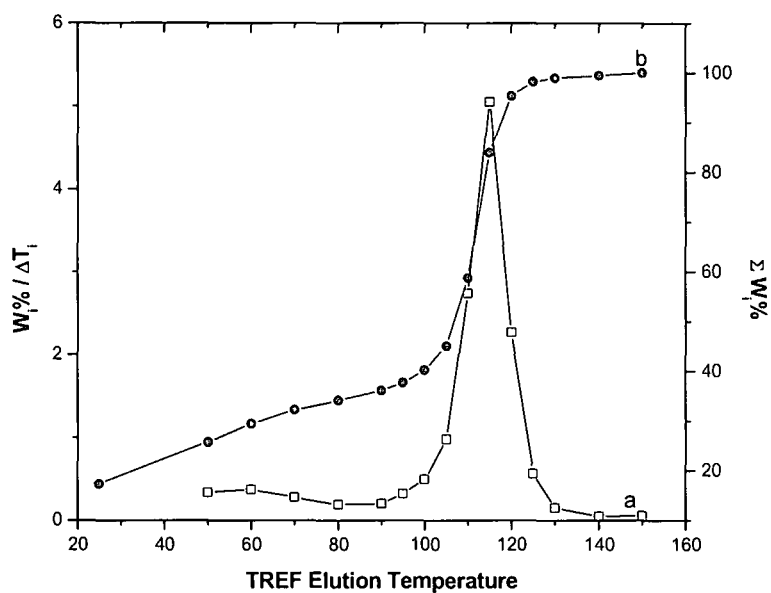


Figure A.11. The curves of TREF for polymer C₃. The weight of the fractions as a function of the elution temperature (°C), (a) the differential weight fraction to temperature, $W_i\%/\Delta T_i$, (b) accumulative weight fraction, $\Sigma W_i\%$.

Table A.11. Fractionation data of polymer C₃:

Fraction no.	T _e (°C)	W _i	W _i (%)	ΣW _i (%)	W _i %/ΔT
1	25	0.540	17.32	17.32	n/a
2	50	0.263	8.43	25.75	0.34
3	60	0.115	3.67	29.42	0.37
4	70	0.086	2.77	32.19	0.28
5	80	0.060	1.91	34.10	0.19
6	90	0.061	1.97	36.07	0.20
7	95	0.050	1.59	37.66	0.32
8	100	0.077	2.47	40.13	0.49
9	105	0.153	4.89	45.02	0.98
10	110	0.427	13.70	58.72	2.74
11	115	0.788	25.27	83.99	5.05
12	120	0.354	11.36	95.35	2.27
13	125	0.089	2.87	98.22	0.57
14	130	0.024	0.77	98.99	0.15
15	140	0.014	0.45	99.44	0.05
16	150	0.018	0.56	100.00	0.06

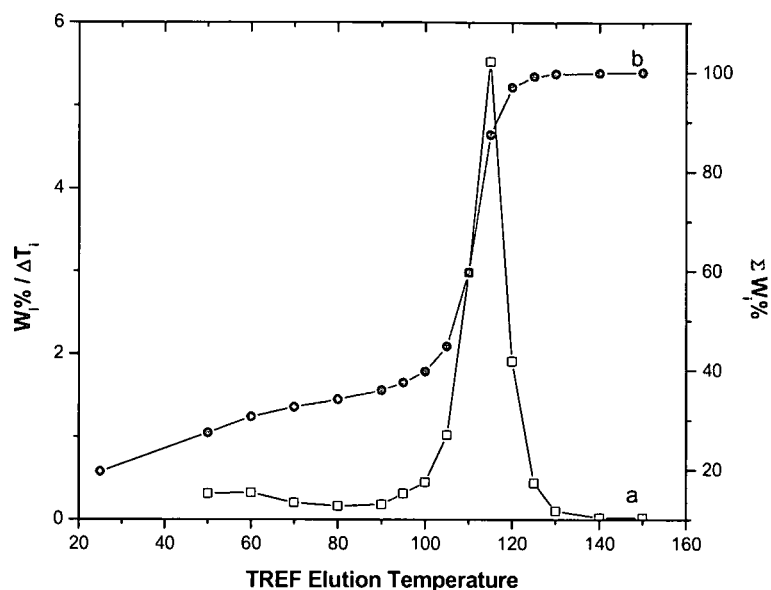


Figure A.12. The curves of TREF for polymer D₃. The weight of the fractions as a function of the elution temperature (°C), (a) the differential weight fraction to temperature, $W_i\%/\Delta T_i$, (b) accumulative weight fraction, $\Sigma W_i\%$.

Table A.12. Fractionation data of polymer D₃:

Fraction no.	T_c (°C)	W_i	W_i (%)	ΣW_i (%)	$W_i\%/\Delta T$
1	25	0.603	19.61	19.61	n/a
2	50	0.239	7.78	27.39	0.31
3	60	0.099	3.22	30.62	0.32
4	70	0.060	1.96	32.58	0.20
5	80	0.048	1.57	34.14	0.16
6	90	0.056	1.83	35.97	0.18
7	95	0.047	1.54	37.50	0.31
8	100	0.069	2.25	39.76	0.45
9	105	0.156	5.08	44.83	1.02
10	110	0.458	14.91	59.75	2.98
11	115	0.850	27.65	87.39	5.53
12	120	0.293	9.54	96.94	1.91
13	125	0.068	2.22	99.16	0.44
14	130	0.016	0.52	99.67	0.10
15	140	0.005	0.17	99.84	0.02
16	150	0.005	0.16	100.00	0.02

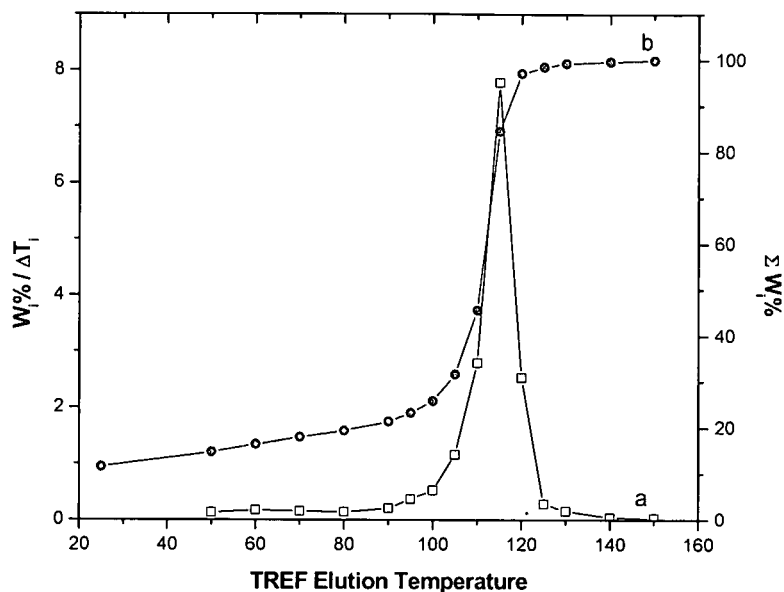


Figure A.13. The curves of TREF for polymer E₁. The weight of the fractions as a function of the elution temperature (°C), (a) the differential weight fraction to temperature, $W_i\%/\Delta T_i$, (b) accumulative weight fraction, $\Sigma W_i\%$.

Table A.13. Fractionation data of polymer E₁:

Fraction no.	T _e (°C)	W _i (g)	W _i (%)	ΣW _i (%)	W _i %/ΔT
1	25	0.348	11.53	11.53	n/a
2	50	0.097	3.21	14.74	0.13
3	60	0.051	1.68	16.42	0.17
4	70	0.045	1.50	17.93	0.15
5	80	0.043	1.41	19.34	0.14
6	90	0.061	2.03	21.37	0.20
7	95	0.056	1.87	23.24	0.37
8	100	0.079	2.60	25.84	0.52
9	105	0.175	5.79	31.62	1.16
10	110	0.421	13.95	45.57	2.79
11	115	1.174	38.89	84.46	7.78
12	120	0.382	12.64	97.10	2.53
13	125	0.042	1.39	98.49	0.28
14	130	0.023	0.75	99.24	0.15
15	140	0.013	0.43	99.67	0.04
16	150	0.010	0.33	100	0.03

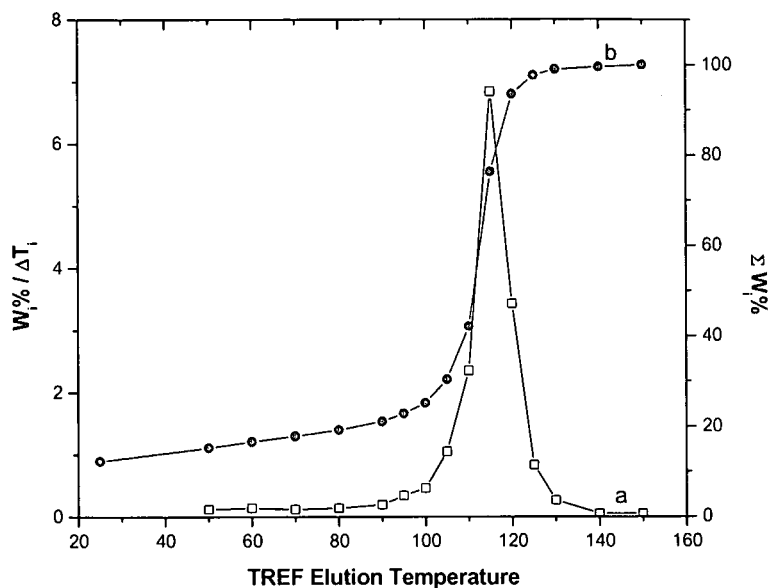
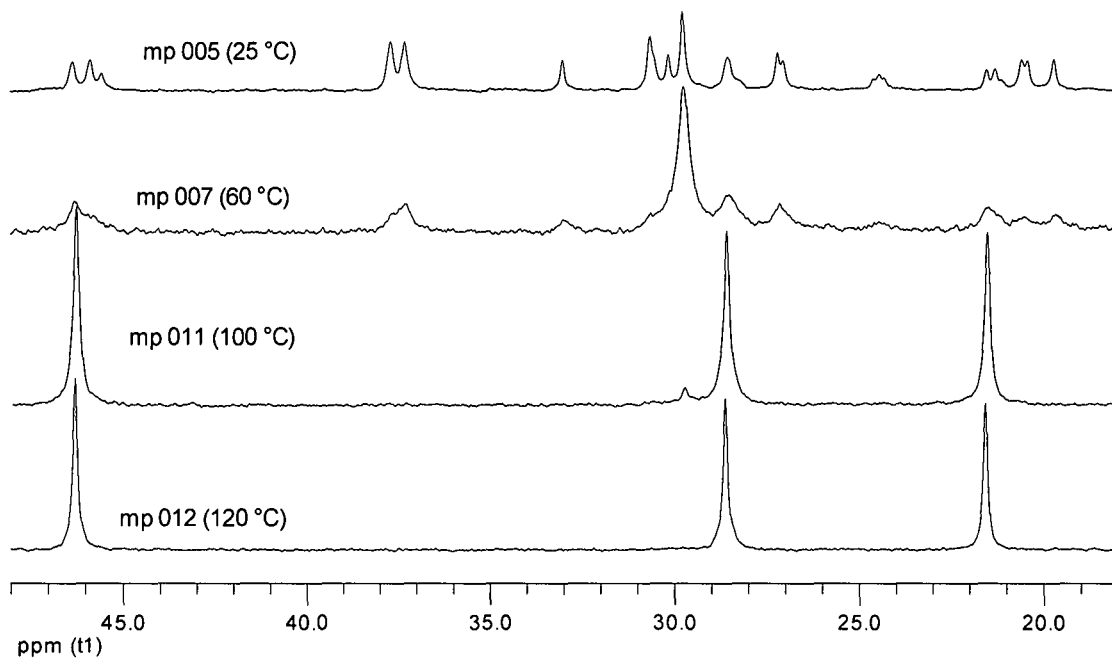
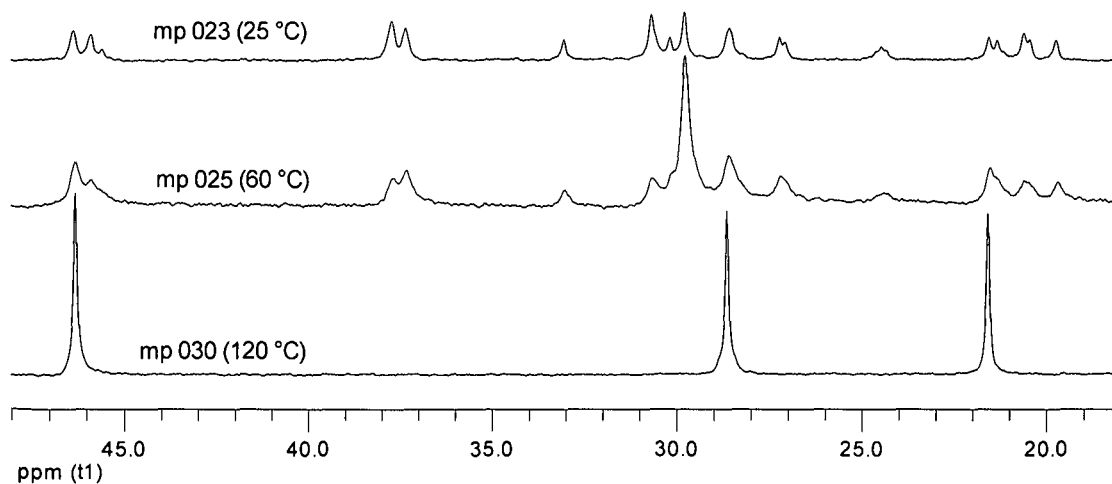


Figure A.14. The curves of TREF for polymer E₂. The weight of the fractions as a function of the elution temperature (°C), (a) the differential weight fraction to temperature, $W_i/\Delta T_i$, (b) accumulative weight fraction, $\Sigma W_i\%$.

Table A.14. Fractionation data of polymer E₂:

Fraction no.	T_e (°C)	W_i (g)	W_i (%)	ΣW_i (%)	$W_i/\Delta T$
1	25	0.371	12.29	12.29	n/a
2	50	0.089	2.96	15.25	0.12
3	60	0.042	1.41	16.66	0.14
4	70	0.036	1.21	17.86	0.12
5	80	0.042	1.38	19.24	0.14
6	90	0.056	1.86	21.10	0.19
7	95	0.052	1.72	22.82	0.34
8	100	0.070	2.32	25.13	0.46
9	105	0.159	5.26	30.39	1.05
10	110	0.355	11.75	42.15	2.35
11	115	1.031	34.18	76.33	6.84
12	120	0.517	17.15	93.48	3.43
13	125	0.126	4.17	97.65	0.83
14	130	0.040	1.32	98.97	0.26
15	140	0.015	0.50	99.47	0.05
16	150	0.016	0.53	100	0.05

Appendix B

A. ^{13}C NMR ResultsFigure B.1. ^{13}C NMR Spectra for Polymer A₁Figure B.2. ^{13}C NMR Spectra for Polymer C₁

(Note: A₁ refers to the author's first fractionation run of polymer A; A₂ refers to the second fractionation run of polymer A, etc.)

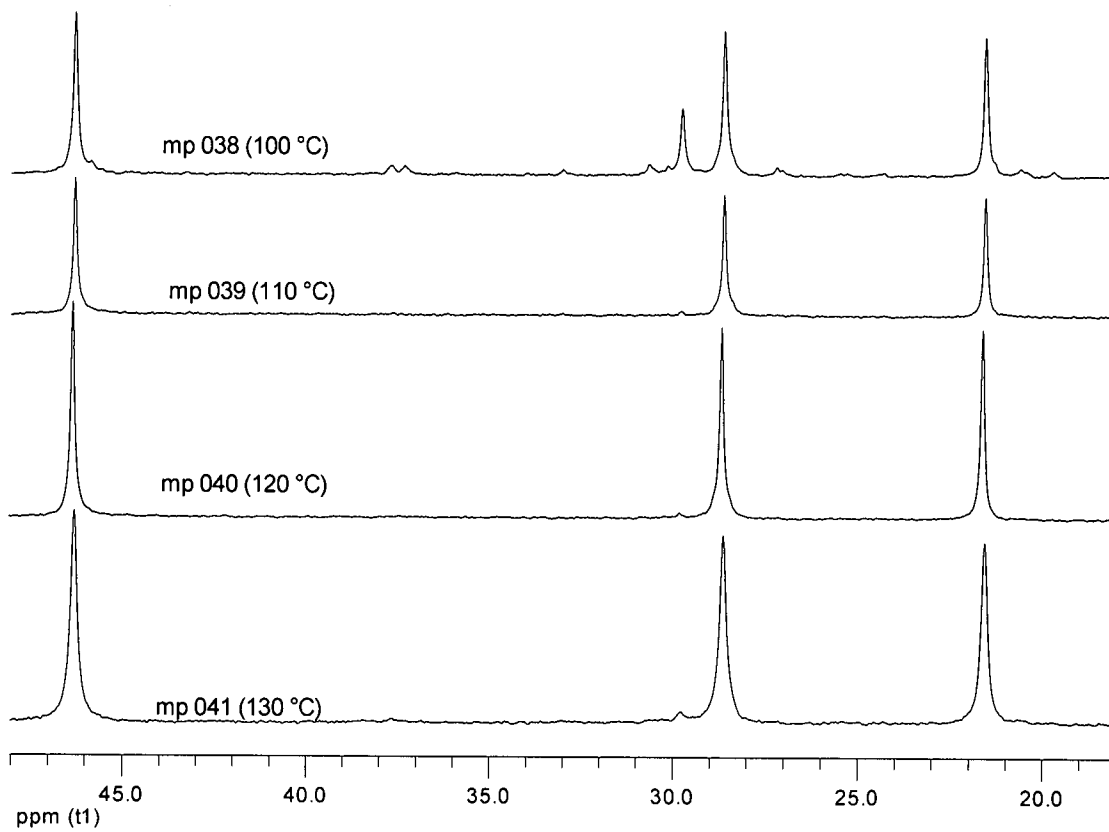
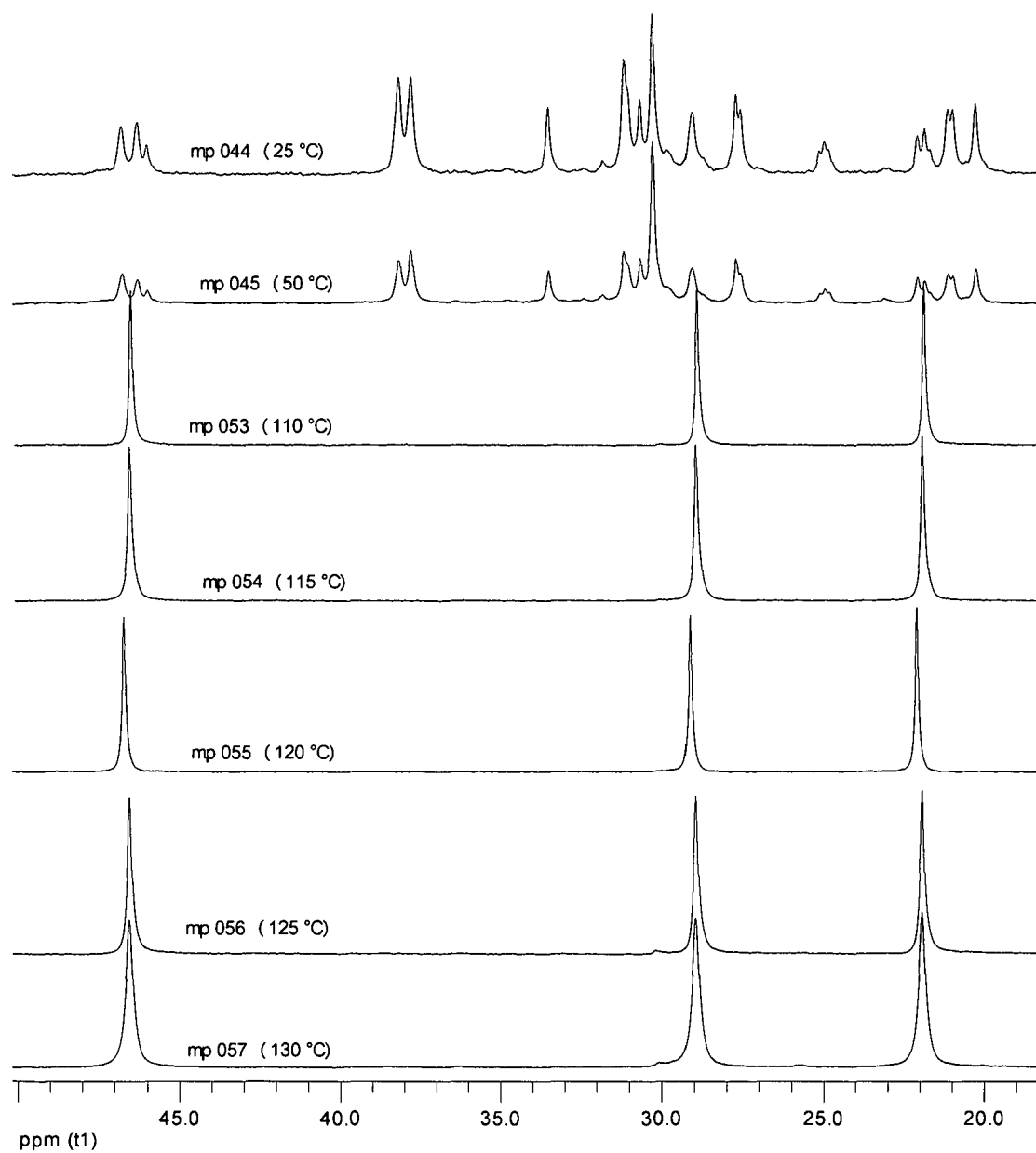


Figure B.3. ^{13}C NMR Spectra for Polymer D₁

**Figure B.4.** ^{13}C NMR Spectra for Polymer A₂

B. CRYSTAF Results

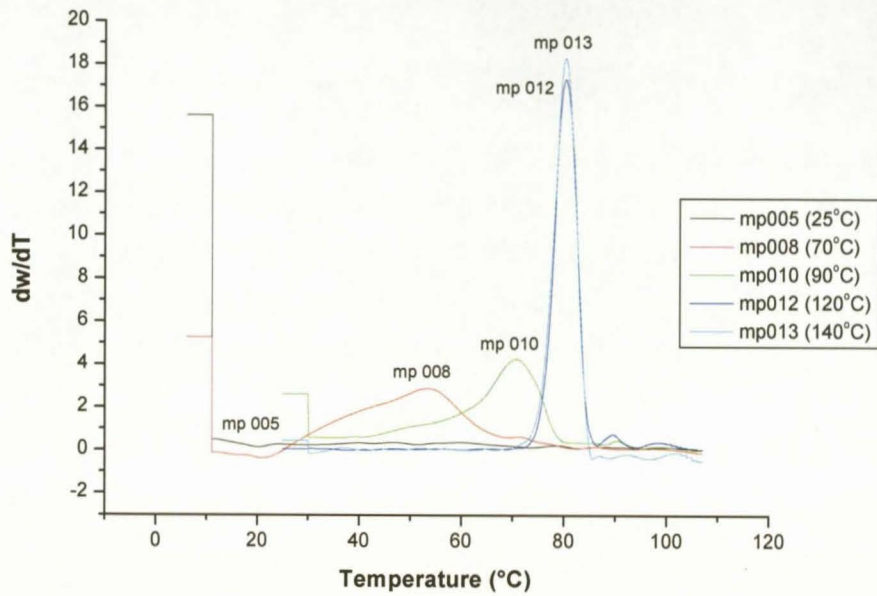


Figure B.5. CRYSTAF traces for Polymer A₁

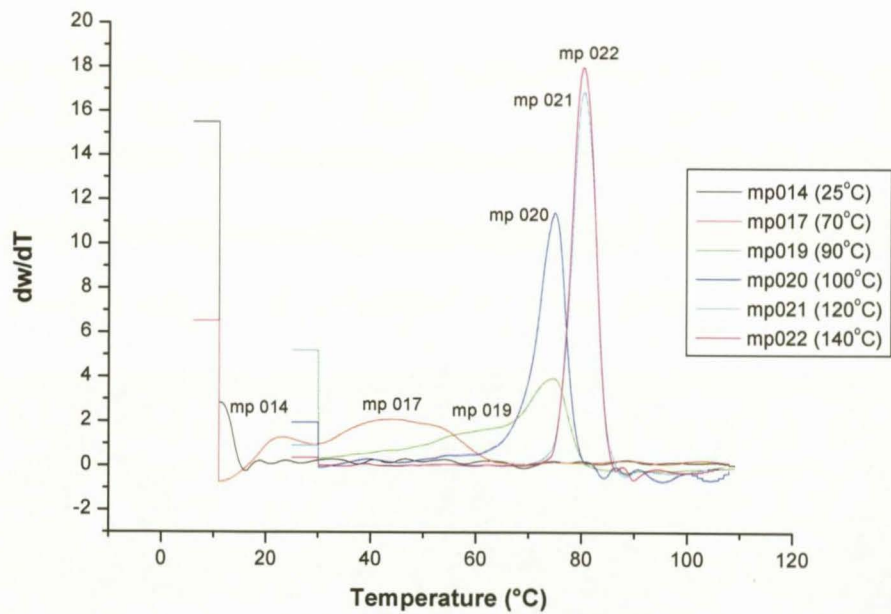


Figure B.6. CRYSTAF traces for Polymer B₁

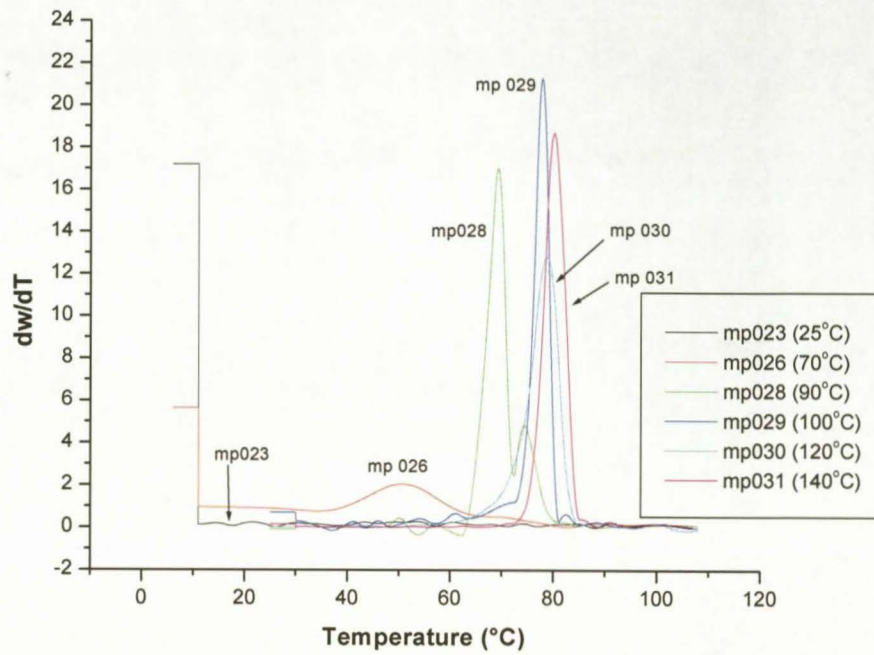


Figure B.7. CRYSTAF traces for Polymer C₁

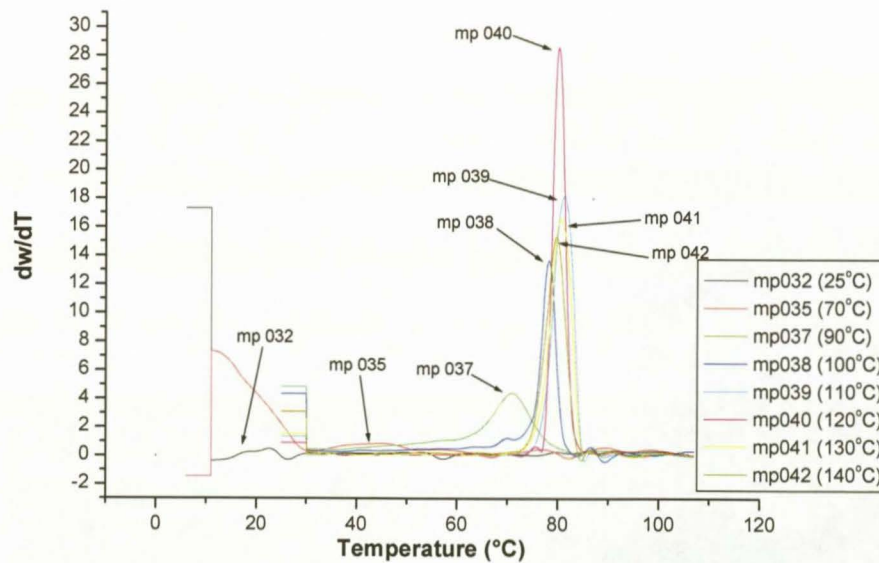


Figure B.8. CRYSTAF traces for Polymer D₁

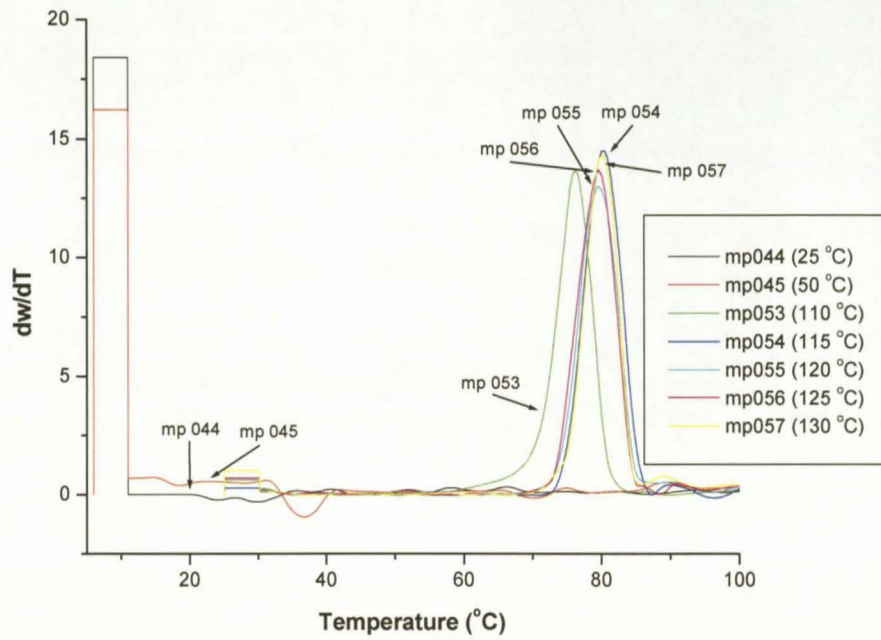


Figure B.9. CRYSTAF traces for Polymer A₂

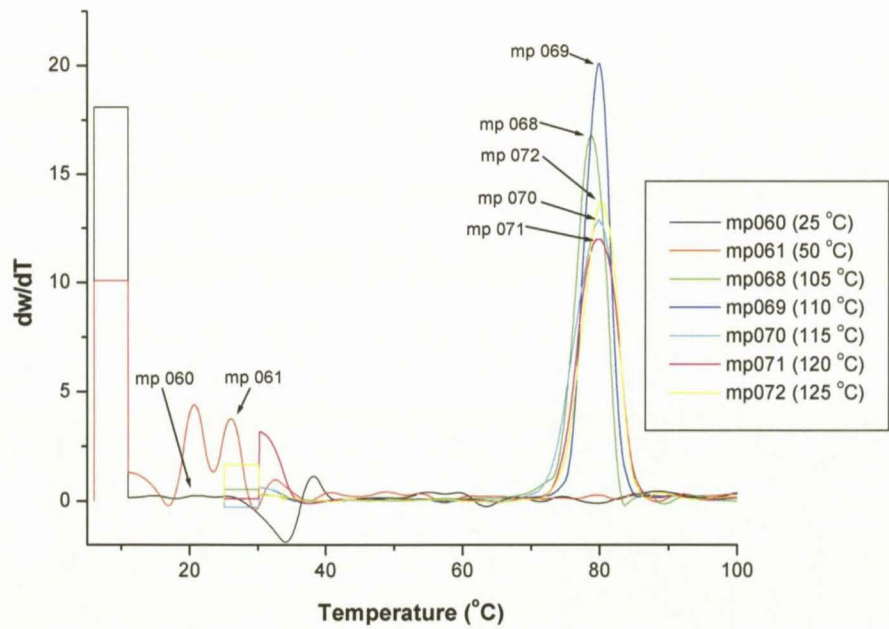


Figure B.10. CRYSTAF traces for Polymer B₂

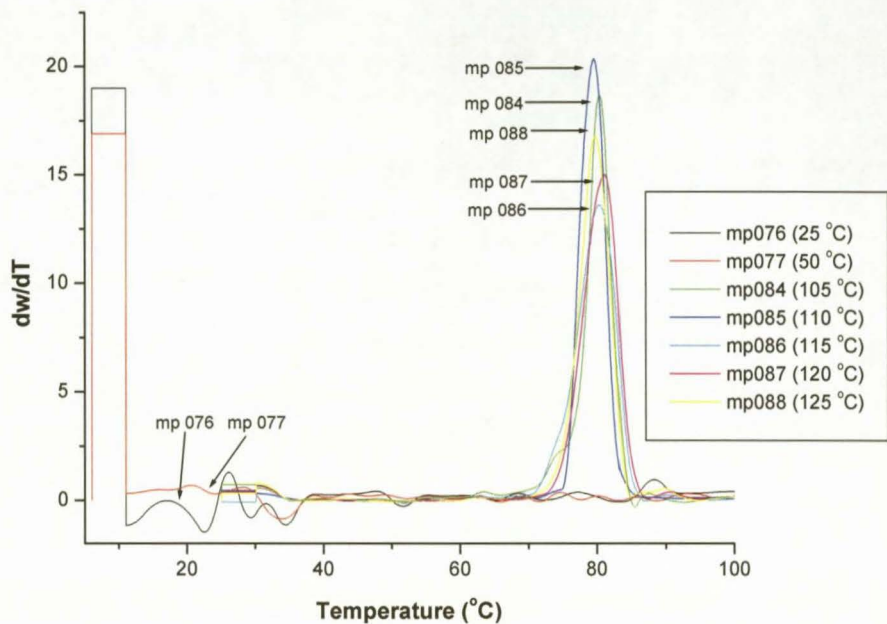


Figure B.11. CRYSTAF traces for Polymer C₂

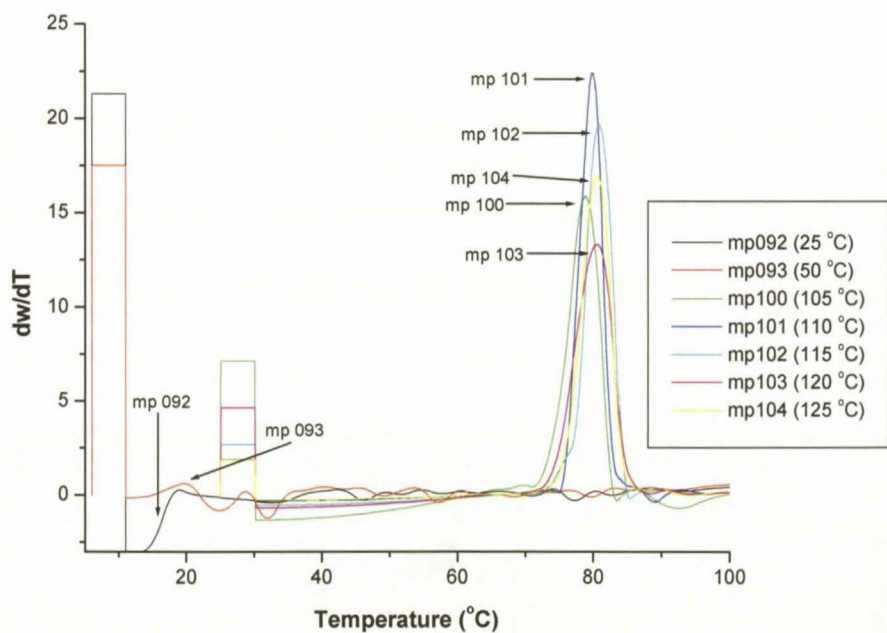


Figure B.12. CRYSTAF traces for Polymer D₂

C. DSC Results

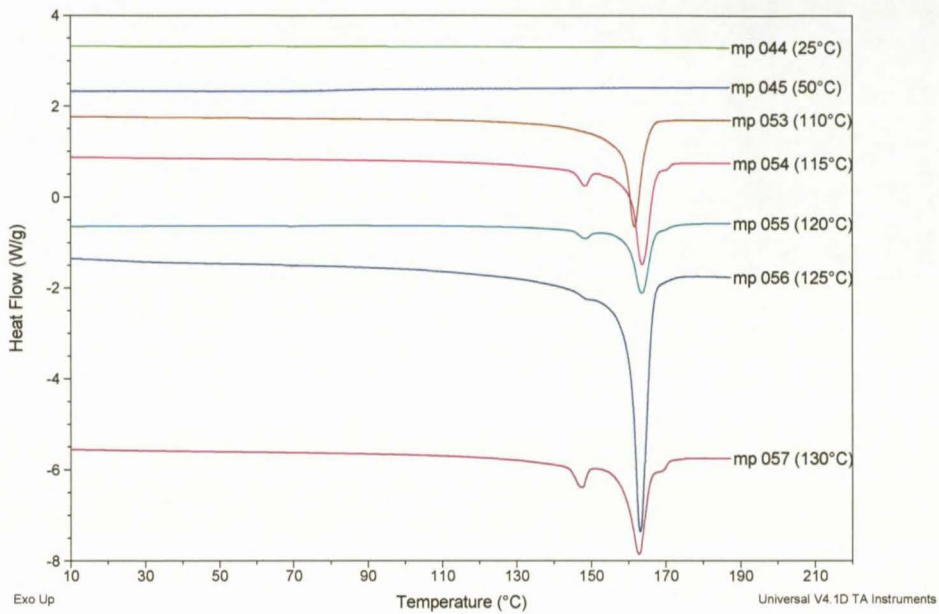


Figure B.13. DSC endothermic curves (2nd heating cycle) for Polymer A₂

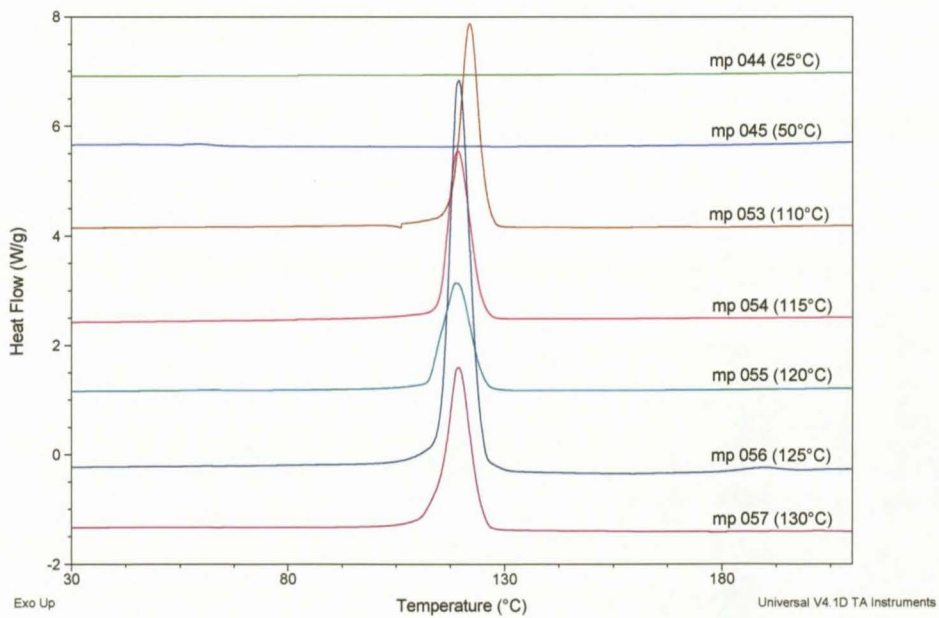


Figure B.14. DSC exothermic curves for Polymer A₂

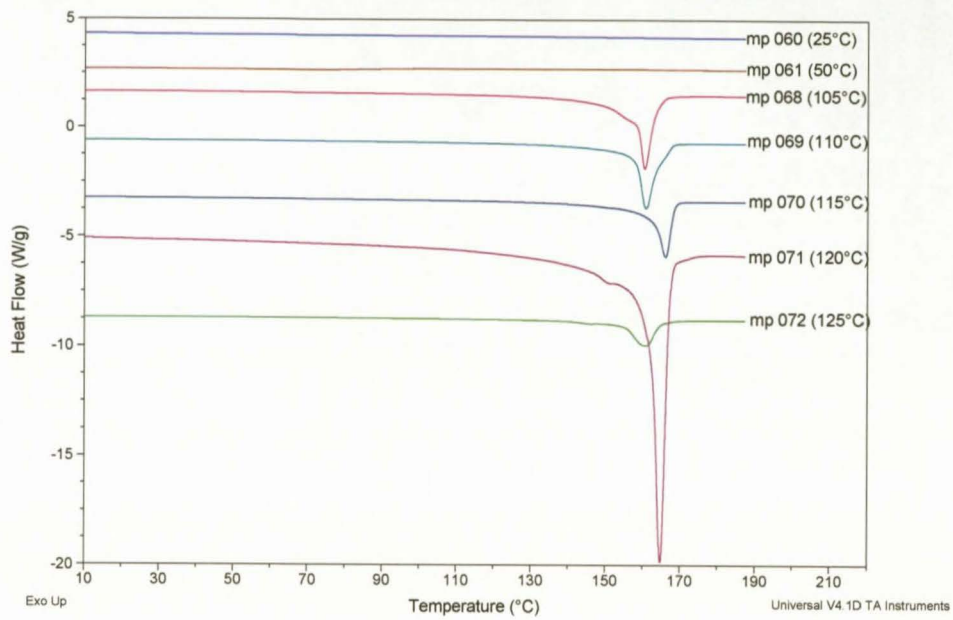


Figure B.15. DSC endothermic curves (2nd heating cycle) for Polymer B₂

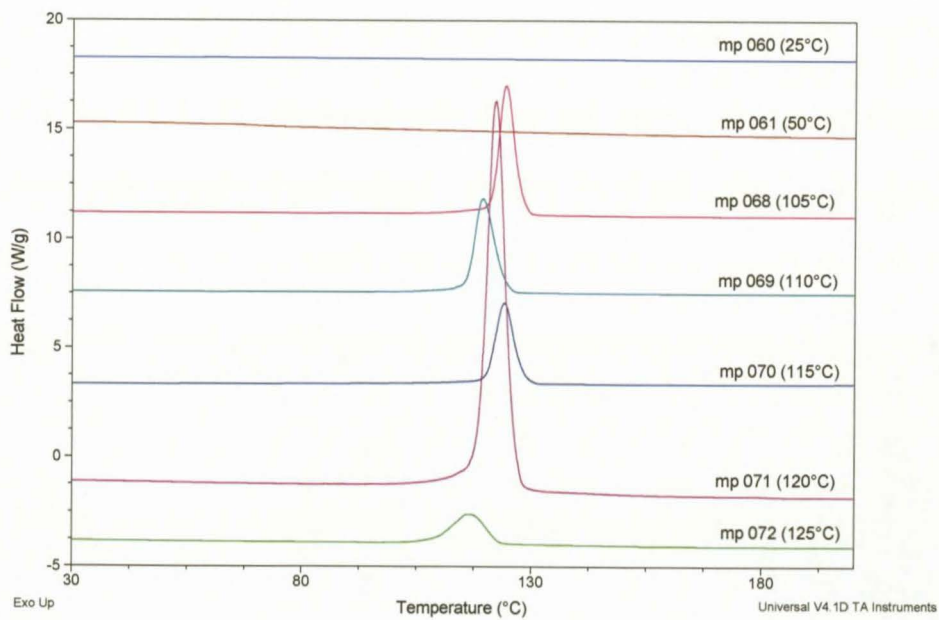


Figure B.16. DSC exothermic curves for Polymer B₂

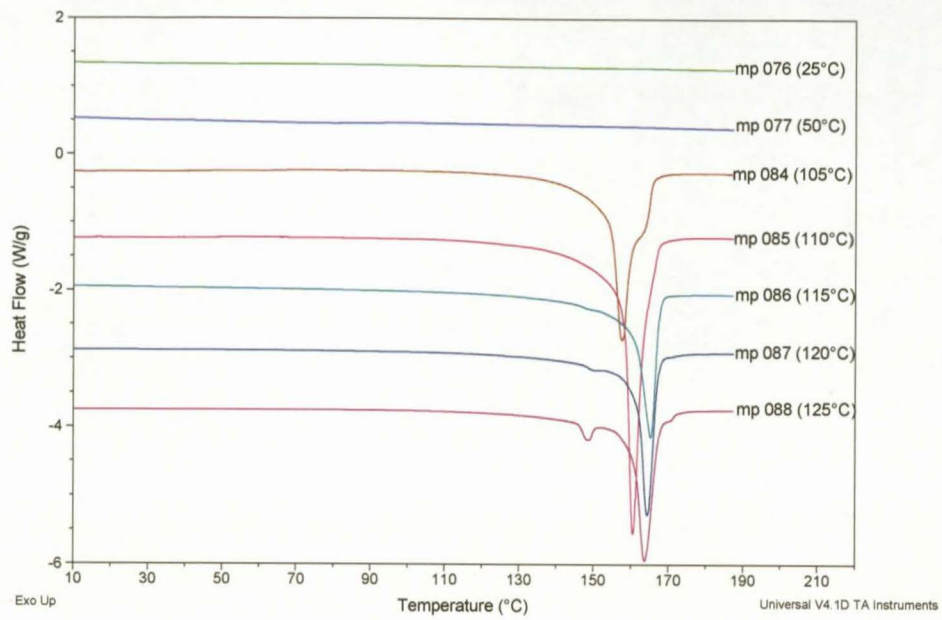


Figure B.17. DSC endothermic curves (2nd heating cycle) for Polymer C₂

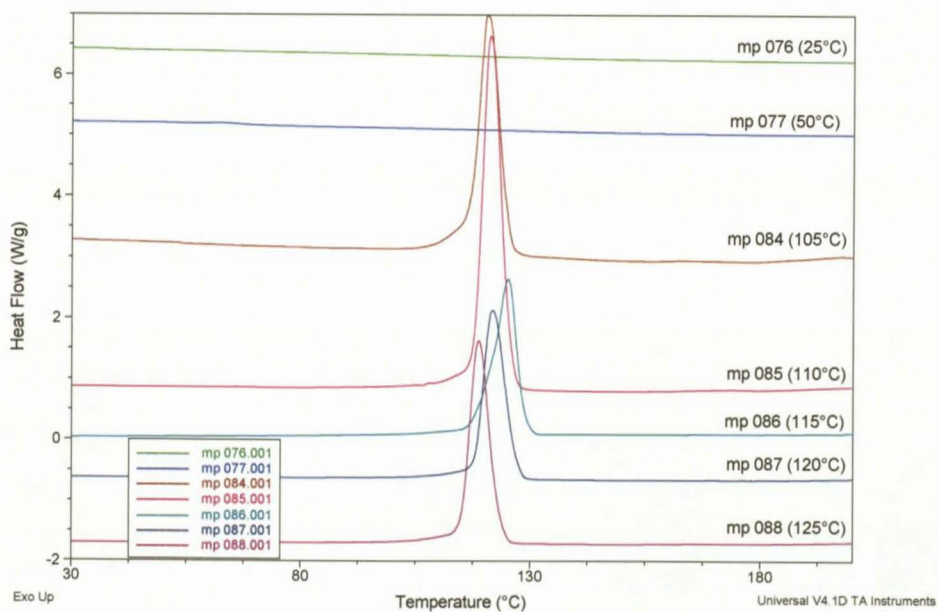


Figure B.18. DSC exothermic curves for Polymer C₂

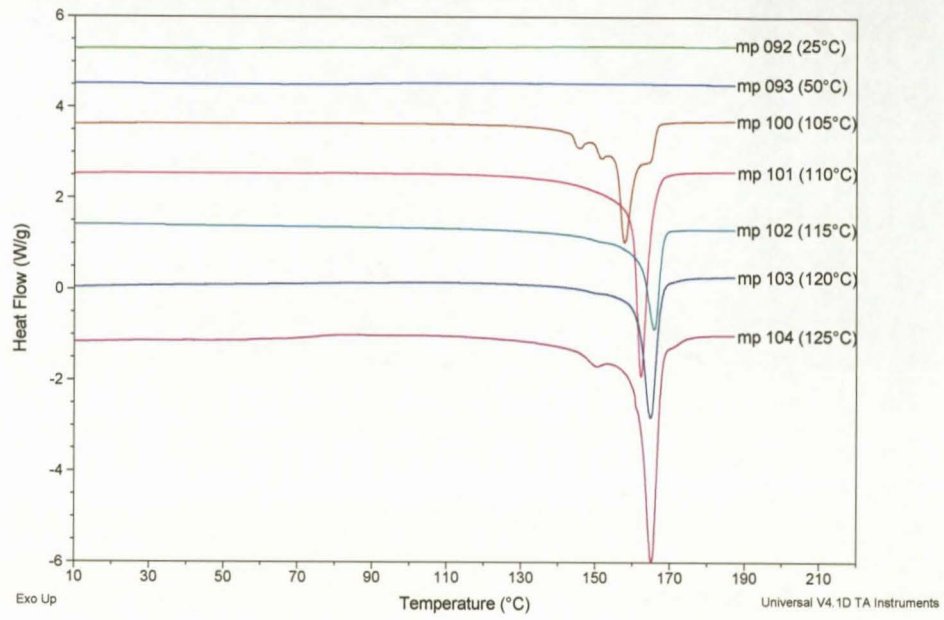


Figure B.19. DSC endothermic curves (2nd heating cycle) for Polymer D₂

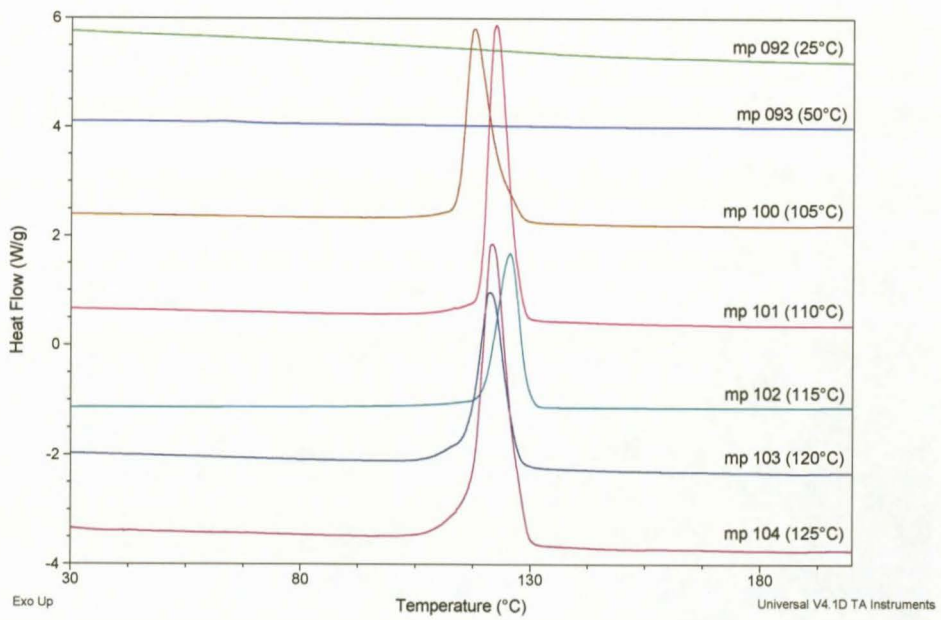


Figure B.20. DSC exothermic curves for Polymer D₂

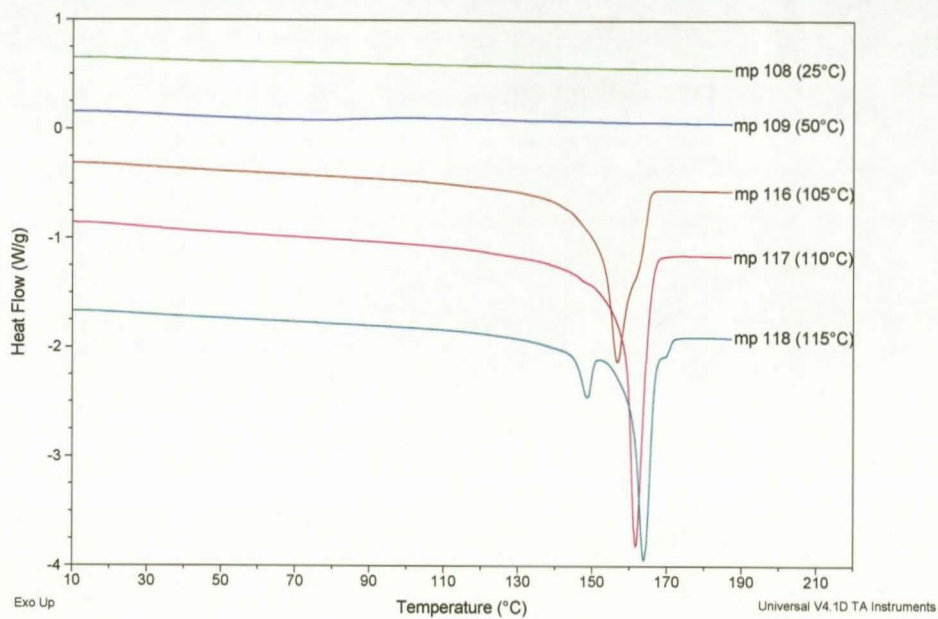


Figure B.21. DSC endothermic curves (2nd heating cycle) for Polymer A₃

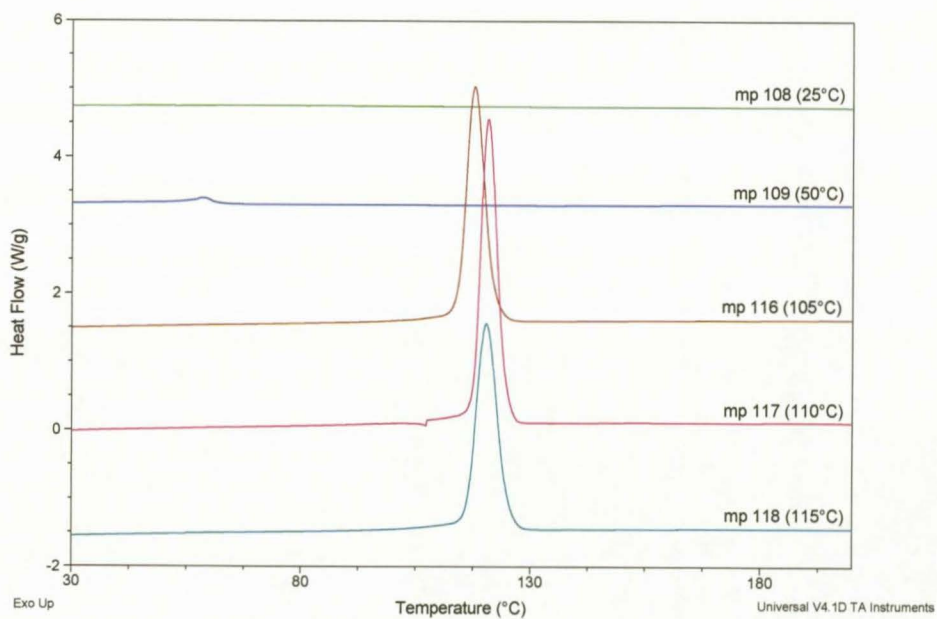


Figure B.22. DSC exothermic curves for Polymer A₃

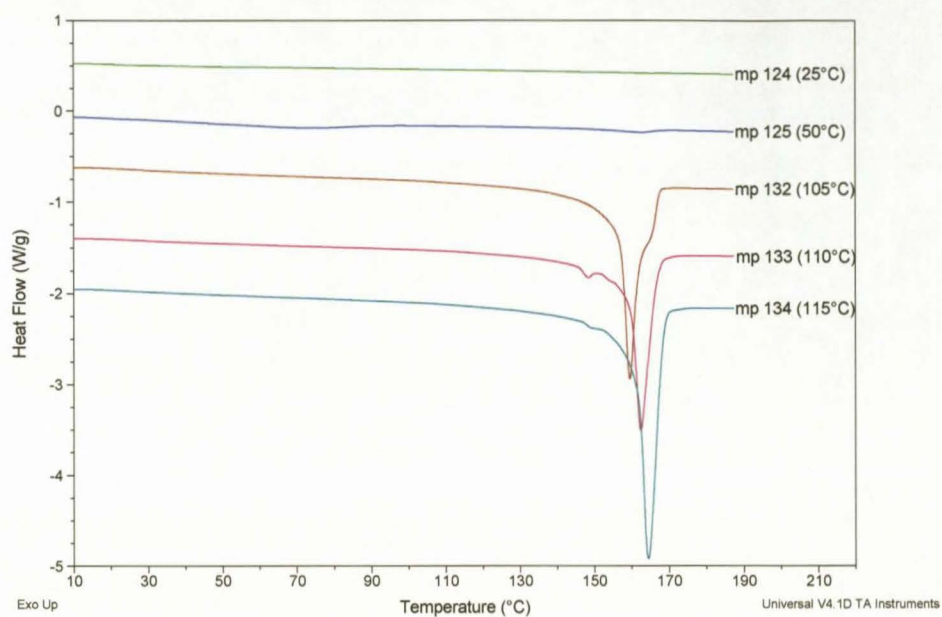


Figure B.23. DSC endothermic curves (2nd heating cycle) for Polymer B₃

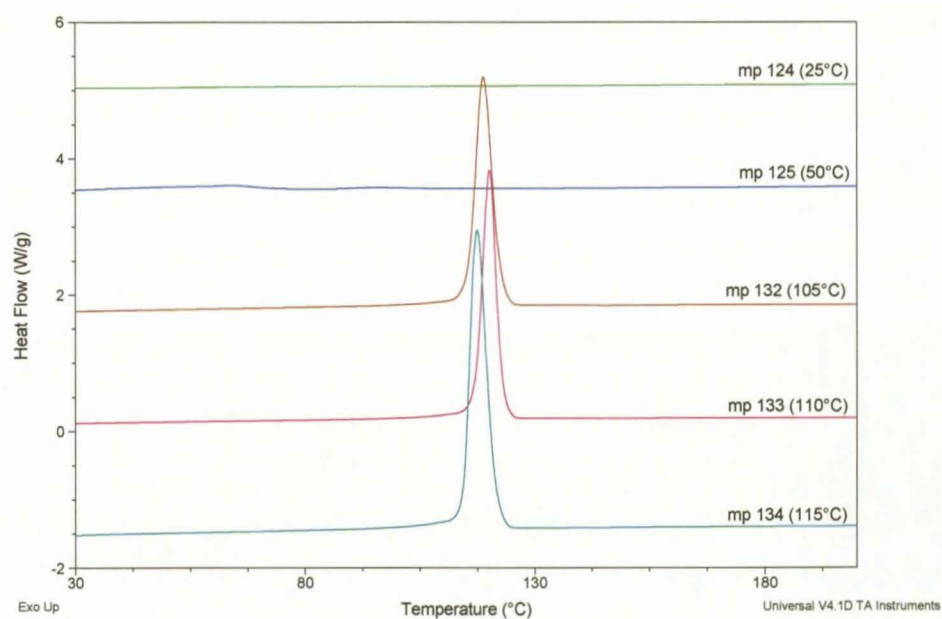


Figure B.24. DSC exothermic curves for Polymer B₃

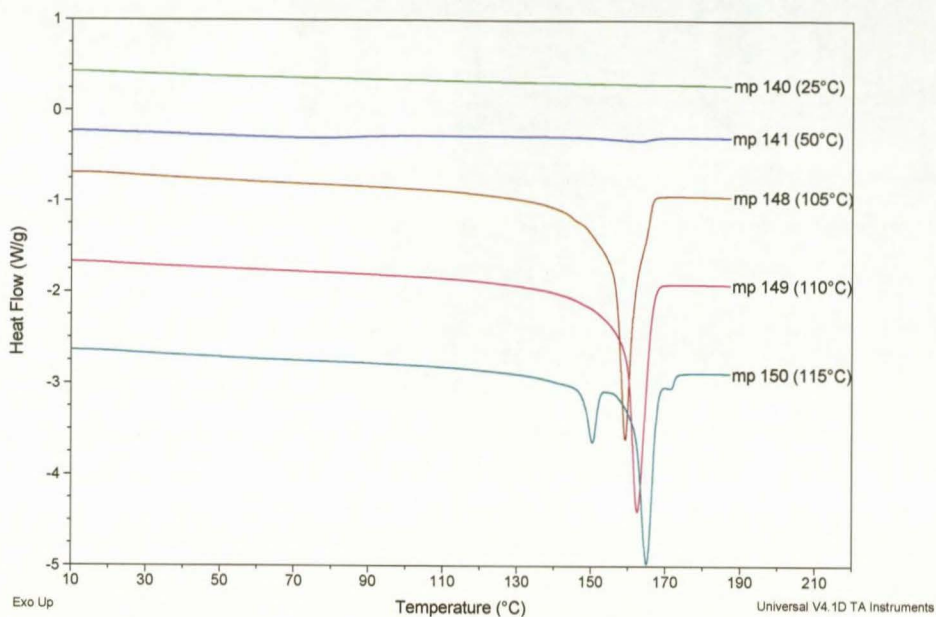


Figure B.25. DSC endothermic curves (2nd heating cycle) for Polymer C₃

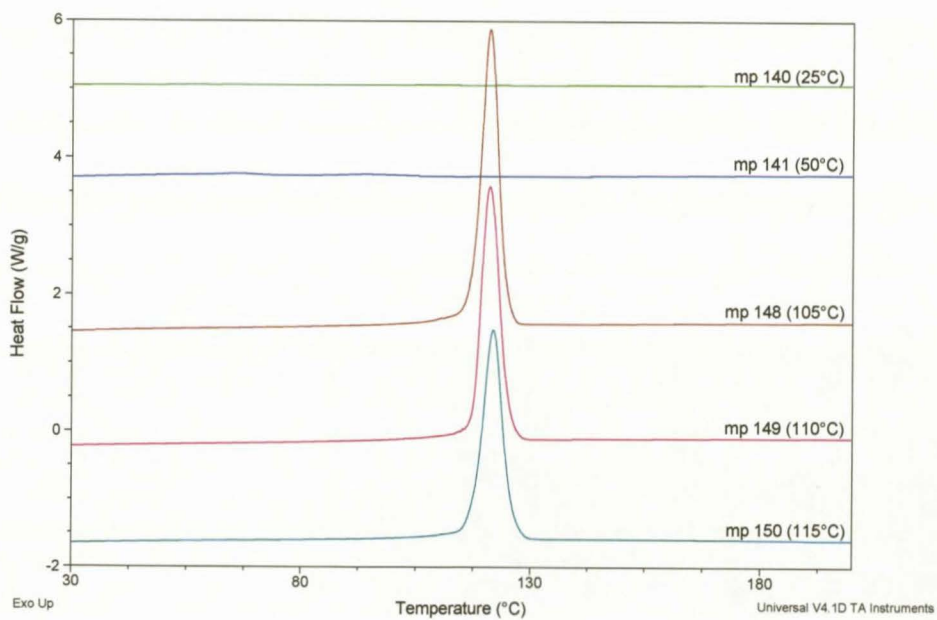


Figure B.26. DSC exothermic curves for Polymer C₃

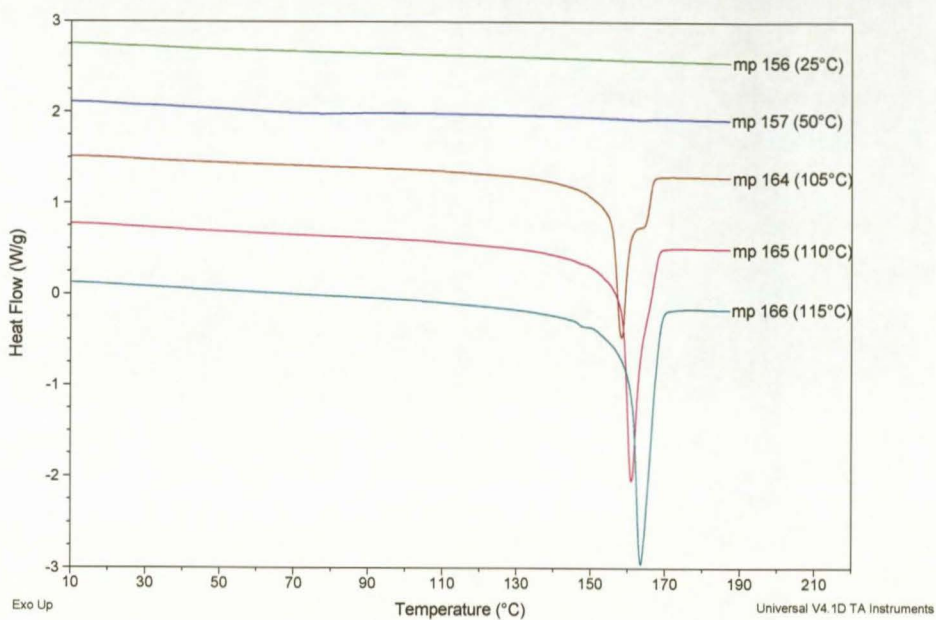


Figure B.27. DSC endothermic curves (2nd heating cycle) for Polymer D₃

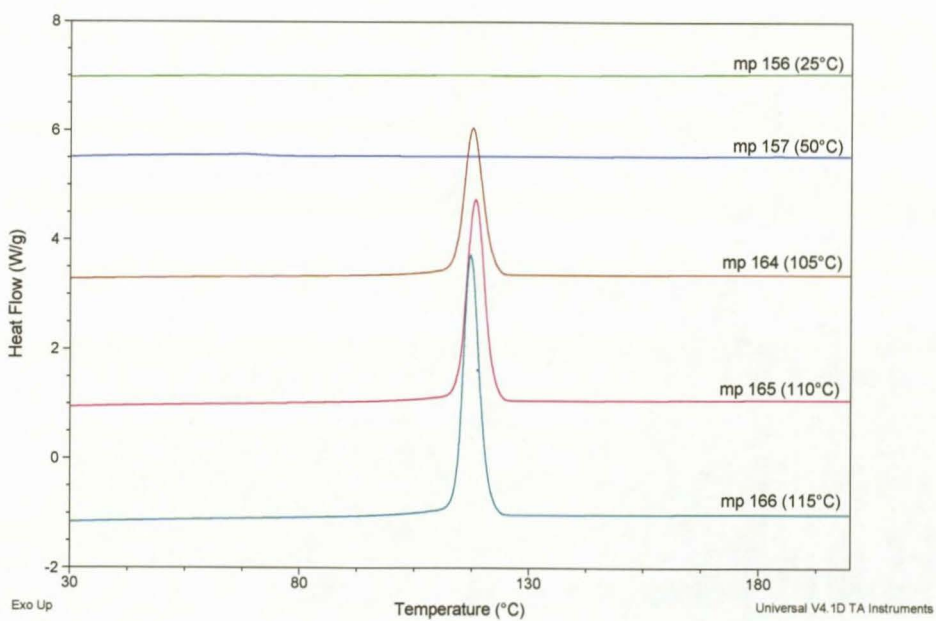


Figure B.28. DSC exothermic curves for Polymer D₃

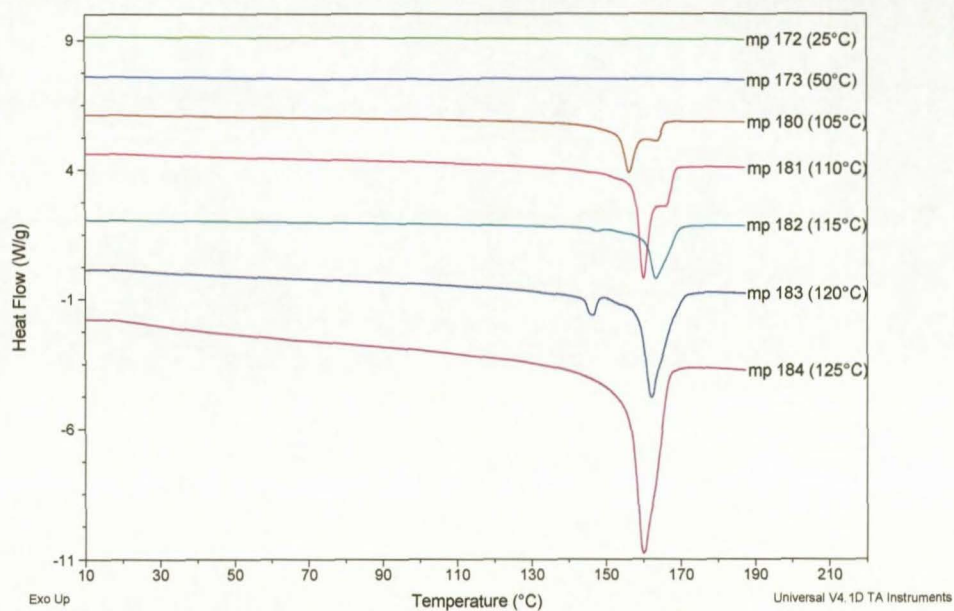


Figure B.29. DSC endothermic curves (2nd heating cycle) for Polymer E₁

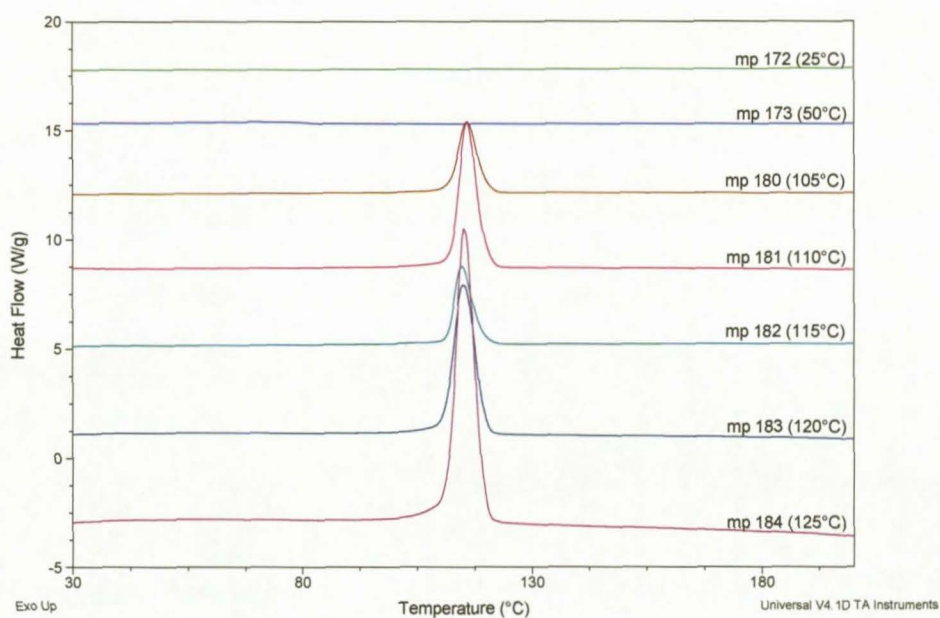


Figure B.30. DSC exothermic curves for Polymer E₁

D. HT-GPC Results

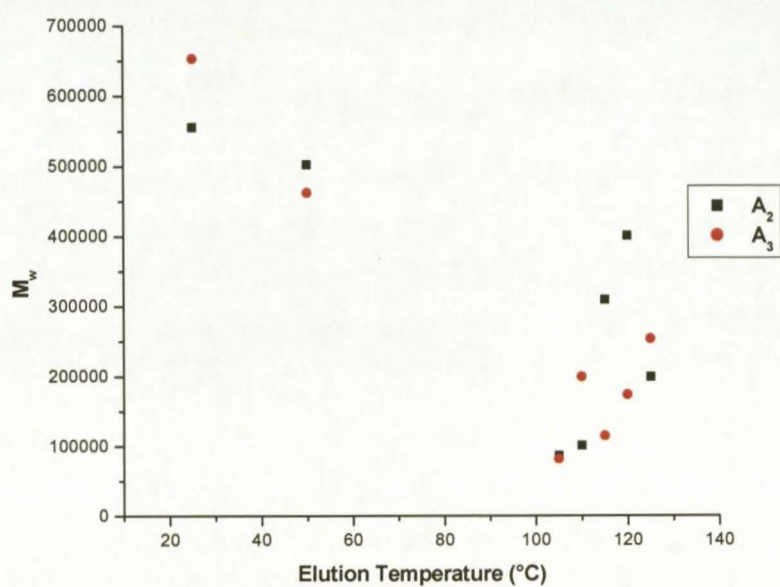


Figure B.31. The weight average molecular weights, M_w , of the fractions from polymers A_2 and A_3 as a function of elution temperature, °C.

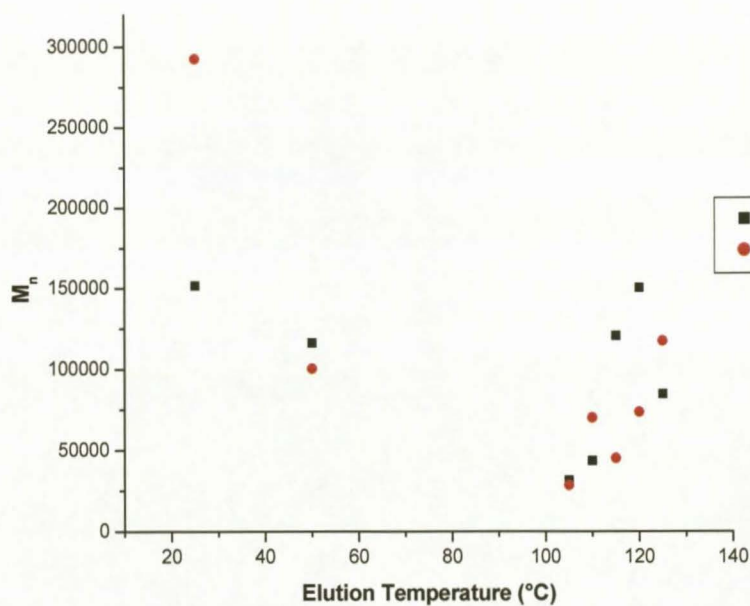


Figure B.32. The number average molecular weights, M_n , of the fractions from polymers A_2 and A_3 as a function of elution temperature, °C.

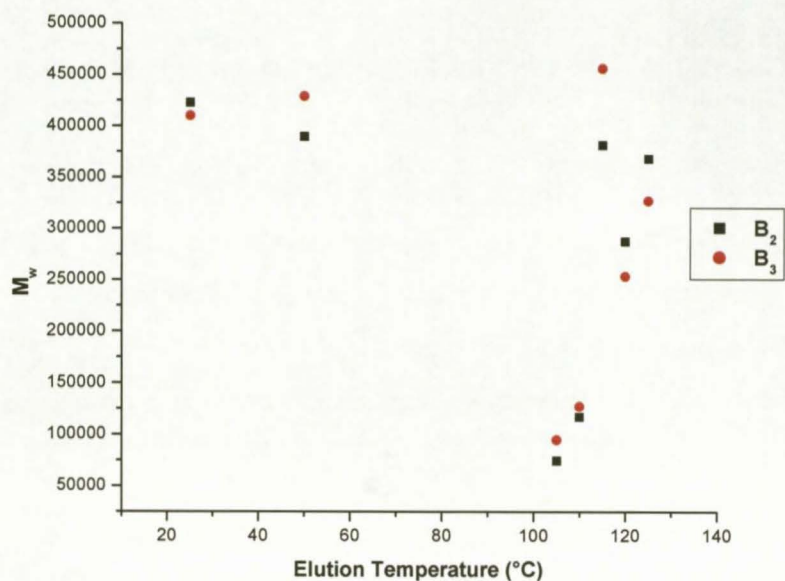


Figure B.33. The weight average molecular weights, M_w , of the fractions from polymers B_2 and B_3 as a function of elution temperature, °C.

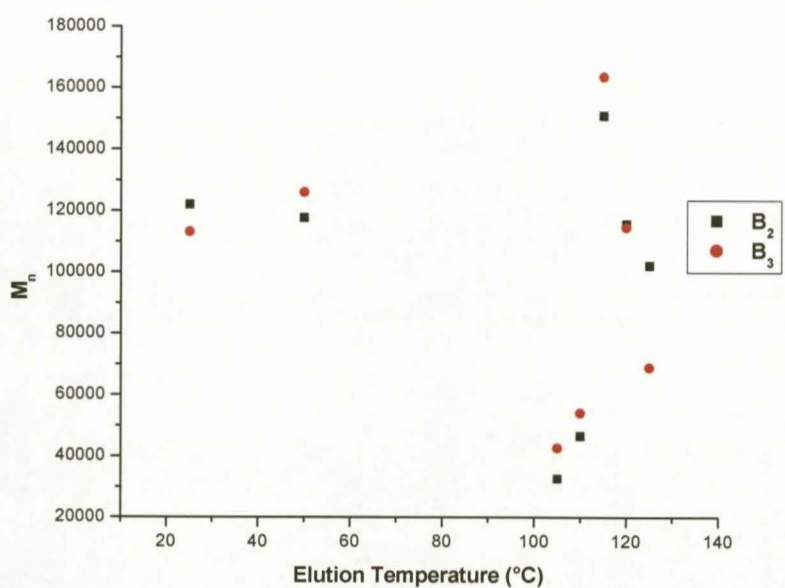


Figure B.34. The number average molecular weights, M_n , of the fractions from polymers B_2 and B_3 as a function of elution temperature, °C.

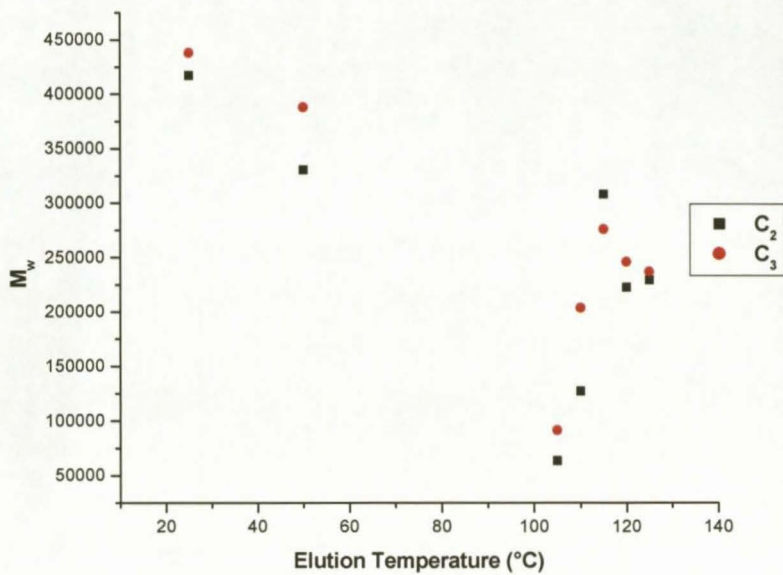


Figure B.35. The weight average molecular weights, M_w , of the fractions from polymers C_2 and C_3 as a function of elution temperature, °C.

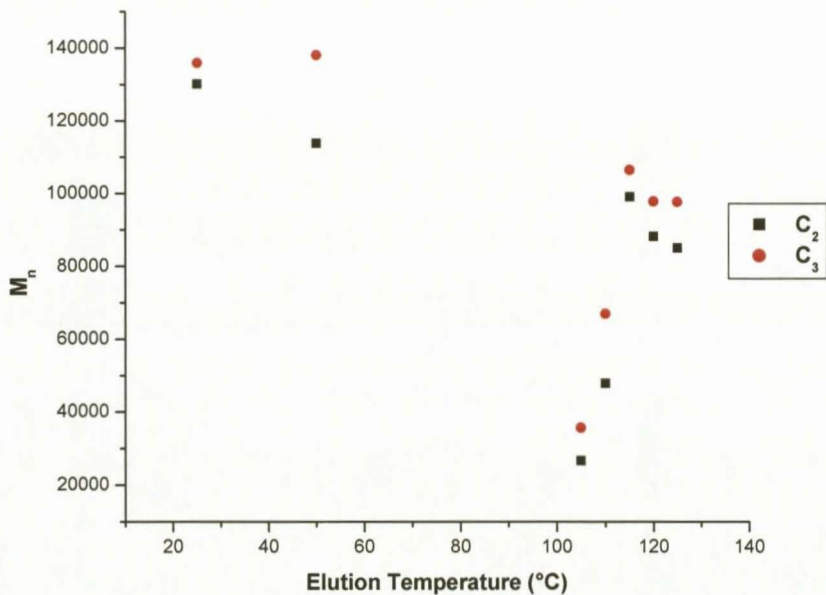


Figure B.36. The number average molecular weights, M_n , of the fractions from polymers C_2 and C_3 as a function of elution temperature, °C.

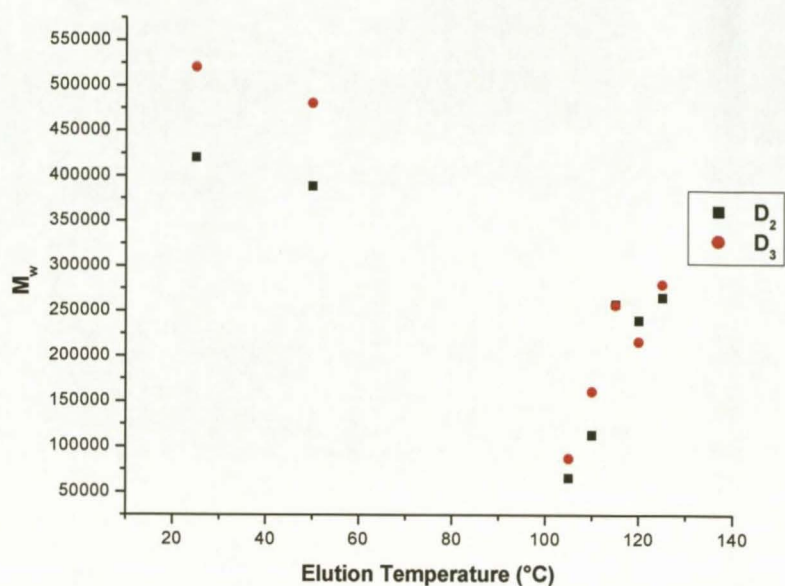


Figure B.37. The weight average molecular weights, M_w , of the fractions from polymers D_2 and D_3 as a function of elution temperature, °C.

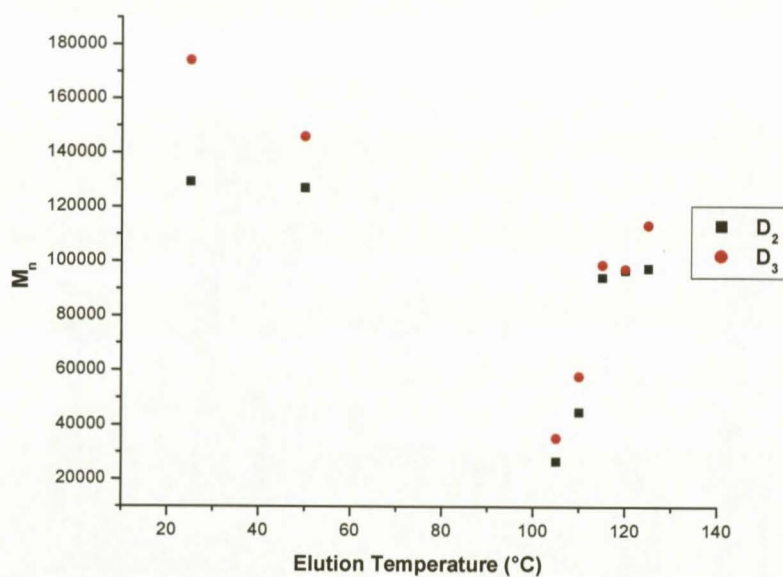


Figure B.38. The number average molecular weights, M_n , of the fractions from polymers D_2 and D_3 as a function of elution temperature, °C.

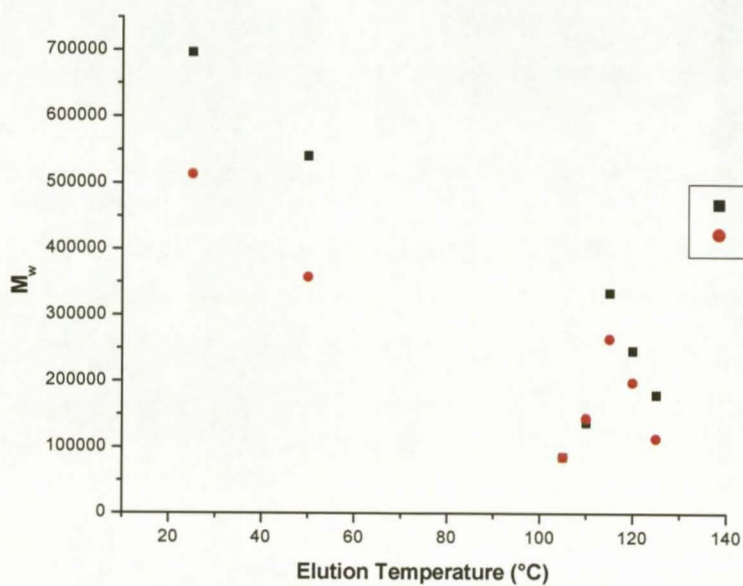


Figure B.39. The weight average molecular weights, M_w , of the fractions from polymers E_1 and E_2 as a function of elution temperature, °C.

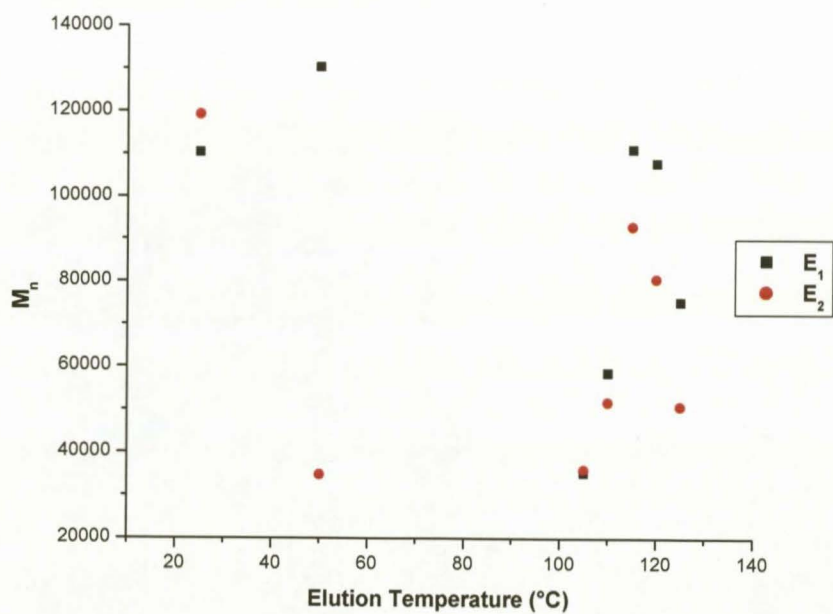


Figure B.40. The number average molecular weights, M_n , of the fractions from polymers E_1 and E_2 as a function of elution temperature, °C.